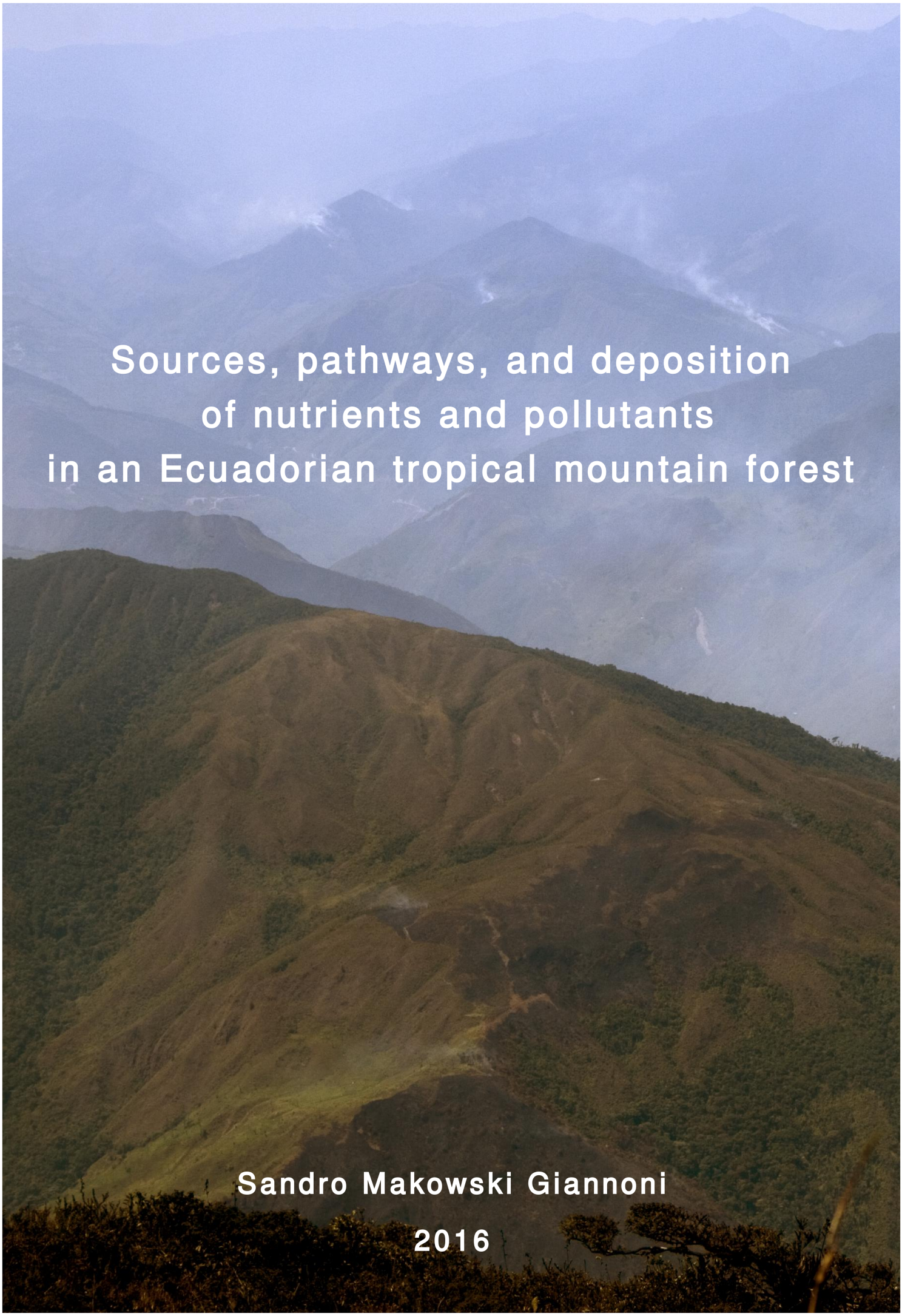

Sources, pathways, and deposition of nutrients and pollutants in an Ecuadorian tropical mountain forest

Sandro Makowski Giannoni

2016

Sources, pathways, and deposition of nutrients and pollutants in an Ecuadorian tropical mountain forest

Kumulative Dissertation

zur Erlangung des

DOKTORGRADES DER NATURWISSENSCHAFTEN

(Dr. rer. nat)

dem FACHBEREICH GEOGRAPHIE

der PHILIPPS-UNIVERSITÄT MARBURG

vorgelegt von

SANDRO MAKOWSKI GIANNONI

aus Lima - Peru

Marburg / Lahn, Januar 2017

Am FACHBEREICH GEOGRAPHIE der PHILIPPS-UNIVERSITÄT MARBURG (Hochschul-kennziffer: 1180) am 24.10.2016 als Dissertation eingereicht

Erstgutachter: Prof. Dr. Jörg Bendix

Zweitgutachter: Prof. Dr. Peter Chifflard

Weitere Mitglieder der Prüfungskomission:

Prof. Dr. Birgit Ziegehagen

Prof. Dr. Maaike Bader

Tag der mündlichen Prüfung am 19.12.2016

A Giulia y Kamil

Prolog

At the end of this very long journey I would like to thank all the people that have supported me, who without them the conclusion of this work would not have been possible.

For their invaluable advice, patience, time, comprehensive feedback and effort in keeping my work on track, all my gratitude goes to my advisors Jörg Bendix, Rütger Rollenbeck and Katja Trachte. Their support and confidence helped me overcome difficulties and, what is more important, learn to face new challenges. I especially thank Jörg Bendix for helping me when applying for financial support and for directly financially supporting me after my scholarship came to an end. Special thanks go to Lukas Lehnert, Wolfgang Obermeier, and Tim Appelhans for taking their time in helping me to find solutions to my problems and to discuss my progress.

I am very grateful to all my colleagues at the LCRS for their support in addressing all kind of difficulties, from computer system dilemmas to day-to-day tasks. In particular, I want to thank Giulia Curatola Fernández, Martin Schulz, Wolfgang Obermeier, Lukas Lehnert, Simone Sollberger, Ximena Fernández Fontenoy, Paulina Alava, and Sebastian Egli for proofreading and language check. I am also appreciative for the collaboration of all students and student assistants in my work. These thank yous go to Alexander Groos, Insa Otte, Julia Tueshaus, Andine Houbé, and Nicolas Caspari.

I am eternally grateful to my life companions Giulia and Kamil for giving me the most important ingredient of life: joy. I thank you both for being so patient and understanding in times of crisis and for bringing happiness into my everyday life in spite of the circumstances. You always made me see the positive side of life. I also want to thank my parents, my brother and rest of the family for their unconditional love and support during all this time. Thank you so much to have taken enough time to share your sensible opinion with me when it came to taking difficult decisions. It has been a long and sometimes bumpy ride and I believe that your support helped me overcome the obstacles I encountered.

Many thanks to Birgit Kühne-Bialozyt, Sonja Häse, and Cristina Philippi for all their support, especially regarding paperwork and formalities. Maik, thank you for the technical support and for being an extremely pleasant neighbour. Our plants would have not survived without your help!

Last but not least, I thank Waltraud Kofer for all her enthusiastic support, as well as the German Academic Exchange Service (DAAD) and the German Research Foundation (DFG) for funding.

Sandro Makowski Giannoni[1]
Marburg, October 2016

[1] sandro.makowski@posteo.org

Summary

The element cycle is an important control of the ecosystem functioning such as the provision of supporting and regulating ecosystem services. Human induced alterations of this cycle could have deleterious effects on the ecosystem and its services, as e.g., carbon sequestration and water supply. The input of atmospheric elements is a key underlying mechanism of this cycle, supplying new nutrients/pollutants to the ecosystem. Therefore, an in-depth knowledge of the fluxes and the complex factors driving the deposition of ecosystem-relevant elements are indispensable to unravel the impacts of element cycle alterations on the mountain forests function, e.g. by nutrient manipulation experiments.

The current work is the first effort in a TMF with a very intricate terrain to reveal the complex causal relationships between the atmospheric fluxes of ecosystem-relevant nutrients and pollutants, the contributing emission sources and the atmospheric circulation drivers responsible for transport. This investigation has shown that the atmospheric deposition is highly conditioned by the interception of OP by vegetation and ground. Therefore, in the study area, the atmospheric constituents explored present a high spatial and temporal heterogeneity mainly based on elevation, aspect, and topographic position of the receptor side, as well as the location and height of the surrounding barriers. In general, the higher the terrain features are, the higher is the frequency of clouds touching the ground and thus, the influence of the synoptical circulation and far-range sources is increased. That is on the condition that the surrounding topography does not act as a barrier for the synoptical winds from specific directions.

The exposed findings stress the importance of considering topographical complexity of the receptor site when assessing atmospheric deposition in mountainous areas and should be considered when designing future nutrient manipulation experiments. Due to the importance of the synoptical circulation in the medium to long range transport of nutrient and pollutants, also the location of the sources with respect to the preponderant transport pathways is an important parameter affecting the observed deposition. Additionally, the seasonality, the surface, and the intensity of the emissions are also highly relevant factors determining the state of deposition at the receptor site.

The sources and transport pathways of the investigated atmospheric constituents in the study area are illustrated in a synthesis map in Fig. 6.1. The anthropogenic sources dominate the sulfur and nitrogen cycles, on which a very high influence of the biomass-burning sources was observed, especially on high elevation and vegetated areas well-exposed to the preponderant wind direction. Atmospheric sodium and chloride deposition at the study area is still dominated by natural sources, especially the Caribbean Sea and the equatorial Pacific Ocean, mostly fertilizing areas at high elevations, more exposed to the synoptic winds.

Zusammenfassung

Der Stoffkreislauf nimmt gegenüber Ökosystemfunktionen eine wichtige Kontrollfunktion ein und damit für die Bereitstellung unterstützender und regulierender Ökosystemdienstleistungen wie z.B. die Kohlenstoffbindung und das Wasserangebot. Anthropogen verursachte Veränderungen dieses Kreislaufs könnten jedoch eine schädliche Wirkung auf das jeweilige Ökosystem und dessen Dienstleistungen haben. Der Eintrag von atmosphärischen Spurenelementen ist dabei ein grundlegender Mechanismus innerhalb des Kreislaufs, der die Ökosysteme mit neuen Nährstoffen versorgt. So ist ein fundiertes Verständnis der zu Grunde liegenden Prozesse sowie der komplexen Faktoren, welche die Deposition ökosystemrelevanter Elemente bestimmen, unabdingbar, um den Einfluss eines veränderten Elementkreislaufs auf die Funktionen des Bergregenwalds zu untersuchen.

Die vorliegende Dissertation ist ein erster Ansatz in dem sehr komplexen Gelände eines Bergregenwalds in Süd-Ecuador die komplexen Kausalzusammenhänge atmosphärischer Flüsse ökosystemrelevanter Nähr- und Schadstoffe, sowie die dazu beitragenden Emissionsquellen und treibenden Kräfte unter Berücksichtigung der atmosphärischen Zirkulation aufzuzeigen. Die Untersuchungen haben gezeigt, dass die atmosphärische Deposition hauptsächlich von der Interzeption okkulten Niederschlags durch die Vegetation und den Boden bestimmt wird. So unterliegt die atmosphärische Deposition der analysierten Stoffe im Untersuchungsgebiet einer hohen räumlichen und zeitlichen Heterogenität, welche hauptsächlich durch Höhe, Exposition und topographische Position des Immissionsortes sowie Lage und Höhe der ihn umgebenden topographischen Barrieren hervorgerufen wird. Im Allgemeinen gilt, je höher das Gelände desto häufiger haben Wolken Bodenkontakt, wodurch der Einfluss der synoptischen Zirkulation und damit die Bedeutung weit entfernter Quellen erhöht wird. Dies gilt so lange, bis die umgebende Topographie keine Barriere mehr für die synoptischen Winde darstellt.

Diese Erkenntnisse betonen die Notwendigkeit, die komplexe Struktur der Topographie bei der Untersuchung atmosphärischer Deposition sowie auch bei der Planung von künftigen Nährstoffmanipulationsexperimenten im Hochgebirgsraum zu berücksichtigen. Da die synoptische Zirkulation einen wichtigen Teil der mittel bis weiten Transportweg von Nähr- und Schadstoffen darstellt, ist auch die Lage der Quellen

relativ zu den überwiegend vorherrschenden Transportwegen ein wesentlicher Faktor, welcher die beobachtete Deposition beeinflusst. Darüber hinaus steuern die Saisonalität der atmosphärischen Zirkulation sowie Oberfläche und Intensität der Emmissionen die Deposition am Immissionsort.

Die Quellen und Transportwege der untersuchten Spurenstoffe im Untersuchungsgebiet sind in einer Synthesekarte zusammengefasst (siehe Fig. 6.1). Anthropogene Quellen dominieren sowohl den Schwefel- als auch den Stickstoffkreislauf, wobei ein sehr starker Einfluss aus den aus der Verbrennung von Biomasse resultierenden Quellen beobachtet wurde. Dies trifft insbesondere in bewachsenen Flächen in großen Höhen auf, die zudem in Richtung der vorherrschenden Windrichtung exponiert sind. Die Deposition von atmosphärischem Natrium und Chlorid im Untersuchungsgebiet ist nach wie vor von natürlichen Quellen geprägt, vor allem der Karibischen See und dem äquatornahen Pazifischen Ozean; auch hier profitieren insbesondere die höher gelegenden Gebiete. Des Weiteren sind diese höher gelegenen Gebiete stärker von mittel- bis -weit entfernten herantransportierten Luftschadstoffen betroffen als die tieferen Gebiete, da sie der atmosphärischen Zirkulation weniger ausgesetzt sind.

Resumen

El ciclo de los elementos es un componente importante del funcionamiento del ecosistema como lo es la provisión de servicios ecosistémicos de soporte y regulación. Las alteraciones de este ciclo, inducidas por el hombre, podrían tener efectos negativos en el ecosistema y sus servicios, como por ejemplo en la captación de carbono y en el suministro de agua. La entrada de elementos atmosféricos al ecosistema es un mecanismo clave de este ciclo que provee nuevos nutrientes al ecosistema. Por lo tanto, un conocimiento profundo de los flujos y de los factores complejos que llevan a la deposición de elementos importantes para el ecosistema es indispensable para desentrañar el impacto de las alteraciones del ciclo de los elementos al funcionamiento de los bosques de montaña, por ejemplo, a través de experimentos de manipulación de nutrientes.

El presente trabajo es el primer esfuerzo para revelar las complejas relaciones causales entre los flujos atmosféricos de nutrientes relevantes para el ecosistema y los contaminantes, la contribución de sus fuentes de emisión, así como los elementos de la circulación atmosférica responsables de su transporte, en un bosque tropical de montaña topográficamente complejo. Esta investigación ha mostrado que la deposición atmosférica está fuertemente influenciada por la captación de precipitación oculta por la vegetación y el suelo. Por lo tanto, en el área de estudio, los elementos estudiados presentan una alta heterogeneidad espacial y temporal principalmente causada por la altitud, la orientación de la ladera y la posición topográfica, así como por la posición y la altura de las barreras circundantes. En general, cuanto más alto se encuentra el terreno, más alta es la frecuencia de nubes que tocan el terreno y la influencia de la circulación sinóptica y las fuentes alejadas. Esto siempre y cuando la topografía circundante no actúe como barrera para los vientos sinópticos provenientes de direcciones específicas.

Los hallazgos aquí expuestos resaltan la importancia de considerar la complejidad topográfica cuando se estudia la deposición atmosférica en áreas montañosas y deberán ser considerados en el momento de diseñar experimentos de manipulación de nutrientes futuros. Dado que la circulación sinóptica es un factor importante en el transporte de nutrientes y contaminantes de mediano y largo rango, la localización de las fuentes con respecto a las vías de transporte preponderantes es un parámetro importante que afecta la

deposición observada. Adicionalmente, la estacionalidad, la superficie y la intensidad de las emisiones también son factores altamente relevantes que determinan el estado de la deposición en el lugar receptor.

Las fuentes y las vías de transporte de los elementos atmosféricos estudiados están ilustradas en un mapa de síntesis (Fig. 6.1). Las fuentes antropogénicas dominan el ciclo del sulfuro y del nitrógeno. Se ha observado que, entre estas, las fuentes de quema de biomasa tienen una gran influencia especialmente en las zonas altas y con vegetación bien expuesta a la dirección del viento preponderante. La deposición de sodio y cloruro en el área de estudio está todavía dominada por fuentes naturales, en particular en el mar Caribe y en el océano Pacífico ecuatorial, y fertiliza principalmente las áreas más elevadas y más expuestas a los vientos sinópticos.

Contents

List of Figures

List of Tables

List of acronyms

Acronym		Meaning
Aerocom	-	Aerosol comparisons between emissions and models
CAMS	-	Copernicus atmosphere monitoring system
CASA-GFED	-	Carnegie Ames Stanford approach - global fire emission database
CF	-	Concentration field
COSPEC	-	Correlation spectrometer
CWT	-	Concentration weighted trajectory
DFG	-	German Research Council
DJF	-	December, January, February
ECSF	-	Estación científica San Francisco
ECMWF	-	European Center for Medium-range Weather Forecast
EDGAR	-	Emission database for global atmospheric research
EMEP	-	European Monitoring and Evaluation Programme
ERA 40	-	ECMWF reanalysis 40
ERA Interim	-	ECMWF reanalysis interim
FLEXPART	-	Flexible Particle dispersion model
FLEXTRA	-	Flexible Trajectory model
GAW	-	Global Atmosphere Watch
GFAS	-	Global fire assimilation system
GFEDv3	-	Global fire emission database version 3
GISTEMP	-	Goddard institute for space studies surface - temperature analysis
GOME	-	Global ozone monitoring experiment
HYSPLIT	-	Hybrid single particle lagrangian integrated trajectory model
INEC	-	Instituto Nacional de Estadística y Censos (Ecuador)
INPE	-	Instituto Nacional de Pesquisas Espaciais (Brazil)
ITCZ	-	Inter tropical convergence zone

JJA	-	June, July, August
LCRS	-	Laboratory for Climatology and Remote Sensing
MACC	-	Monitoring atmospheric composition and climate
MAD	-	Median absolute deviation
MAM	-	March, April, May
MCS	-	Mesoscale convective system
MS	-	Meteorological station
MTOP	-	Ministerio de Transporte y Obras Públicas (Ecuador)
NCAR	-	National Center for Atmospheric Research (USA)
NCEP	-	National Centers for Environment Prediction (USA)
Nr	-	Reactive nitrogen
NPP	-	Net primary productivity
NUMEX	-	Nutrient manipulation experiment
OMI	-	Ozone monitoring instrument
OP	-	Occult precipitation
PFA	-	Principal factor analysis
PREDICT	-	Precipitation dynamics and chemical properties in tropical mountain forests of southern Ecuador
PSCF	-	Probability source contribution function
RBSF	-	Reserva biológica San Francisco
RETRO	-	Reanalysis of the Tropospheric chemical composition over the past 40 years
SA-INV	-	Regional vehicle emissions inventory
SCIAMACHY	-	Scanning imaging absorption spectrometer for atmospheric chartography
SFC	-	Standard fog collector
SON	-	September, October, November
TMF	-	Tropical mountain forest
TOMS	-	Total ozone mapping spectrometer
TS1	-	Transecto 1
TUM-WZW	-	Technische Universität München - Wissenschaftszentrum Weihenstephan
VSI	-	Volcanic sulfur index
VWMM	-	Volume-weighted monthly mean
WMO	-	World Meteorological Organization
WRF	-	Weather research and forecasting model

Chapter 1

Introduction

Tropical rainforests contribute with 44 % to the global forest cover and harbor a great plant and animal species diversity (Fao 2011). Tropical mountain forests (TMFs) represent a small proportion of these forests (around 20 %, Scatena et al. 2010). In the mountainous terrains, the intricated net of valleys and ridges and the consequent variety of climatic conditions are positive factors favoring speciation and endemism (Kessler and Kluge 2008). This results in an extraordinary high biodiversity of the TMFs which consequently have an invaluable ecological importance, as, for instance, diversity supports ecosystems' resilience to environmental changes (Rockström et al. 2009). To this ecological relevance a socio-economic importance is added, as TMFs supply water for irrigation and drinking and many other ecosystem services that support the livelihood and promote the well-being of millions of people living in the tropics (Barkmann et al. 2013; Hölscher 2008; Tognetti et al. 2010).

TMFs' distribution is governed by a diversity of factors. Some of these are the altitude of the upper cloud boundary (influenced by the global-scale atmospheric circulation), the lower cloud limit (determined by local moisture and temperature gradients), and topography (altitude, slope aspect, etc.) (Scatena et al. 2010). A spatial cluster of TMFs is found in South America, at the eastern escarpment of the Andes mountains, where the *cordillera* acts as a natural barrier for the humid Amazon air masses.

TMFs are generally well adapted to nutrient-poor conditions, because most soils in tropical mountain areas are scarce in nutrients (Vitousek 1984; Tanner et al. 1998). Consequently, the fertilization of the TMF by atmospheric deposition represents important nutrient additions to the ecosystem. These atmospheric inputs have long been dominated by natural emission sources. However, the increase of anthropogenic emissions in rapidly developing tropical countries (e.g. forest clearing, industrial, and urban/transportation emissions) has led to a fast increment of the deposition with likely relevant impacts on the TMFs' ecosystem. More precisely, according to a recent review, the increased

deposition of nitrogen and acidic compounds is one of the most important drivers of global environmental change on tropical forests (Lewis et al. 2004).

The increase of nitrogen deposition could lead to a substantial loss in species richness. The excess of this nutrient gives a competitive advantage to generalist species, while species adapted to nitrogen-poor conditions are reduced systematically (Phoenix et al. 2006; Unger et al. 2012; Homeier et al. 2012; Stevens et al. 2004). Besides changing species composition and reducing plant diversity, the increase in nitrogen deposition is expected to have consequences on the nitrogen and carbon dioxide cycles, the acidification of soils, and to increase the susceptibility to secondary stress and disturbance factors, as e.g. drought, pathogens, herbivory, etc. (Bobbink et al. 2010; Boy et al. 2008; Homeier et al. 2012; Matson et al. 2002).

TMFs are very sensitive to acidifying atmospheric deposition because of their highly weathered and naturally acidic soils. Acidic atmospheric deposition has increased in several tropical forests, and in some cases surpassed critical loads likely to cause detrimental impacts on the ecosystem function (Kuylenstierna et al. 2001). An excess of acidic element-influxes, as e.g. sulfur containing components, leads to the acidification of soils and to the consequent decline of the cationic exchange capacity and base metal supply of the vegetation. In a very acidic soil environment, aluminum comes into solution, which is toxic for plant roots and locks up phosphate, an essential macro-nutrient for plant growth (Boy et al. 2008; Rehmus et al. 2015, 2014).

Salt has long been overlooked as an important nutrient in tropical ecosystems. However, according to a recent study, sea salt (NaCl) availability is important for herbivory, carbon cycling, and organic matter decomposition in tropical forests (Dudley et al. 2012). Undoubtedly, the oceans are the most important sources of continental sea salt deposition. Thus, in the Amazon a gradient of sea salt availability as a function of the distance from the Atlantic coast has been assumed, because sea salt transport from the Pacific is blocked by the Andean range. According to this, the sea salt scarcity in the vegetation of the eastern Andean tropical forests would explain the practice of visiting other salt sources (e.g. mineral licks) observed in some herbivore and arthropod species in the Amazon of Peru, Colombia, and central and western Brazil (Dudley et al. 2012; Kaspari et al. 2008; Lee et al. 2009; Lizcano and Cavelier 2004; Powell et al. 2009; Voigt et al. 2008). However, because of the high biomass-burning emissions in tropical South America (Andreae et al. 2004), which contain relevant amounts of chloride salts (Akagi et al. 2011), this type of anthropogenic emissions is likely to play a relevant role in the deposition of salt to Andean TMFs as well.

Therefore, the atmospheric deposition of nutrients, as e.g. nitrogen, sulfur, and sea salt in the TMF has two facets. On the one hand, as already specified, it is an important source of nutrients for the ecosystem (Homeier et al. 2012; Artaxo et al. 2009), also conditioning the behavior of animals (Dudley et al. 2012), as e.g. herbivores and decomposers. On the other hand, atmospheric fertilization can have direct and indirect negative consequences on the TMFs. The continuous increase of influxes of some nutrients as a consequence of higher anthropogenic emissions can destabilize the equilibrium of the ecosystem by affecting its composition and function (Bendix et al. 2013; Harpole and Tilman 2007; Homeier et al. 2012; Lewis et al. 2004), as well as causing acidification of soils (Kuylenstierna et al. 2001).
Despite its importance for the TMF, such as the supply of ecosystem services (e.g. supply and purification of potable water, and nutrient retention in vegetation and soil), knowledge on the state of the deposition regarding the elements mentioned, its sources, and its atmospheric transport pathways are clearly understudied and thus, so far poorly understood.

1.1 Motivation

As already mentioned in section 1, in the Andean TMF the nutrient scarcity in the soil limits the growth of the forest. In this context, the atmospheric deposition of nutrients, long time dominated by natural sources, fertilizes the TMF, being an important component of the element cycle. However, the excess of nutrient inputs related to the increment of anthropogenic emissions represents a negative aspect of atmospheric nutrient deposition. Additional inputs above certain boundaries alter the nutrient balance, with a likely impact on the health of the vegetation, the species composition, the biodiversity and the biogeochemical cycles (Homeier et al. 2012). Considering the current increase in human-related emissions throughout the tropics and the likely impacts on the TMF ecosystem and the ongoing global climate change, new knowledge is needed regarding the nutrient cycles in the TMF. Of special interest are the delineation of the deposition sources and the determination of their nature (natural or anthropogenic) and their contribution to the deposition. In this way it is possible to estimate to what extent natural or human emission sources are contributing to the fertilization of the TMF and which specific sources are dominant (e.g. urban, biomass burning, biogenic, volcanoes, etc.). It is also of great importance how the deposition of nutrients varies in space and time in the local scale, given the likely impacts of the high terrain complexity in areas where TMFs occur (Weathers et al. 2000; Scatena et al. 2010).

In spite of its importance, to my knowledge, intense research in element cycling and atmospheric transport and deposition in the Amazon have been mainly restricted to the lowland forests of Brazil (Vet et al. 2014). Apart from the Andes of eastern

Ecuador, no intensive research initiatives have taken place in other Andean TMFs (Jarvis and Mulligan 2010). Here, a multidisciplinary research platform (FOR 816, Bendix et al. 2013) investigates the atmospheric deposition of nutrients and its impacts on the TMF ecosystem. The present work is part of a subproject investigating the dynamics of precipitation and atmospheric deposition of nutrients (precipitation dynamics and chemical properties in tropical mountain forests of southern Ecuador – project PREDICT –). PREDICT also supplies essential data and information for a running nutrient manipulation experiment (NUMEX - Homeier et al. 2012), which is investigating the response of the TMF ecosystem to the atmospheric nutrient inputs.

In Ecuador, some work regarding the state of atmospheric deposition and the localization and contribution of potential deposition sources has been already done by Fabian et al. (2005, 2009), Rollenbeck et al. (2006), Boy and Wilcke (2008), and Boy et al. (2008). Boy and Wilcke (2008) presented evidence showing that calcium and magnesium from saharan dust sources transported over the Amazon and reaching the tropical mountains of the Ecuadorian Andes contributed to the nutrient balance of this forest ecosystem. With support of wind back-trajectories and a fire pixels product from the Instituto Nacional de Pesquisas Espaciais (INPE), Fabian et al. (2005) and Boy et al. (2008) revealed the fertilizing and acidifying effect of biomass-burning sources in the ecosystem. Fabian et al. (2009), Rollenbeck et al. (2006), and Rollenbeck (2010) also explored the application of wind back-trajectories to estimate general transport pathways of different atmospheric constituents to the study area in South Ecuador and the latter introduced an emission inventory as input for transport modelling by a trajectory tool. None of the studies mentioned, however, has done an in-depth analysis of the deposition and source-receptor relationships of ecosystem-relevant nutrient species which explicitly accounts for topography, and integrates the advances of emission inventories, satellite products, atmospheric reanalysis, and wind trajectory analysis techniques.

Several studies have demonstrated that topography affects the deposition in mountainous areas such as the Andes of Ecuador (Griffith et al. 2015; Kirchner et al. 2014; Lovett and Kinsman 1990; Hofhansl et al. 2011; Weathers et al. 2000). Studies in these regions should account for the effects of the different topographic features in the deposition. Furthermore, since the studied nutrient species can have different anthropogenic as well as natural sources, and therefore different atmospheric pathways, a more comprehensive analysis of ecosystem-relevant individual species (i.e. nitrogen, sulfur, sodium, and chloride, see section 1) is needed. The required approach should synergistically combine state-of-the-art source receptor models, wind trajectory statistical techniques, emission inventories, atmospheric reanalysis, and satellite data. This will allow a more accurate definition of the emission sources and the atmospheric circulation features driving to the

observed deposition, which is hitherto lacking.

1.2 Aims and hypotheses

Considering the knowledge gaps mentioned in the previous chapter, the main aims of this work are to gain new insights into the spatial and temporal variability of the deposition of some key nutrients into the ecosystem of the San Francisco river catchment in the South of Ecuador and to shed new light on its potential sources and its drivers.

The specific aims are:

- To analyze the deposition of nitrate, sulfate, sodium, and chloride along an altitudinal gradient with different wind exposures, given the high complexity of the terrain and related heterogeneity of precipitation and cloud water inputs.
- To locate the potential sources of nitrate, sulfate, sodium, and chloride that contribute to the observed deposition.
- To identify the atmospheric circulation and pathways as well as source emission features that led to the observed nitrate, sulfate, sodium, and chloride deposition events.

To achieve the aforementioned objectives, the following central hypotheses will be tested:

H1. Nitrate deposition is determined by **a)** the complex interaction of the site's topographic characteristics, more precisely the topographic position and terrain aspect, the elevation, the type of precipitation, and the cross-scale circulation patterns, as well as by **b)** the emission patterns of Amazon biomass-burning sources.

H2. Sulfate deposition depends on **a)** the interplay between the type of precipitation, the altitude, the relief's characteristics, i.e. topographic position and aspect, and the cross-scale circulation, and on **b)** several emission sources: anthropogenic (urban/industrial emissions) and natural local sources (volcanic degassing).

H3. As for nitrate and sulfate, the deposition of sodium and chloride along the evaluated transect relies on **a)** the topographical attributes of the measurement sites, the precipitation type, and the variability of the cross-scale circulation. Furthermore, contrary to the general current opinion of a unique Atlantic origin at the eastern Andean slopes and the Amazon, **b)** sodium and chloride at the South-Ecuadorian Andes is to a great extent provided by Pacific sources as well.

1.3 Thesis outline

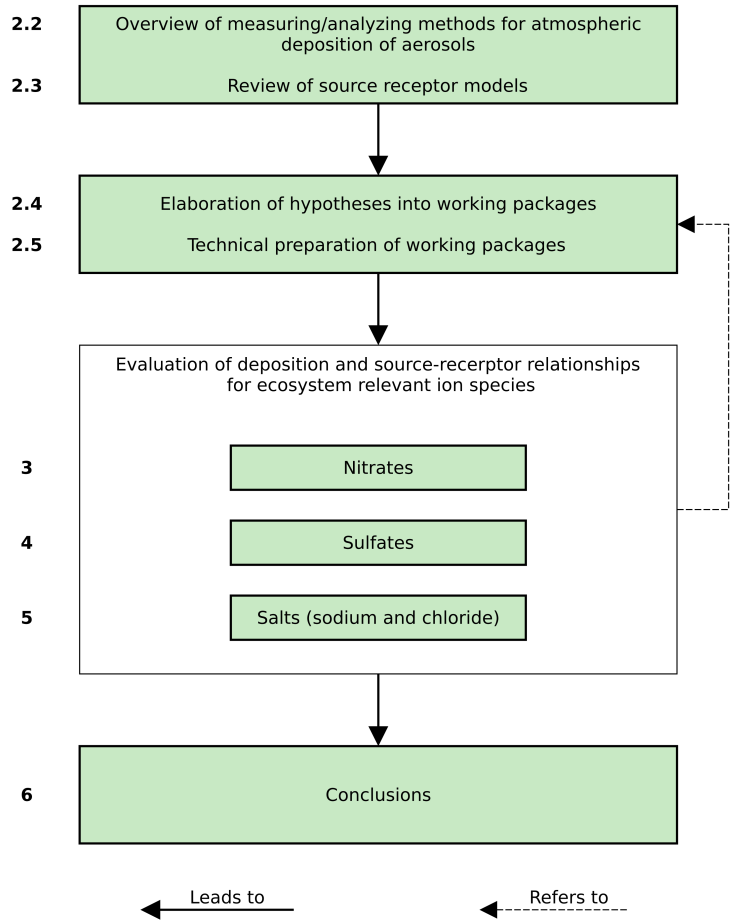

Figure 1.1: Outline of the thesis.

The structure of this work is depicted in Fig. 1.1. Following a methodological framework on the methods for analyzing the nutrient deposition in mountainous areas (section 2.2) and a review on source-receptor models (section 2.3) for the allocation of potential sources related to the observed deposition, sections 2.4 and 2.5 deal with the elaboration of ad-hoc working packages that will allow to test the defined hypotheses.

The results of this investigation have been published in recognized peer-reviewed scientific journals and are presented in Chapters 3, 4, and 5. In these publications the authors analyze the wet deposition of individual nutrient species important for the ecosystem function, namely nitrates, sulfates, and sea salt (NaCl), and its source-receptor relationships. Even though other nutrient/pollutant species were analyzed, the selection of these individual elements for the analysis responds to its relevance as limiting nutrients or pollutants of great importance for the ecosystem function of the TMF studied (see section 1). Furthermore, the study of individual nutrient/pollutant species allows for a more in-

depth analysis of the sources of these species and their relevance in the observed deposition.

Finally, chapter 6.1 summarizes the knowledge gained in chapters 3 to 5 by answering the central hypotheses drawn in section 1.2 and gives a short outlook.

Bibliography

State of world's forests, Tech. rep., Food and Agricultural Organization, Rome, 2011.

Akagi, S. K., Yokelson, R. J., Wiedinmyer, C., Alvarado, M. J., Reid, J. S., Karl, T., Crounse, J. D., and Wennberg, P. O.: Emission factors for open and domestic biomass burning for use in atmospheric models, Atmos. Chem. Phys., 11, 4039–4072, doi: 10.5194/acp-11-4039-2011, URL http://www.atmos-chem-phys.net/11/4039/2011/, 2011.

Andreae, M. O., Rosenfeld, D., Artaxo, P., Costa, A. A., Frank, G. P., Longo, K. M., and Silva-Dias, M. A. F.: Smoking rain clouds over the Amazon., Science, 303, 1337–42, doi: 10.1126/science.1092779, URL http://www.ncbi.nlm.nih.gov/pubmed/14988556, 2004.

Artaxo, P., Rizzo, L. V., Paixão, M., De Lucca, S., Oliveira, P. H., Lara, L. L., Wiedemann, K. T., Andreae, M. O., Holben, B., Schafer, J., Correia, A. L., and Pauliquevis, T. M.: Aerosol Particles in Amazonia: Their Composition, Role in the Radiation Balance, Cloud Formation, and Nutrient Cycles, in: Amazonia and global change, pp. 233–250, American Geophysical Union, doi:10.1029/2008GM000847, URL http://dx.doi.org/10.1029/2008GM000847, 2009.

Barkmann, J., Hillmann, B. M., and Marggraf, R.: The Research Unit RU 816: Overall Approach in the Light of the Ecosystem Services Concept BT - Ecosystem Services, Biodiversity and Environmental Change in a Tropical Mountain Ecosystem of South Ecuador, in: Ecosystem services, biodiversity and environmental change in a tropical mountain ecosystem of South Ecuador, edited by Bendix, J., Beck, E., Bräuning, A., Makeschin, F., Mosandl, R., Scheu, S., and Wilcke, W., pp. 41–49, Springer Berlin / Heidelberg, doi:10.1007/978-3-642-38137-9_4, URL http://dx.doi.org/10.1007/978-3-642-38137-9{_}4, 2013.

Bendix, J., Beck, E., Bräuning, A., Makeschin, F., Mosandl, R., Scheu, S., and Wilcke, W., eds.: Ecosystem services, biodiversity and environmental change in a tropical mountain ecosystem of South Ecuador, vol. 221 of *Ecological Studies*, Springer Berlin / Heidelberg, doi:10.1007/978-3-642-38137-9, URL http://link.springer.com/10.1007/978-3-642-38137-9, 2013.

Bobbink, R., Hicks, K., Galloway, J., Spranger, T., Alkemade, R., Ashmore, M., Bustamante, M., Cinderby, S., Davidson, E., Dentener, F., Emmett, B., Erisman, J. W., Fenn, M., Gilliam, F., Nordin, A., Pardo, L., and De Vries, W.: Global assessment of nitrogen deposition effects on terrestrial plant diversity: a synthesis, Ecol. Appl., 20, 30–59, doi:10.1890/08-1140.1, URL http://www.esajournals.org/doi/abs/10.1890/08-1140.1, 2010.

Boy, J. and Wilcke, W.: Tropical Andean forest derives calcium and magnesium from Saharan dust, Glob. Biogeochem. Cycles, 22, GB1027, URL http://dx.doi.org/10.1029/2007GB002960, 2008.

Boy, J., Rollenbeck, R., Valarezo, C., and Wilcke, W.: Amazonian biomass burning-derived acid and nutrient deposition in the north Andean montane forest of Ecuador, Global Biogeochem. Cycles, 22, GB4011, URL http://dx.doi.org/10.1029/2007GB003158, 2008.

Dudley, R., Kaspari, M., and Yanoviak, S. P.: Lust for salt in the western Amazon, Biotropica, 44, 6–9, doi:10.1111/j.1744-7429.2011.00818.x, URL http://doi.wiley.com/10.1111/j.1744-7429.2011.00818.x, 2012.

Fabian, P., Kohlpaintner, M., and Rollenbeck, R.: Biomass burning in the Amazon–fertilizer for the mountaineous rain forest in Ecuador, Environ. Sci. Pollut. Res., 12, 290–296, URL http://dx.doi.org/10.1065/espr2005.07.272http://www.ncbi.nlm.nih.gov/pubmed/16206723, 2005.

Fabian, P., Rollenbeck, R., Spichtinger, N., Brothers, L., Dominguez, G., and Thiemens, M.: Sahara dust, ocean spray, volcanoes, biomass burning: pathways of nutrients into Andean rainforests, Adv. Geosci., 22, 85–94, doi:10.5194/adgeo-22-85-2009, URL http://www.adv-geosci.net/22/85/2009/, 2009.

Griffith, K. T., Ponette-González, A. G., Curran, L. M., and Weathers, K. C.: Assessing the influence of topography and canopy structure on Douglas fir throughfall with LiDAR and empirical data in the Santa Cruz mountains, USA., Environ. Monit. Assess., 187, 4486, doi:10.1007/s10661-015-4486-6, URL http://www.ncbi.nlm.nih.gov/pubmed/25893759, 2015.

Harpole, W. S. and Tilman, D.: Grassland species loss resulting from reduced niche dimension., Nature, 446, 791–3, doi:10.1038/nature05684, URL http://www.ncbi.nlm.nih.gov/pubmed/17384633, 2007.

Hofhansl, F., Wanek, W., Drage, S., Huber, W., Weissenhofer, A., and Richter, A.: Topography strongly affects atmospheric deposition and canopy exchange processes in different types of wet lowland rainforest, Southwest Costa Rica, Biogeochemistry, 106, 371–396, doi:10.1007/s10533-010-9517-3, URL http://link.springer.com/10.1007/s10533-010-9517-3, 2011.

Hölscher, D.: Hydrology of natural and anthropogenically altered tropical montane rainforests with special reference to rainfall interception, in: The tropical mountain forest – patterns and processes in a biodiversity hotspot, edited by Gradstein, S. R., Homeier, J.,

and Gansert, D., vol. 2, pp. 129–136, Göttingen Centre for Biodiversity and Ecology, Göttingen, 2008.

Homeier, J., Hertel, D., Camenzind, T., Cumbicus, N. L., Maraun, M., Martinson, G. O., Poma, L. N., Rillig, M. C., Sandmann, D., Scheu, S., Veldkamp, E., Wilcke, W., Wullaert, H., and Leuschner, C.: Tropical andean forests are highly susceptible to nutrient inputs–rapid effects of experimental N and P addition to an ecuadorian montane forest., PLoS One, 7, e47 128, doi:10.1371/journal.pone.0047128, URL http://www.pubmedcentral.nih.gov/articlerender.fcgi?artid=3468540{&}tool=pmcentrez{&}rendertype=abstract, 2012.

Jarvis, A. and Mulligan, M.: The climate of cloud forests, in: Tropical montane cloud forests: science for conservation and management, edited by Bruijnzeel, L. A., Scatena, F. N., and Hamilton, L. S., pp. 3–13, Cambridge University Press, Cambridge, 2010.

Kaspari, M., Yanoviak, S. P., and Dudley, R.: On the biogeography of salt limitation: a study of ant communities., Proc. Natl. Acad. Sci. U.S.A., 105, 17 848–51, doi:10.1073/pnas.0804528105, URL http://www.pubmedcentral.nih.gov/articlerender.fcgi?artid=2584704{&}tool=pmcentrez{&}rendertype=abstract, 2008.

Kessler, M. and Kluge, J.: Diversity and endemism in tropical montane forests - from patterns to processes, in: The tropical mountain forest – patterns and processes in a biodiversity hotspot, edited by Gradstein, S. R., Homeier, J., and Gansert, D., vol. 2, pp. 35–50, Göttingen Centre for Biodiversity and Ecology, Göttingen, 2008.

Kirchner, M., Fegg, W., Römmelt, H., Leuchner, M., Ries, L., Zimmermann, R., Michalke, B., Wallasch, M., Maguhn, J., Faus-Kessler, T., and Jakobi, G.: Nitrogen deposition along differently exposed slopes in the Bavarian Alps, Sci. Total Environ., 470-471, 895–906, doi:10.1016/j.scitotenv.2013.10.036, URL http://www.sciencedirect.com/science/article/pii/S0048969713011807, 2014.

Kuylenstierna, J. C. I., Rodhe, H., Cinderby, S., and Hicks, K.: Acidification in developing countries: ecosystem sensitivity and the critical load approach on a global scale, Ambio, 30, 20–28, doi:10.1579/0044-7447-30.1.20, URL http://www.bioone.org/doi/pdf/10.1579/0044-7447-30.1.20http://dx.doi.org/10.1579/0044-7447-30.1.20, 2001.

Lee, A. T. K., Kumar, S., Brightsmith, D. J., and Marsden, S. J.: Parrot claylick distribution in South America: do patterns of "where" help answer the question "why"?, Ecography, doi:10.1111/j.1600-0587.2009.05878.x, URL http://doi.wiley.com/10.1111/j.1600-0587.2009.05878.x, 2009.

Lewis, S. L., Malhi, Y., and Phillips, O. L.: Fingerprinting the impacts of global change on tropical forests., Philos. Trans. R. Soc. Lond. B. Biol. Sci., 359, 437–62, doi:10.1098/rstb.2003.1432, URL http://www.pubmedcentral.nih.gov/articlerender.fcgi?artid=1693339{&}tool=pmcentrez{&}rendertype=abstract, 2004.

Lizcano, D. J. and Cavelier, J.: Características químicas de salados y hábitos alimenticios de la Danta de montaña (Tapirus pinchaque Roulin, 1829) en los Andes Centrales de Colombia, Mastozoología Neotrop., 11, 193–201, URL http://www.scielo.org.ar/scielo.php?script=sci{_}arttext{&}pid=S0327-93832004000200004{&}lng=es{&}nrm=iso{&}tlng=es, 2004.

Lovett, G. and Kinsman, J.: Atmospheric pollutant deposition to high-elevation ecosystems, Atmos. Environ., 24, 2767–2786, URL http://www.sciencedirect.com/science/article/pii/096016869090164I, 1990.

Matson, P., Lohse, K. A., and Hall, S. J.: The globalization of nitrogen deposition: Consequences for terrestrial ecosystems, Ambio, 31, 113–119, URL http://www.jstor.org/stable/4315223, 2002.

Phoenix, G. K., Hicks, K. W., Cinderby, S., Kuylenstierna, J. C. I., Stock, W. D., Dentener, F. J., Giller, K. E., Austin, A. T., Lefroy, R. D. B., Gimeno, B. S., Ashmore, M. R., and Ineson, P.: Atmospheric nitrogen deposition in world biodiversity hotspots: the need for a greater global perspective in assessing N deposition impacts, Glob. Chang. Biol., 12, 470–476, doi:10.1111/j.1365-2486.2006.01104.x, URL http://dx.doi.org/10.1111/j.1365-2486.2006.01104.x, 2006.

Powell, L. L., Powell, T. U., Powell, G. V. N., and Brightsmith, D. J.: Parrots take it with a grain of salt: available sodium content may drive collpa (Clay Lick) selection in southeastern Peru, Biotropica, 41, 279–282, doi:10.1111/j.1744-7429.2009.00514.x, URL http://doi.wiley.com/10.1111/j.1744-7429.2009.00514.x, 2009.

Rehmus, A., Bigalke, M., Valarezo, C., Castillo, J. M., and Wilcke, W.: Aluminum toxicity to tropical montane forest tree seedlings in southern Ecuador: response of biomass and plant morphology to elevated Al concentrations, Plant Soil, 382, 301–315, doi:10.1007/s11104-014-2110-0, URL http://link.springer.com/10.1007/s11104-014-2110-0, 2014.

Rehmus, A., Bigalke, M., Valarezo, C., Castillo, J. M., and Wilcke, W.: Aluminum toxicity to tropical montane forest tree seedlings in southern Ecuador: response of nutrient status to elevated Al concentrations, Plant Soil, 388, 87–97, doi:10.1007/s11104-014-2276-5, URL http://link.springer.com/10.1007/s11104-014-2276-5, 2015.

Rockström, J., Steffen, W., Noone, K., Persson, Å., Chapin, F. S., Lambin, E., Lenton, T. M., Scheffer, M., Folke, C., Schellnhuber, H. J., Nykvist, B., de Wit, C. A., Hughes, T., van der Leeuw, S., Rodhe, H., Sörlin, S., Snyder, P. K., Costanza, R., Svedin, U., Falkenmark, M., Karlberg, L., Corell, R. W., Fabry, V. J., Hansen, J., Walker, B., Liverman, D., Richardson, K., Crutzen, P., and Foley, J.: Planetary boundaries: exploring the safe operating space for humanity, Ecol. Soc., 14, doi: 10.1038/461472a, URL http://www.nature.com/nature/journal/v461/n7263/full/461472a.html, 2009.

Rollenbeck, R.: Global sources-local impacts: natural and anthropogenic sources of matter deposition in the Andes of Ecuador, Geo-öko, pp. 5–27, 2010.

Rollenbeck, R., Fabian, P., and Bendix, J.: Precipitation dynamics and chemical properties in tropical mountain forests of Ecuador, Adv. Geosci., 6, 73–76, doi:10.5194/adgeo-6-73-2006, URL http://www.adv-geosci.net/6/73/2006/, 2006.

Scatena, F. N., Bruijnzeel, L. A., Bubb, P., and Das, S.: Setting the stage, in: Tropical montane cloud forests: science for conservation and management, edited by Bruijnzeel, L. A., Scatena, F. N., and Hamilton, L. S., pp. 3–13, Cambridge University Press, Cambridge, 2010.

Stevens, C. J., Dise, N. B., Mountford, J. O., and Gowing, D. J.: Impact of nitrogen deposition on the species richness of grasslands., Science, 303, 1876–9, doi:10.1126/science.1094678, URL http://www.ncbi.nlm.nih.gov/pubmed/15031507, 2004.

Tanner, E. V. J., Vitousek, P. M., and Cuevas, E.: Experimental investigation of nutrient limitation of forest growth on wet tropical mountains, Ecology, 79, 10–22, doi:10.1890/0012-9658(1998)079[0010:EIONLO]2.0.CO;2, URL http://www.esajournals.org/doi/abs/10.1890/0012-9658(1998)079[0010:EIONLO]2.0.CO;2, 1998.

Tognetti, S., Aylward, B., and Bruijnzeel, L. A.: Assessment needs to support the development of arrangements for payments for ecosystem services from tropical montane cloud forests, in: Tropical montane cloud forests: science for conservation and management, edited by Bruijnzeel, L. A., Scatena, F. N., and Hamilton, L. S., pp. 671–685, Cambridge University Press, Cambridge, 2010.

Unger, M., Homeier, J., and Leuschner, C.: Effects of soil chemistry on tropical forest biomass and productivity at different elevations in the equatorial Andes, Oecologia, 170, 263–274, doi:10.1007/s00442-012-2295-y, URL http://link.springer.com/10.1007/s00442-012-2295-y, 2012.

Vet, R., Artz, R. S., Carou, S., Shaw, M., Ro, C. U., Aas, W., Baker, A., Bowersox, V. C., Dentener, F., Galy-Lacaux, C., Hou, A., Pienaar, J. J., Gillett, R., Forti, M. C., Gromov, S., Hara, H., Khodzher, T., Mahowald, N. M., Nickovic, S., Rao, P. S. P., and Reid, N. W.: A global assessment of precipitation chemistry and deposition of sulfur, nitrogen, sea salt, base cations, organic acids, acidity and pH, and phosphorus, Atmos. Environ., 93, 3–100, doi:10.1016/j.atmosenv.2013.10.060, URL `http://www.sciencedirect.com/science/article/pii/S1352231013008133`, 2014.

Vitousek, P. M.: Litterfall, nutrient cycling, and nutrient limitation in tropical forests, 65, 285–298, URL `http://www.esajournals.org/doi/abs/10.2307/1939481`, 1984.

Voigt, C. C., Capps, K. A., Dechmann, D. K. N., Michener, R. H., and Kunz, T. H.: Nutrition or detoxification: why bats visit mineral licks of the Amazonian rainforest, PLoS One, 3, e2011, doi:10.1371/journal.pone.0002011, URL `http://journals.plos.org/plosone/article?id=10.1371/journal.pone.0002011`, 2008.

Weathers, K. C., Lovett, G. M., Likens, G. E., and Lathrop, R.: The effect of landscape features on deposition to hunter mountain, Catskill Mountains, New York, Ecol. Appl., 10, 528–540, doi:10.1890/1051-0761(2000)010[0528:TEOLFO]2.0.CO;2, 2000.

Chapter 2

Conceptual design

This chapter summarizes the current state of research regarding the methodological options to investigate the atmospheric deposition of nutrients/pollutants in tropical forest ecosystems. Based on theoretical considerations, the chapter describes how the thesis is structured into different working packages to test the hypotheses. The methodological overview is divided in two main parts: field observation of the deposition (precipitation chemistry) and identification of potential sources and transport pathways (transport modelling). Thus, the first section of this chapter (2.1) presents a general description of the study area that puts this investigation into a geographical context. The second section (2.2) gives a brief overview of the most important existing sampling and analyzing methods in precipitation chemistry, as well as a short description of the methods applied in the current research. The third section (2.3) shortly reviews common methods suitable to evaluate source-receptor relationships and nutrient/pollutant transport. Section 2.3 is an important part of this investigation because a great emphasis is given to the allocation of potential sources and the drivers behind the observed deposition. After this short review, the methods applied in the current work are described. The fourth and final sections (2.4 and 2.5) of this chapter describe the design of working packages and its implementation in order to facilitate the testing of the hypotheses defined.

2.1 Study area

The research area is split into two different spatial domains. The local domain includes the TMF of the San Francisco river valley in southern Ecuador, where an atmospheric deposition survey was undertaken (Fig. 2.1a). This is surrounded by the continental domain, which covers potential nutrient/pollutant source-emission areas and allows to investigate the large scale factors causing deposition, such as atmospheric transport pathways an its seasonality (Fig. 2.1b).

The San Francisco river valley is located on the eastern declivity of the southern Andes of Ecuador, between 1800 and 3200 m a.s.l., near the western geographical margin of the Amazon forest. The topography in this part of the Andes forms the so called Huancabamba depression. The mountains here are lower and narrower than in the rest of the range (Fig. 2.1b). The natural vegetation in the valley is composed of evergreen montane forest reaching altitudes up to 2700 m a.s.l., elfin forest (2700-3100 m a.s.l.) and finally paramo in the highest parts of the mountains (above 3100 m a.s.l.) (Homeier et al. 2008). Because of its very high species diversity and high rates of deforestation, the TMF of South Ecuador is part of the list of hotspots of biodiversity (Marchese 2015; Myers et al. 2000). Especially on the south-facing slopes, the natural vegetation has been mostly replaced by grazing areas for livestock, successional forest areas and areas invaded by the bracken fern (Curatola Fernández et al. 2015; Göttlicher et al. 2009). A precipitation chemistry survey was performed at different altitudes in the valley where natural vegetation dominates (See Fig. 2.1a).

The climate of the valley is a typical tropical climate, with low seasonal but high daily variations in temperature. Precipitation rates are very high due to the effect of the constant easterly winds that carry moisture from the lowlands of the Amazon and produce heavy orographic rainfall as they meet the mountains. Precipitation varies depending on the behavior of the dominant winds and especially the tropical easterlies, but also with altitude and aspect of the relief.

The highest and most exposed parts to moist air masses have a larger volume of precipitation. The tops of the mountains are often immersed in clouds because of forced uplifting of the easterly air masses by the topography. This causes not only heavy rainfall but also a high deposition of cloud water directly onto the vegetation and soil (Bendix et al. 2006, 2008; Richter et al. 2013; Rollenbeck et al. 2011). Therefore, the precipitation varies between 1900 and 6000 mm per year between the valley and the peaks of the mountain range, where the cloud water deposition contributes to up to 35 % of the total precipitation (Rollenbeck et al. 2011). The large volume of precipitation causes leaching of nutrients resulting in a nutrient-poor and therefore infertile substrate (Wilcke et al. 2008).

The main synoptic wind systems that affect the study area are the northern easterlies (with greater intensity in February), the southern easterlies (with greater intensity in July) and the westerlies (with greater intensity between November and December) (Bendix et al. 2008; Emck 2007; Rollenbeck et al. 2011). At the local scale, the regional pressure and temperature gradients of the relief create regular winds, commonly known as mountain-valley breezes. At the daytime, the difference in temperature between the heated summits and the cooler valleys generate upward-flowing anabatic winds. During

the late afternoon and night the opposite occurs, as katabatic winds flow downslope from the upper parts of the *cordillera* to the valley bottoms (Bendix et al. 2008; Emck 2007). At night, katabatic winds along the slopes and drainage flows along the valley have been recognized as drivers involved in the formation of a mesoscale convective system (MCS) at the foothills of the *cordillera*, where local and synoptic scale systems interact (Trachte et al. 2010).

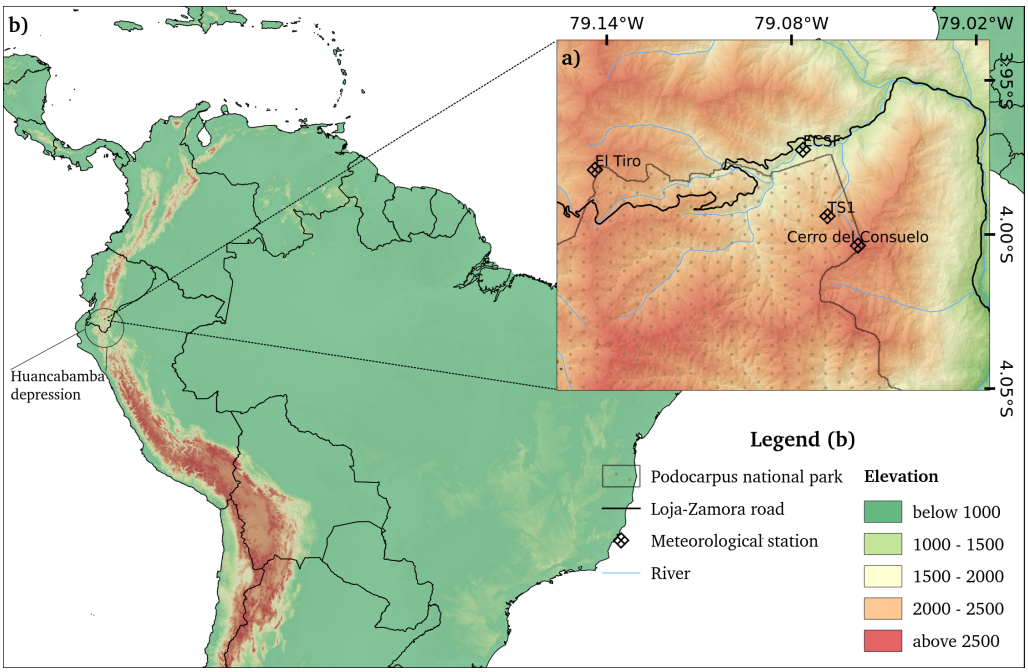

Figure 2.1: Study area map.

Local strong sources of pollution such as big industrial complexes and big urban areas do not exist in the area. The small city of Loja ($\sim$ 214 855 inhabitants) is located about 10 km towards the west (INE 2010). Land use in the vicinity of the research area is mainly dominated by small-scale farming where extensive cattle ranching is practiced (Gerique Zipfel 2011). Potential local minor pollution sources are the Loja-Zamora road (unpaved until 2008; MTO 2008), and the recurrent slash and burn practice which is used to clean and to extend the pasture-lands during the dry season, between November and December (Curatola Fernández et al. 2015; Gerique Zipfel 2011).

At the regional scale, the burning of biomass in forests, savannas and agricultural fields of the Brazilian Amazon emits a large quantity of a variety of pollutants every year between August and October (Akagi et al. 2011; Crutzen and Andreae 1990), which are transported downwind from the emission sources (Longo et al. 2009). In February, during the dry season in northern South America, big vegetated areas are also burned with large emissions into the tropical atmosphere (Hamburger et al. 2013). Large coastal cities as

e.g. Guayaquil are other sources of pollution for the area of investigation. Furthermore, Ecuador possesses a large number of active volcanoes. These can inject a large volume of gases and particles into the atmosphere impacting the regional chemical composition of the air and precipitation (Carn et al. 2008; Mahowald et al. 2008).

2.2 Overview of sampling/analyzing methods

Mountainous areas represent a challenge for atmospheric deposition experiments due to the high spatio-temporal heterogeneity of precipitation and wind systems resulting from the interaction of the atmosphere with the roughness of the terrain. In the TMF of South Ecuador, an additional factor further complicates the measurements of atmospheric deposition: the increasing contribution of cloud-fog to the total water inputs at higher altitudes, as mentioned in subsection 2.1. As a consequence, any atmospheric deposition survey in mountain areas should be designed in such a way that it accounts for this variability, e.g., by covering different altitudes and differently exposed sites.

In general, elevation and topographic characteristics of the landscape, such as slope, aspect, as well as location and height of surrounding barriers, are essential parameters in mountainous regions determining the local deposition (Griffith et al. 2015; Lovett and Kinsman 1990; Weathers et al. 2000, 2006). The contribution of cloud-fog to the water inputs and thus to the deposition is closely related to the specific elevation and topographic location. As nutrient/pollutant deposition by cloud-fog can largely contribute to the total deposition in TMFs, this should be taken into account in precipitation chemistry studies at TMFs as well. Nonetheless, until now no other precipitation chemistry studies in the tropical Andes of South America have taken into account these factors (topography and rain/cloud-fog< deposition) in their experimental design.

There are two mechanisms underlying wet deposition of nutrients/pollutants from the atmosphere to the land cover/ground in mountainous regions. These are rain scavenging and fog deposition - including both radiation fog and advective fog - (Lovett and Kinsman 1990; Schemenauer and Cereceda 1994). The relative importance of each of these mechanisms depends on the geographical conditions of the sampling sites. In tropical mountain cloud forests, the cloud-fog deposition contributes substantially to the total deposition, due to the high cloud immersion frequencies of the mountain tops (Rollenbeck et al. 2011). Thus, the deposition sampling in a tropical mountain environment should definitely incorporate cloud-fog deposition measurements. Nonetheless, given the difficulty of measuring cloud-fog only without the interference of wind-driven precipitation, many studies refer to the combination of cloud-fog and wind-driven rain, as well as light drizzle as occult precipitation (OP) (Bruijnzeel and Proctor 1995; Frumau

et al. 2011; Nyaga et al. 2015; Rollenbeck et al. 2007, 2011).

Standard sampling units for measuring wet atmospheric deposition are summarized in Amodio et al. (2014). Two different types of samplers can be used: wet-only and bulk collectors. The wet-only collector accumulates only rain-scavenged particles, while the bulk collectors are designed to account for all wet and dry particles.

For the measurement of OP deposition a large variety of devices is available. They can be grouped mainly into passive and active collectors. The passive collectors depend on the wind speed, that moves a mass of air charged with cloud particles through the collectors. In contrast, in the more complex active devices the air is mechanically forced to flow through the collector. This makes the latter manyfold more expensive, as they require an adequate infrastructure (e.g., electricity supply, good accessibility) and maintenance, all common issues in many developing countries. Furthermore, their benefits are low compared to passive samplers if the purpose is to estimate water interception by the vegetation and the soil as well as the deposition of nutrients/pollutants.

Because the use of different types of collection devices could hamper the comparison of deposition rates in different locations, Schemenauer and Cereceda (1994) proposed an inexpensive and simple standard fog collector (SFC) to be used in high-elevation regions. This device has been widely used in many studies and in different countries to study OP in mountainous areas (Cereceda et al. 2008; Molina and Escobar 2008; Schemenauer et al. 1995; Marzol et al. 2011) and to estimate the deposition to trees (Schemenauer and Cereceda 1994).

Comprehensive guides for handling and analyzing atmospheric deposition samples are given in the manual of the Global Atmosphere Watch (GAW) precipitation chemistry program `https://www.wmo.int/pages/prog/arep/gaw/precip_chem.html` of the World Meteorological Organization (WMO) and the manual for sampling and chemical analysis `http://www.nilu.no/projects/ccc/manual/index.html` from the European Monitoring and Evaluation Programme (EMEP). The summary of methods for sample handling and analysis discussed hereinafter refers to the information given in these bibliographical sources.

The principal guidelines for handling precipitation water samples for chemical analysis refer to the preservation of samples during sample collection, storage, and shipping. It is recommended that all surfaces that come in contact with the samples at all steps, from the measurements to the analysis in the laboratory, should be chemically

inert for the atmospheric constituents measured. For the precipitation and fog sample collectors, tests have shown that polyethylene, polypropylene, and Teflon are suitable materials. To avoid the contamination of the samples nothing should interfere with the water droplets falling/impacting into/onto the samplers and the samplers should also be designed to prevent splash from entering or exiting the container.

To minimize the degradation of the samples, their handling should be reduced to the minimum before laboratory for analysis. Since the arrival of the samples at the analytical laboratory can sometimes take longer than the recommended time, especially in cases of international shipping, the precipitation chemistry manuals strongly advise to keep the samples refrigerated below 4° C and in the dark until they are analyzed. These procedure reduces ammonium and nitrate losses upon arrival to the laboratory.

In order to obtain a measure of the ion concentration of the different nutrient/pollutant species in precipitation water, the major ion species in the samples have to be determined by chemical analytical methods. Different methods can be used depending on the ion species. A very common method in most precipitation chemistry studies is ion chromatography. This technique can be applied to almost all major cations and anions found in precipitation samples. However, for some species like sodium, potassium, magnesium, and calcium more accurate results are yielded using mass spectrometry methods as e.g. ICP-MS.

In the light of state-of-research on precipitation chemistry and deposition in mountain sites, the effect of elevation on the deposition as well as the difference in exposure (topographic location) and the inputs by OP have are taken into account in this investigation. Bulk totalizers are selected for rain sampling because, as already explained, the dense vegetation and wet environment in the study area are unfavorable conditions for turbulent generation and transport of local aerosols, which means that the contribution of dry particulate to the total deposition might be neglected. For OP water, the sampling is done by cost-effective SFC that have delivered good results in other mountainous areas. The samples from the four meteorological stations (MSs) are handled following the recommendations of the GAW precipitation chemistry and EMEP programms and analyzed for ion concentrations in the TUM-WZW (Technische Universität München - Wissenschaftszentrum Weihenstephan). For details on rain and OP water measurements, the readers should refer to Fabian et al. (2005) and Rollenbeck et al. (2007, 2011).

2.3 Methods for assessing source-receptor relationships

There are several methods to unveil the relationship between nutrient/pollutant sources and its receptors. The majority of them are based on wind trajectories, which are computed from the wind fields included in atmospheric reanalysis data. By concatenating the wind fields forward or backward in time from one starting position, the air mass pathways can be reconstructed. Given that the chemical composition of an air parcel is inherently associated to its passage through the atmosphere, the pathway reconstruction by wind trajectories is adequate to investigate the connections between emissions, transport, and in situ deposition measurements.

According to a recent review by Fleming et al. (2012), three main types of models are appropriate for analyzing source-receptor relationships: trajectory models, dispersion models, and chemistry transport models. The complexity increases from the first to the last in this list, but the accuracy of the results is not always improved because of their specific drawbacks, as indicated by the authors. Compared to the other two approaches, chemistry transport models are based on many more assumptions (emission inventories and physics and chemistry schemes). Thus, each assumption includes specific uncertainties which in combination can lead to biases in the results (Fleming et al. 2012). The chemical dispersion models represent an intermediate option in which more complexity is gained without incurring relevant biases. As stated by the review's authors, the main improvement of these models is that they reproduce turbulent air flow with higher accuracies, offering a more realistic representation of transport in the atmospheric boundary layer. For the purpose of this study, however, this improvement does not have real advantages as compared to trajectory models. Local relief features in areas of very complex terrain are not taken into account by the coarse underlying meteorological datasets; hence, the meso-scale turbulence features cannot be correctly simulated by the dispersion analysis tools only, if not coupled with meso-scale climate models (Brioude et al. 2012; Hernández-Ceballos et al. 2014). Consequently, source-receptor trajectory techniques have been used in this study, which are shortly described in the next paragraphs. For more detail on the different methods for assessing the interface between sources and receptors the reader is referred to Fleming et al. (2012).

Following previous work on source attribution of observed deposition in the FOR 816 project in southern Ecuador (Fabian et al. 2005, 2009; Rollenbeck 2010), and in cases when emission inventories are available, this work adapts and uses a trajectory-emission integration tool - Emisstraject - implemented in Visual Basic and developed by Rütger Rollenbeck (Rollenbeck 2010) in the Laboratory for Climatology and Remote Sensing (LCRS) at the

University
constituents from upwind emission sources to the receptor area. The modelling scheme combines 10 days Flexible Trajectory model (FLEXTRA, Stohl et al. 1995) backward wind trajectories with gridded emission/concentration from inventory and satellite data. During the execution, the path of the trajectories are followed; all emission values of the respective data set where temporal and spatial coincidence between air mass passage and emissions exist, are integrated until the receptor site. A buffer of 25 km radius from the trajectory point was applied to account for inaccuracies related to the resolution of the underlying European Centre for Medium-range Weather Forecasts (ECMWF) global reanalysis data set. After each run, the sum of the emissions integrated along the back-trajectories yields an estimate of the final concentration at the receptor site produced by atmospheric transport.

To account for in-cloud and below-cloud scavenging in the atmosphere, a decay function was implemented into the algorithm:

$$\mathrm{C}_t = \frac{\mathrm{C}_0}{\mathrm{e}^{\frac{t}{k}}} \tag{2.1}$$

where C_t is the concentration at time t in days, C_0 is the initial concentration value at the emission point, and k is the mean lifetime constant in days.

In those cases where no emission inventories for the analyzed atmospheric constituents are available, hybrid source-receptor models are used which do not require emission information. Nevertheless, because this modelling approach needs high temporal resolution concentration data, which is not the case of that measured on the ground, reanalysis data was used as proxy of the concentration at the receptor site. The models are based on the "residence time analysis", a technique to classify air mass pathways to find the geographical sectors that mostly influence the highest species concentration observed at the receptor site. It relies on the idea that air parcels rapidly overflying polluted areas have less time to accumulate pollutants than those that spend longer times over these regions.

The two commonly used state-of-the-art models are the potential source contribution function (PSCF) and the concentration field (CF) or concentration weighted trajectory (CWT). Both rely on wind back-trajectories of air masses that were generated with the hybrid single particle lagrangian integrated trajectory model (HYSPLIT) (Draxler and Hess 1998) from reanalysis wind fields. The PSCF (Ashbaugh 1983; Zeng and Hopke 1989) overlays grid cells over specific regions of interest and calculates a probability function for each grid cell, representing the probability of an air parcel reaching the receptor site to

cause high concentrations of a given constituent at its arrival. The function is defined by:

$$\text{PSCF}_{ij} = \frac{m_{ij}}{n_{ij}}, \tag{2.2}$$

where n_{ij} is the number of trajectory points that passed through cell (i, j) and m_{ij} is the number of times that trajectory points passing through the cell (i, j) are associated to high concentration values given by a defined threshold at the air mass arrival time to the receptor site.

The CF or CWT model builds upon a grid domain over which a grid-wise logarithmic mean concentration of a nutrient or pollutant is calculated (Seibert et al. 1994). The function is defined by the following formula:

$$\ln\left(\overline{C}_{ij}\right) = \frac{1}{\sum_{k=1}^{N} t_{ij}} \sum_{k=1}^{N} \ln\left(\overline{C}_{k}\right) t_{ijk}, \tag{2.3}$$

where i and j are the grid indexes, k the trajectory index, N the total number of trajectories, $\overline{C}_k$ the pollutant concentration measured upon arrival of trajectory k, and t_{ijk} the residence time of trajectory k in grid cell (i, j). A weighted concentration is then assigned to each pixel in the grid, which represents the average of the observed concentration at the measurement site which have related trajectories passing over the respective cell. In this technique, contrary to the PSCF, the time spent in each grid cell by a trajectory is weighted by the concentration at the receptor point.

2.4 Design of hypotheses into working packages

To achieve the aims defined in section 1.2 a methodological workflow is needed to test the defined hypotheses. This methodological workflow is organized into working packages with specific aims that elaborate from the hypotheses. Figure 2.2 gives an overview of the conceptual design of this work and the interrelationships between hypotheses and working packages.

Three specific aims have been set: (1) to assess the role of topography in the deposition of nitrate, sulfate, sodium, and chloride aerosols and its variability, (2) to identify potential sources for the evaluated nutrients/pollutants, and (3) to explain the possible drivers leading to the observed deposition. To achieve these, the hypotheses in section 1.2 need to be evaluated. For this, a two-step approach is developed: first, a precipitation chemistry experiment adequate for areas with complex terrain is needed to address the role of topography in the deposition; second, the observed deposition must

be traced back in time by wind trajectory modelling to identify potential sources of the observed deposition and to identify the drivers behind the observed deposition at the receptor site.

Regarding the first methodological step, some specificities need to be considered regarding the sampling design. As Lovett and Kinsman (1990) and Weathers et al. (2000) have already stressed for mountainous areas, the sampling stations should be installed at different altitudinal levels which, if possible, span the whole altitudinal gradient of the study site. Additionally, the different topography aspects should be taken into account. Furthermore, samples must be collected not only from rain but also from OP, given the rising importance of the latter type of precipitation in the total water deposition with increasing elevation (Bendix et al. 2008; Rollenbeck et al. 2011). OP water involves all kinds of light precipitation, from wind-driven drizzle down to fog and cloud droplets (Rollenbeck et al. 2007, 2011). All the samples must be analyzed for the major ion concentrations by appropriate chemical analytical techniques such as ion chromatography and mass spectrometry.

In the second methodological step the contribution of sources and transport pathways need to be tested. To do this it is first necessary to locate the sources by back-trajectory statistical and modelling techniques. These techniques allow to determine the transport pathways and the potential sources in order to associate them with the observed deposition at the receptor site. For this purpose, first back-trajectories need to be calculated and therefore correctly parameterized prior to calculation. These encompass, for instance, the length in time of the trajectories and their temporal resolution. It has to be considered that the longer the trajectories are, the larger the uncertainty. The temporal resolution depends on the meteorological data chosen for running the trajectory model. The ECMWF reanalysis 40 (ERA 40) and ECMWF reanalysis Interim (ERA Interim) meteorological data have a maximal temporal resolution of 6 hours and a spatial resolution of $2.5°$ and $0.7°$, respectively. Many models offer higher temporal and spatial resolution by interpolating the values in the default data set. The selection of the optimal temporal resolution of the trajectories will, however, depend more on that of the deposition measurements and/or the emission data sets that will be used for further analysis.

To evaluate the hypotheses, the methodological steps mentioned are translated into the following working packages:

WP1 Analysis of the atmospheric deposition of nitrate along an altitudinal gradient and attribution of its potential sources by a source-receptor modelling approach that includes source-emission information.

WP2 Analysis of the atmospheric deposition of sulfate at two elevated sites and attribution of its potential sources by a source-receptor modelling approach that includes source-emission information.

WP3 Analysis of the atmospheric deposition of sodium and chloride along an altitudinal gradient and attribution of its potential sources by a source-receptor modelling approach not including source-emission information and back-trajectory statistical methods.

2.5 Technical preparation of working packages

In the previous chapter the defined hypotheses have been elaborated into three working packages. This chapter is dedicated to its technical implementation and application.

WP 1 Atmospheric nitrate deposition can strongly vary across rugged terrain areas, so this complexity has to be taken into account in such places prior to the sampling and analysis. This work uses the operating MSs at the study area to consider the likely impact of topography in the deposition. Here, an experimental sampling design was set up which fulfills this need of representing different topographical features and elevation layers in a heterogeneous terrain configuration. Three MSs are installed following an altitudinal gradient in the core investigation area in the San Francisco river catchment, the Reserva Biológica San Francisco (RBSF). A fourth MS is located on a mountain pass around four kilometers upriver in the direction of the city of Loja (see Fig. 2.1). All these MSs are equipped with conventional rain samplers and fog collectors, wind speed, and direction instruments.

From all four MSs, rain and OP samples, as well as precipitation and wind data are collected weekly. At least 100 ml of collected water from each sampler are put into a polyethylene bottle and labeled accordingly. The samples are stored frozen at the Estación Científica San Francisco (ECSF) until shipped to Germany. The shipment takes place every three months.

The samples are analyzed for pH, (Methron 73065/682), conductivity (WTW-LF 90) and nitrate ion concentrations at TUM-WZW. The concentration of nitrate is determined by ion chromatography (Dionex DX-210). The measurements are repeated whenever unlikely values are yielded.

The analysis of weekly nitrate concentration values from each MS is done to gain information on the concentration of nitrate ions in rain and OP water collected at different

elevations and topographic locations, which is necessary to subsequently evaluate the impact of topography on the deposition. Thus, to test the topographic effect on the deposition, the nitrate concentration data is compiled in time-series for each MS and the statistical distributions are compared. Being wind an important driving factor of the deposition, wind data from each MS is analyzed to evaluate the presence of different wind systems along the altitudinal gradient. Since OP highly contributes to the water inputs and is driven by wind, if different wind systems are present, heterogeneous chemical compositions in sampled water are to be expected.

To simulate the air mass pathways of the air masses reaching the study area, back-trajectories are calculated over a period from 2005-2009 starting at the receptor site, the San Francisco river valley, located at 4°00 S and 79°00 W. To trace-back nitrate depositions FLEXTRA back-trajectories were calculated based on ERA 40 reanalysis data (Stohl et al. 1995). The length of the trajectories was 10 days back in time. This value is assumed as being the maximal length for which trajectories can be calculated without incurring into relevant inaccuracies (Andreas Stohl, personal communication). The FLEXTRA model was used with the Emisstraject source-receptor model described in section 2.3. Source receptor models are build upon back-trajectories and intend to unravel the relationship between the observed nitrate deposition and the emission sources, that is the allocation of the sources responsible for the observed deposition. The Emisstraject model accounts for the source emissions by incorporating emission inventories (Global Fire Emission Database – GFED – NO_x emissions and the South American Regional Emission Inventory – SA-INV – NO_x emissions) and satellite data (Scanning Imaging Absorption Spectrometer for Atmospheric Chartography – SCIAMACHY – NO_2 concentration) to model the transport of nitrogen precursors to the receptor site. Emission inventories and satellite data need to be preprocessed and the Emisstraject's algorithm adapted to the new data sets prior to execution of the model. The link between the modeled concentration by Emisstraject and the observed concentration is done by cross-correlation analysis and time-series interpretation, which enables to evaluate the contribution of the analyzed sources and the transport pathways.

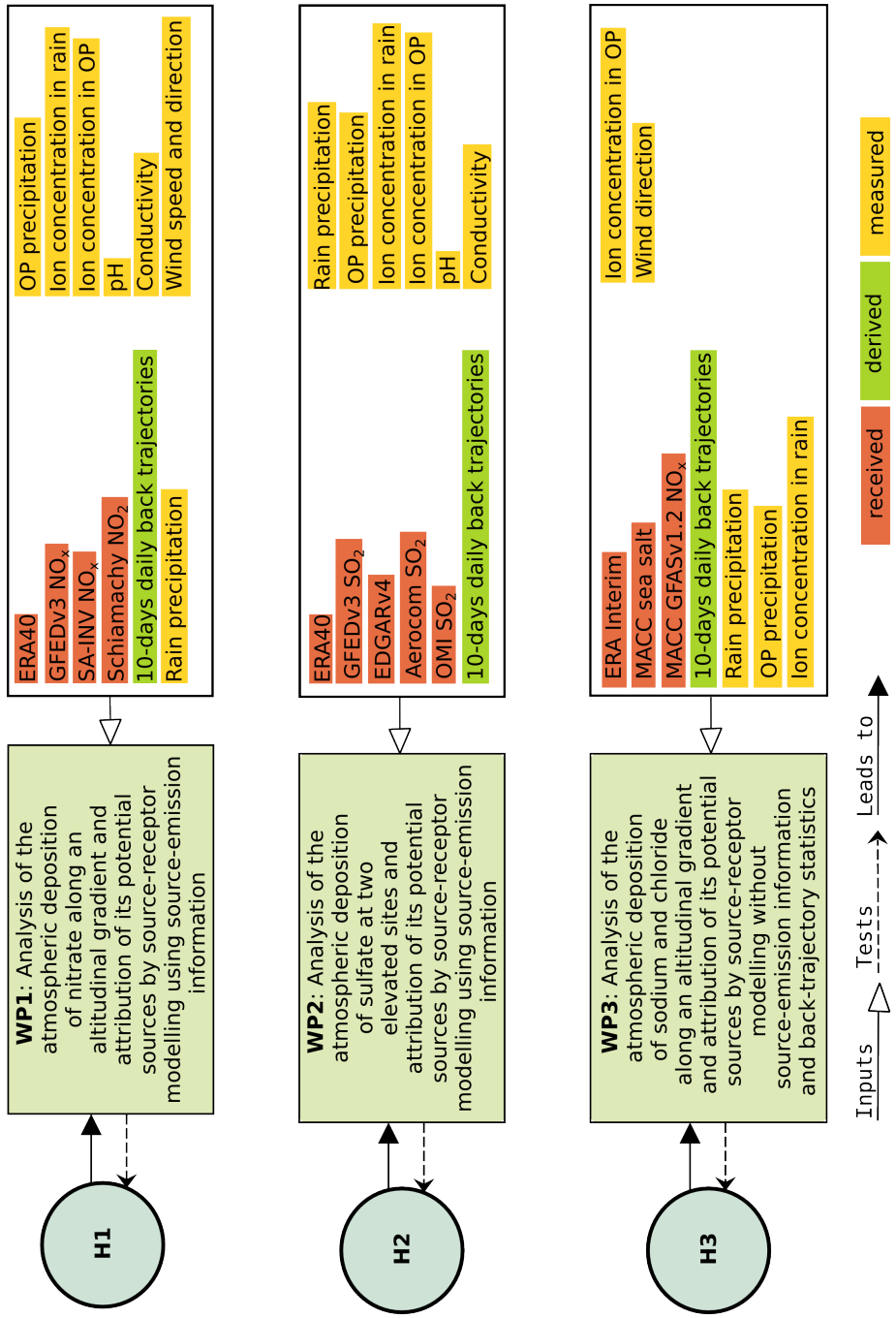

Figure 2.2: Conceptual workflow from WP1 to WP3.

WP2 In order to analyze the deposition of sulfate the same experimental sampling setup and procedure as in **WP1** is used. To test the link between sulfate concentration and the acidifying effect in the ecosystem, pH (Methron 73065/682) and conductivity (WTW-LF 90) are measured in rain and OP water samples. The concentration of sulfate ions was measured in rain and OP samples by ion chromatography technique (Dionex DX-210) at the TUM-WZW. The measurements are reiterated whenever unlikely values are returned. Wind data from MSs at different elevations are evaluated in **WP1** and are therefore not analyzed in **WP2**.

Once again ERA 40 reanalysis wind fields are used for air-mass pathway reconstruction to derive 10-days daily FLEXTRA back-trajectories for the period between 2005 and 2009. The Emisstraject model is used to disentangle the relationship between sulfate deposition at the receptor site and its potential emission sources. For this purpose, three emission inventories and one satellite product are integrated into Emisstraject's modelling scheme: SO_2 biomass burning emissions from the GFED inventory, SO_2 urban emissions from the Emissions Database for Global Atmospheric Research (EDGAR), SO_2 volcanic emissions from the Aerosol Comparisons Between Observations and Models (AeroCom) emissions inventory, and SO_2 concentration in the atmosphere from the Ozone Monitoring Instrument (OMI) on board the Aura satellite. Emisstraject returns estimated SO_2 concentration time-series at the receptor site which can be statistically compared to the observed sulfate concentration at MSs in the research area.

WP3 The topic of the third working package is the analysis of sodium and chloride deposition and related source-receptor dynamics at the research area in South Ecuador. The same experimental setup as in **WP1** and **WP2** is used here to characterize the deposition of sodium and chloride in four MSs covering an altitudinal gradient of 1220 m. The volume of rain and OP was measured in week intervals at all MSs and samples taken for further analysis of ion concentration. The concentration of sodium ions is measured by the inductively coupled plasma method (Perkin Elmer Optima 3000) and ion chromatography (Dionex DX-210) is used to assess the concentration of chloride ions.

HYSPLIT trajectories are calculated directly from ERA Interim reanalysis data within the R software (R Core Team 2015) using the Openair package (Carslaw and Ropkins 2012). This package incorporates a set of functions to statistically post-process trajectories and analyze source-receptor relationships. For sodium and chloride no adequate emission inventories are available. Therefore, two other source-receptor modelling approaches are chosen within Openair that do not require emission information. These approaches use the concentration at the receptor to look back in time which trajectory pixels have the highest probability of being responsible for those concentrations. The results are maps representing

the potential source areas of the investigated atmospheric constituents. One issue related to these models is that a relatively high temporal resolution of the concentration data is needed, which is not the case of the ground measured data from the MSs used. Thus, it is necessary to introduce proxies of the measured concentrations that fulfill the requirements of the model. For sea-salt, MACC reanalysis sea-salt concentration with a daily temporal resolution is used as a proxy for Na^+ and Cl^- measured concentrations.

Given the specific proxy available for sea-salt, the direct output of the source-receptor models is used here to link field observations to the potential emission sources. Additionally, cluster analysis is applied to identify general pathways relevant in estimating the contribution of the sources to the measured concentration.

Bibliography

Informe del examen especial de ingeniería y control ambiental a los proyectos viales emergentes a cargo del Ministerio de Transporte y Obras Públicas y el Cuerpo de Ingenieros del Ejército, Tech. rep., Ministerio de transporte y obras públicas (MTO), Quito, Ecuador, 2008.

Resultados del censo de población y vivienda, Tech. rep., Instituto Nacional de Estadística y Censos (INEC), URL http://www.ecuadorencifras.gob.ec/wp-content/descargas/Manu-lateral/Resultados-provinciales/, 2010.

Akagi, S. K., Yokelson, R. J., Wiedinmyer, C., Alvarado, M. J., Reid, J. S., Karl, T., Crounse, J. D., and Wennberg, P. O.: Emission factors for open and domestic biomass burning for use in atmospheric models, Atmos. Chem. Phys., 11, 4039–4072, doi:10.5194/acp-11-4039-2011, URL http://www.atmos-chem-phys.net/11/4039/2011/, 2011.

Amodio, M., Catino, S., Dambruoso, P. R., De Gennaro, G., Di Gilio, A., Giungato, P., Laiola, E., Marzocca, A., Mazzone, A., Sardaro, A., and Tutino, M.: Atmospheric deposition: sampling procedures, analytical methods, and main recent findings from the scientific literature, Adv. Meteorol., 2014, doi:10.1155/2014/161730, 2014.

Ashbaugh, L. L.: A statistical trajectory technique for determining air pollution source regions, J. Air Pollut. Control Assoc., 33, 1096–1098, doi:10.1080/00022470.1983.10465702, URL http://www.tandfonline.com/doi/abs/10.1080/00022470.1983.10465702, 1983.

Bendix, J., Rollenbeck, R., and Reudenbach, C.: Diurnal patterns of rainfall in a tropical Andean valley of southern Ecuador as seen by a vertically pointing K-band Doppler radar, Int. J. Climatol., 26, 829–846, doi:10.1002/joc.1267, URL http://onlinelibrary.wiley.com/doi/10.1002/joc.1267/fullhttp://doi.wiley.com/10.1002/joc.1267, 2006.

Bendix, J., Rollenbeck, R., Richter, M., Fabian, P., and Emck, P.: Climate, in: Gradients in a tropical mountain ecosystem of Ecuador, edited by Beck, E., Bendix, J., Kottke, I., Makeschin, F., and Mosandl, R., chap. 1, pp. 63–74, Springer Berlin / Heidelberg, ecological edn., URL http://dx.doi.org/10.1007/978-3-540-73526-7{\protect\T1\textbraceleft}{_}{\protect\T1\textbraceright}8, 2008.

Brioude, J., Angevine, W. M., McKeen, S. A., and Hsie, E.-Y.: Numerical uncertainty at mesoscale in a Lagrangian model in complex terrain, Geosci. Model Dev., 5, 1127–1136,

doi:10.5194/gmd-5-1127-2012, URL http://www.geosci-model-dev.net/5/1127/2012/, 2012.

Bruijnzeel, L. A. and Proctor, J.: Hydrology and biogeochemistry of tropical montane cloud forests: what do we really know?, in: Tropical montane cloud forests, pp. 38–78, Springer US, doi:10.1007/978-1-4612-2500-3_3, URL http://dx.doi.org/10.1007/978-1-4612-2500-3{_}3$\delimiter"026E30F$nhttp://link.springer.com/10.1007/978-1-4612-2500-3{_}3, 1995.

Carn, S. A., Krueger, A. J., Arellano, S., Krotkov, N. A., and Yang, K.: Daily monitoring of Ecuadorian volcanic degassing from space, J. Volcanol. Geotherm. Res., 176, 141–150, doi:DOI:10.1016/j.jvolgeores.2008.01.029, URL http://www.sciencedirect.com/science/article/B6VCS-4S0205V-1/2/2fe6d1fb29c1168746aed55392f8981a, 2008.

Carslaw, D. C. and Ropkins, K.: Openair - An R package for air quality data analysis, Environ. Model. Softw., 27-28, 52–61, doi:10.1016/j.envsoft.2011.09.008, URL http://linkinghub.elsevier.com/retrieve/pii/S1364815211002064, 2012.

Cereceda, P., Larrain, H., Osses, P., Farías, M., and Egaña, I.: The spatial and temporal variability of fog and its relation to fog oases in the Atacama Desert, Chile, Atmos. Res., 87, 312–323, doi:10.1016/j.atmosres.2007.11.012, 2008.

Crutzen, P. J. and Andreae, M. O.: Biomass burning in the tropics: impact on atmospheric chemistry and biogeochemical cycles., Science, 250, 1669–78, doi:10.1126/science.250.4988.1669, URL http://www.ncbi.nlm.nih.gov/pubmed/17734705, 1990.

Curatola Fernández, G., Obermeier, W., Gerique, A., López Sandoval, M. F., Lehnert, L. W., Thies, B., and Bendix, J.: Land Cover Change in the Andes of Southern Ecuador - Patterns and Drivers, Remote Sens., 7, 2509–2542, doi:10.3390/rs70302509, URL http://www.mdpi.com/2072-4292/7/3/2509/, 2015.

Draxler, R. and Hess, G.: An overview of the HYSPLIT_4 modeling system of trajectories, dispersion, and deposition, Aust. Meteorol. Mag., 47, 295–308, 1998.

Emck, P.: A climatology of South Ecuador, Phd thesis, Fachbereich Geographie der Friedrich-Alexander-Universität Erlangen-Nürnberg, Germany, URL http://www.opus.ub.uni-erlangen.de/opus/volltexte/2007/656/, 2007.

Fabian, P., Kohlpaintner, M., and Rollenbeck, R.: Biomass burning in the Amazon–fertilizer for the mountaineous rain forest in Ecuador, Environ. Sci. Pollut. Res., 12,

290–296, URL http://dx.doi.org/10.1065/espr2005.07.272http://www.ncbi.nlm.nih.gov/pubmed/16206723, 2005.

Fabian, P., Rollenbeck, R., Spichtinger, N., Brothers, L., Dominguez, G., and Thiemens, M.: Sahara dust, ocean spray, volcanoes, biomass burning: pathways of nutrients into Andean rainforests, Adv. Geosci., 22, 85–94, doi:10.5194/adgeo-22-85-2009, URL http://www.adv-geosci.net/22/85/2009/, 2009.

Fleming, Z. L., Monks, P. S., and Manning, A. J.: Review: untangling the influence of air-mass history in interpreting observed atmospheric composition, Atmos. Res., 104-105, 1–39, doi:10.1016/j.atmosres.2011.09.009, URL http://linkinghub.elsevier.com/retrieve/pii/S0169809511002948, 2012.

Frumau, K. F. A., Burkard, R., Schmid, S., Bruijnzeel, L. A. S., Tobón, C., and Calvo-Alvarado, J. C.: A comparison of the performance of three types of passive fog gauges under conditions of wind-driven fog and precipitation, Hydrol. Process., 25, 374–383, doi:10.1002/hyp.7884, URL http://doi.wiley.com/10.1002/hyp.7884, 2011.

Gerique Zipfel, A.: Biodiversity as a resource: plant use and land use among the Shuar, Saraguros, and Mestizos in tropical rainforest areas of southern Ecuador, Phd thesis, Fachbereich Geographie der Friedrich-Alexander-Universität Erlangen-Nürnberg, Germany, URL https://opus4.kobv.de/opus4-fau/frontdoor/index/index/docId/1860, 2011.

Göttlicher, D., Obregón, A., Homeier, J., Rollenbeck, R., Nauss, T., and Bendix, J.: Land-cover classification in the Andes of southern Ecuador using Landsat ETM+ data as a basis for SVAT modelling, Int. J. Remote Sens., 30, 1867–1886, doi:10.1080/01431160802541531, URL http://www.tandfonline.com/doi/abs/10.1080/01431160802541531, 2009.

Griffith, K. T., Ponette-González, A. G., Curran, L. M., and Weathers, K. C.: Assessing the influence of topography and canopy structure on Douglas fir throughfall with LiDAR and empirical data in the Santa Cruz mountains, USA., Environ. Monit. Assess., 187, 4486, doi:10.1007/s10661-015-4486-6, URL http://www.ncbi.nlm.nih.gov/pubmed/25893759, 2015.

Hamburger, T., Matisāns, M., Tunved, P., Ström, J., Calderon, S., Hoffmann, P., Hochschild, G., Gross, J., Schmeissner, T., Wiedensohler, A., and Krejci, R.: Long-term in situ observations of biomass burning aerosol at a high altitude station in Venezuela – sources, impacts and interannual variability, Atmos. Chem. Phys., 13, 9837–9853, doi:10.5194/acp-13-9837-2013, URL http://www.atmos-chem-phys.net/13/9837/2013/, 2013.

Hernández-Ceballos, M. A., Skjøth, C. A., García-Mozo, H., Bolívar, J. P., and Galán, C.: Improvement in the accuracy of back trajectories using WRF to identify pollen sources in southern Iberian Peninsula., Int. J. Biometeorol., 58, 2031–43, doi:10.1007/s00484-014-0804-x, URL http://link.springer.com/10.1007/s00484-014-0804-x, 2014.

Homeier, J., Werner, F. A., Gradstein, S. R., Breckle, S. W., and Richter, M.: Potential Vegetation and Floristic Composition of Andean Forests in South Ecuador, with a Focus on the RBSF, in: Gradients in a tropical mountain ecosystem of Ecuador, edited by Beck, E., Bendix, J., Kottke, I., Makeschin, F., and Mosandl, R., chap. Flora and, pp. 87–100, Springer Berlin / Heidelberg, doi:10.1007/978-3-540-73526-7, URL http://link.springer.com/chapter/10.1007/978-3-540-73526-7{_}10, 2008.

Longo, K., Freitas, S., Andreae, M., Yokelson, R., and Artaxo, P.: Biomass burning in Amazonia: emissions, long-range transport of smoke and its regional and remote impacts, in: Amaz. Glob. Chang., edited by Keller, M., Bustamante, M., Gash, J., and Silva Dias, P., chap. Section II, pp. 207–232, American Geophysical Union, Washington, D. C., doi:10.1029/GM186, URL http://www.agu.org/books/gm/v186/, 2009.

Lovett, G. and Kinsman, J.: Atmospheric pollutant deposition to high-elevation ecosystems, Atmos. Environ., 24, 2767–2786, URL http://www.sciencedirect.com/science/article/pii/096016869090164I, 1990.

Mahowald, N., Jickells, T. D., Baker, A. R., Artaxo, P., Benitez-Nelson, C. R., Bergametti, G., Bond, T. C., Chen, Y., Cohen, D. D., Herut, B., Kubilay, N., Losno, R., Luo, C., Maenhaut, W., McGee, K. A., Okin, G. S., Siefert, R. L., and Tsukuda, S.: Global distribution of atmospheric phosphorus sources, concentrations and deposition rates, and anthropogenic impacts, Global Biogeochem. Cycles, 22, n/a–n/a, doi:10.1029/2008GB003240, URL http://doi.wiley.com/10.1029/2008GB003240, 2008.

Marchese, C.: Biodiversity hotspots: a shortcut for a more complicated concept, Glob. Ecol. Conserv., 3, 297–309, doi:10.1016/j.gecco.2014.12.008, URL http://www.sciencedirect.com/science/article/pii/S235198941400095X, 2015.

Marzol, M. V., Sanchez, J. L., and Yanes, A.: Meteorological patterns and fog water collection in Morocco and the Canary Islands, Erdkunde, 65, 291–303, doi:10.3112/erdkunde.2011.03.06, URL http://www.erdkunde.uni-bonn.de/archive/2011/meteorological-patterns-and-fog-water-collection-in-morocco-and-the-canary-islands, 2011.

Molina, J. M. and Escobar, C. M.: Fog collection variability in the Andean mountain range of southern Colombia, Erde, 139, 127–140, 2008.

Myers, N., Mittermeier, R. A., Mittermeier, C. G., da Fonseca, G. A. B., and Kent, J.: Biodiversity hotspots for conservation priorities, Nature, 403, 853–858, doi:10.1038/35002501, URL http://www.ncbi.nlm.nih.gov/pubmed/10706275$\delimiter"026E30F$nhttp://www.nature.com/doifinder/10.1038/35002501, 2000.

Nyaga, J. M., Neff, J. C., and Cramer, M. D.: The contribution of occult precipitation to nutrient deposition on the west coast of South Africa, PLoS One, 10, 1–21, doi:10.1371/journal.pone.0126225, 2015.

R Core Team: R: A Language and Environment for Statistical Computing, R Foundation for Statistical Computing, Vienna, Austria, URL https://www.r-project.org, 2015.

Richter, M., Beck, E., Rollenbeck, R., and Bendix, J.: The study area, in: Ecosystem services, biodiversity and environmental change in a tropical mountain ecosystem of South Ecuador, edited by Bendix, J., Beck, E., Brauning, A., Makeschin, F., Mosandl, R., Scheu, S., and Wilcke, W., chap. 1, Springer Berlin / Heidelberg, Berlin, Germany, doi:10.1007/978-3-642-38137-9_1, URL http://link.springer.com/chapter/10.1007/978-3-642-38137-9{_}1, 2013.

Rollenbeck, R.: Global sources-local impacts: natural and anthropogenic sources of matter deposition in the Andes of Ecuador, Geo-öko, pp. 5–27, 2010.

Rollenbeck, R., Bendix, J., Fabian, P., Boy, J., Wilcke, W., Dalitz, H., Oesker, M., and Emck, P.: Comparison of different techniques for the measurement of precipitation in tropical montane rain forest regions, J. Atmos. Ocean. Technol., 24, 156–168, doi:10.1175/JTECH1970.1, URL http://journals.ametsoc.org/doi/abs/10.1175/JTECH1970.1, 2007.

Rollenbeck, R., Bendix, J., and Fabian, P.: Spatial and temporal dynamics of atmospheric water inputs in tropical mountain forests of South Ecuador, Hydrol. Process., 25, 344–352, doi:10.1002/hyp.7799, URL http://doi.wiley.com/10.1002/hyp.7799, 2011.

Schemenauer, R., Banic, C., and Urquizo, N.: High elevation fog and precipitation chemistry in southern Quebec, Canada, Atmos. Environ., 29, 2235–2252, URL http://www.sciencedirect.com/science/article/pii/135223109500153P, 1995.

Schemenauer, R. S. and Cereceda, P.: A proposed standard fog collector for use in high-elevation regions, J. Appl. Meteorol., 33, 1313–1322, URL http://adsabs.harvard.edu/abs/1994JApMe..33.1313S, 1994.

Seibert, P., Kromb-Kolb, H., Baltensperger, U., Jost, D., and Schwikowski, M.: Trajectory analysis of high-alpine air pollution data, in: NATO challenges Mod. Soc., edited by Gryning, S.-E. and Millán, M. M., pp. 595–596, Springer US, doi:10.1007/978-1-4615-1817-4_65, URL http://link.springer.com/chapter/10.1007/978-1-4615-1817-4{_}65, 1994.

Stohl, A., Wotawa, G., Seibert, P., and Kromp-Kolb, H.: Interpolation errors in wind fields as a function of spatial and temporal resolution and their impact on different types of kinematic trajectories, doi:10.1175/1520-0450(1995)034<2149:IEIWFA>2.0.CO;2, 1995.

Trachte, K., Rollenbeck, R., and Bendix, J.: Nocturnal convective cloud formation under clear-sky conditions at the eastern Andes of south Ecuador, J. Geophys. Res. Atmos., 115, D24 203, doi:10.1029/2010JD014146, URL http://doi.wiley.com/10.1029/2010JD014146, 2010.

Weathers, K. C., Lovett, G. M., Likens, G. E., and Lathrop, R.: The effect of landscape features on deposition to hunter mountain, Catskill Mountains, New York, Ecol. Appl., 10, 528–540, doi:10.1890/1051-0761(2000)010[0528:TEOLFO]2.0.CO;2, 2000.

Weathers, K. C., Simkin, S. M., Lovett, G. M., and Lindberg, S. E.: Empirical modeling of atmospheric deposition in mountainous landscapes, Ecol. Appl., 16, 1590–1607, doi:10.1890/1051-0761(2006)016[1590:EMOADI]2.0.CO;2, 2006.

Wilcke, W., Yasin, S., Fleischbein, K., Goller, R., Boy, J., Knuth, J., Valarezo, C., and Zech, W.: Nutrient status and fluxes at the field and catchment scale, in: Gradients in a tropical mountain ecosysem of Ecuador, edited by Beck, E., Bendix, J., Kottke, I., Makeschin, F., and Mosandl, R., pp. 203–215, Springer Berlin-Heidelberg, doi:10.1007/978-3-540-73526-7_20, URL http://dx.doi.org/10.1007/978-3-540-73526-7{_}20, 2008.

Zeng, Y. and Hopke, P.: A study of the sources of acid precipitation in Ontario, Canada, Atmos. Environ., 23, 1499–1509, doi:10.1016/0004-6981(89)90409-5, URL http://www.sciencedirect.com/science/article/pii/0004698189904095, 1989.

Chapter 3

Complex topography influences atmospheric nitrate deposition in a neotropical mountain rainforest

Sandro Makowski Giannoni, Rütger Rollenbeck, Peter Fabian and Jörg Bendix

ATMOSPHERIC ENVIRONMENT

ATMOS. ENV., 118, 17, 10082-10092, 2013

Received: 20 November 2012
Revised: 23 May 2013
Accepted 10 June 2013
First published online: November 2013
DOI: http://dx.doi.org/10.1016/j.atmosenv.2013.06.023

Abstract

Future increase of atmospheric nitrogen deposition in tropical regions is expected to have negative impacts on forests ecosystems and related biogeochemical processes. In tropical mountain forests topography causes complex streamflow and rainfall patterns, governing the atmospheric transport of pollutants and the intensity and spatial variability of deposition. The main goal of the current study is to link spatio-temporal patterns of upwind nitrogen emissions and nitrate deposition in the San Francisco Valley (eastern Andes of southern Ecuador) at different altitudinal levels. The work is based on Scanning Imaging Absorption SpectroMeter for Atmospheric CHartographY (SCIAMACHY) retrieved-NO_2 concentrations, NO_x biomass burning emissions from the Global Fire Emissions Database (GFEDv3), and regional vehicle emissions inventory (SA-INV) for urban emissions in South America. The emission data is used as input for lagrangian atmospheric backward trajectory modelling (FLEXTRA) to model the transport to the study area. The results show that NO_3^- concentrations in occult precipitation samples are significantly correlated to long-range atmospheric secondary nitrogen transport at the highest meteorological stations (MSs) only, whereas for NO_3^- concentrations in rain samples this correlation is more pronounced at the lower MSs. We conclude that ion concentrations in occult precipitation at the uppermost MSs are mainly linked to distant emission sources via the synoptic circulation impinging the more exposed higher sites. Lower correlations close to the valley bottom are due to a lower occult precipitation frequency and point to a contamination of the samples by local pollution sources not captured by the used emission data sources.

3.1 Introduction

Nitrogen oxide emissions (NO_x) are increasing at a global scale because of population growth, increasing industrial activity, and greater land use change rates (Lewis et al. 2004). This also holds true for nitrate and other nitrogen species (Matson et al. 1999; Galloway et al. 2004). The unfavorable development especially applies to developing countries like the growing economies of South America, which are rapidly becoming the major nitrogen emitters of the world prone to enhanced atmospheric deposition (Vallack and Cinderby 2001). For many of valuable ecoregions, N accumulation is probably the main driver of changes to species composition by changing competitive interactions in the ecosystems. Bobbink et al. (2010) showed that particularly tropical parts of Latin America as the Andes of Ecuador, hitherto not receiving enough attention, belong to the vulnerable regions in the next decades.

The effects of Nr (Reactive nitrogen) deposition in temperate terrestrial ecosystems related to anthropogenic emissions have extensively been addressed in the scientific literature (Matson et al. 1999, 2002). This is not the case for tropical terrestrial ecosystems where some degree of uncertainty about the influence of increasing Nr deposition remains (Matson et al. 1999, 2002; Galloway et al. 2004; Koehler et al. 2009; Wolf et al. 2011). This increase in tropical ecosystems could have a fertilizing effect and boost ecosystem productivity or decrease it through acidification and related nutrient imbalances (Lewis et al. 2004; Unger et al. 2012). These changes in the biogeochemical cycles are expected to have an impact on ecosystem biodiversity (Matson et al. 1999, 2002; Galloway et al. 2004)

Increased deposition from anthropogenic NO_x emissions in Latin America has been observed not only in the vicinity of the emission sources but also in remote neotropical sites (McDowell et al. 1990; Clark et al. 1998; Phoenix et al. 2006). Nitrogen deposition in the form of NO_3^- has been investigated in tropical lowland sites of Costa Rica (Eklund and McDowell 1997), Venezuela (Morales et al. 1998), and central Brazilian Amazon (Williams et al. 1997). Eklund and McDowell (1997) and Williams et al. (1997) found that NO_3^- depositions in Costa Rica and the central Amazon were not contaminated by anthropogenic activities but rather originated from natural sources. Conversely, rain samples from Lake Maracaibo area in Venezuela were strongly contaminated with anthropogenic NO_3^-, potentially originating from industrial and urban upwind emissions (Morales et al. 1998). At high elevation sites, in Costa Rica, Puerto Rico, and Venezuela, cloud water was a significant source of deposition and water input, contributing up to 71 % to the total precipitation. NO_3^- concentrations in cloud water were much higher than in rainfall. Samples strongly charged with nitrate ions point to the likely contamination of the airmasses. In most cases the origin of pollutants are thought to be local anthropogenic

activities. Long distance transport was not identified as an important deposition source at these locations (Asbury et al. 1994; Gordon et al. 1994a,b; Clark et al. 1998).

Boy et al. (2008) and Fabian et al. (2005, 2009) found, that even in remote areas like the tropical mountain forests of the east Ecuadorian Andes, high nitrogen deposition rates were linked to distant continental anthropogenic upwind-sources from the east. Fabian et al. (2005) stressed the importance of occult precipitation water inputs at the upper parts of the *cordillera* and the positive gradient of nitrogen depositions (nitrate and ammonium) with altitude. Both Boy et al. (2008) and Fabian et al. (2005, 2009) observed that deposited nitrate and ammonium were highly correlated, which lead them to the conclusion that they originated from the same source. They pointed out the importance of long-range transport of pollutants for the nutrient budget and identified biomass burning as the most likely source of atmospheric nitrogen deposition to the ecosystem. An explanation is given by Andreae et al. (2004), which studied pyrogenic clouds from biomass burning regions; fires reduce the cloud droplet size, thus delaying precipitation and allowing the polluted air masses to travel greater distances before the pollutants are scavenged by rain. This explains how the polluted air masses may travel as far as the outer rim of the Amazon, where they are finally adiabatically uplifted by the orographic effects when reaching the Andes, causing intense water inputs through impaction of clouds and precipitation (Bendix et al. 2006b,a, 2008).

In mountain areas, the deposition of long-range transported aerosols can be highly variable depending on location, because of the complex weather patterns generated by the interaction of atmospheric features with topography and the particular exposures of the different landscape features (Lovett and Kinsman 1990). In tropical mountain forests it is essential to assess the level of pollutant exposure along altitudinal gradients. Depending on location, pollutant loads can vary considerably. Yet, no studies have addressed differences in atmospheric deposition along altitudinal gradients in tropical mountain forests. Likewise, source areas of nitrate precursors related to nitrate deposition have not been investigated in the light of recent developments in remote sensing of tropospheric chemistry and new emission inventories.

We report long term variations of nitrate deposition in precipitation at different altitudes in the *Reserva Biológica San Francisco* (RBSF), in south-east Ecuador. We combined long-term measurements of nitrate concentrations in rain and occult precipitation samples with pollutant transport modelling using emission inventories and satellite data as inputs. Due to the high wind speeds in this area, occult precipitation water here refers to all kind of light precipitation, from wind-driven drizzle down to fog and cloud droplets (Rollenbeck et al. 2007, 2011).

The aim of the current study was to find out (1) how nitrate deposition by occult precipitation and rain water varies in elevation/location along an altitudinal gradient between 1960 and 3180 m a.s.l. and (2) how the relationship between distant upwind emission events and the deposition varies at different elevations/ locations.

Additionally, this study contributes to a joint ecological fertilization experiment in southern Ecuador, the Nutrient Manipulation Experiment (NUMEX, Homeier et al. 2012), as part of a joint biodiversity research program (Bendix and Beck 2009).

3.2 Study area, data, and methods

To unveil the link between nitrate sources and deposition rates in the RBSF a combination of long-term monitoring of nitrate inputs and nitrogen transport modelling was employed. At the receptor site, in the San Francisco River catchment, in-situ data on NO_3^- deposition by rainfall and occult precipitation was collected on a weekly basis, and time series of nitrate concentrations and total deposition rates were compiled.

Regarding the sources of emissions, gridded emission and satellite data are used to model the NO_x transport to yield NO_x daily transport values up to the target coordinates, corresponding to the observation sites in the San Francisco River catchment. This is done by applying trajectory modelling.

The evaluation of data aims at comparing and correlating the observed concentration values and modeled transport values of the observation sites corresponding pixels.

To test the influence of local and synoptic wind exposure on the deposition process, we used local wind observations of the valley and vectorial averages of NCEP/NCAR wind direction at 500 hPa for the corresponding pixels of the observations sites.

The following sections describe the methods for field data sampling and analyses, and the data sets and tools employed for modelling the transport of nitrate precursors to the study area.

3.2.1 Study site and its climatology

The RBSF (Fig. 3.1) is located in the south-eastern Andes of Ecuador (4°00 S and 79°00 W), on the eastern slope of the Cordillera Real, the weather divide between the

humid Amazon basin and the dryer interandean valleys west of this *cordillera* (Beck et al. 2008).

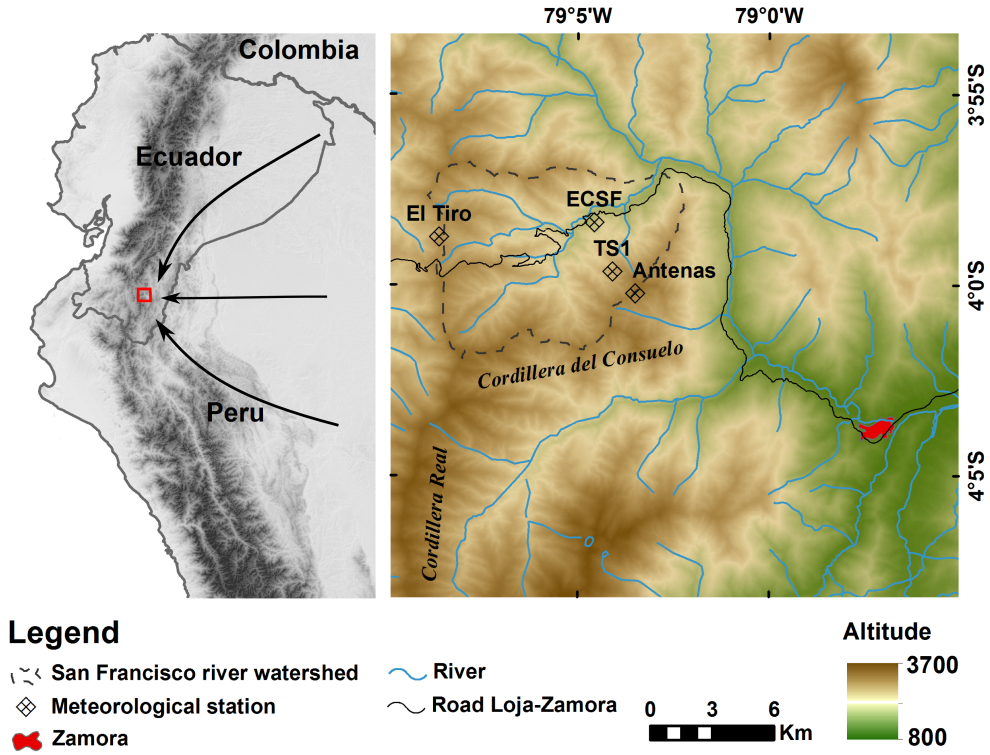

Figure 3.1: a) Location of the study area in the Andes of south-eastern Ecuador. Arrows indicate the funneling of the tropical trades by the effect of the concave shape and the low altitude of the Andes at that point of the *cordillera*. b) Location of meteorological stations (MSs) and fog water collectors along an altitudinal gradient on the north-west facing slopes of the *Reserva Biológica San Francisco* (RBSF) and at the mountain pass El Tiro.

Topography makes the region especially suitable for investigating atmospheric nutrient/pollutant inputs. The area is affected by the Inter-Tropical Convergence Zone (ITCZ) and the influence of the tropical easterlies. The region's relief is lower (less than 3200 m a.s.l.) compared to the northern and central Andes. The latter, combined with the concave shape of the Andes arc at this point of the mountain range, creates a funneling effect (Fig. 3.1a), leading to the convergence of air masses from the Amazon (Rollenbeck et al. 2011). The wind direction and velocity at the core area vary with increasing altitude. The RBSF lower northwest-facing slopes form a sheltered location at the leeward side, and are characterized by low wind velocities and diurnal breeze patterns. At the mountain top, wind comes predominantly from the east and can reach high speeds ($>$20 m s^{-1}), causing a constant exposure to the synoptic winds flowing over the Amazon almost all year long (Bendix et al. 2008).

Precipitation varies, depending mainly on the variations of the tropical easterlies and the associated humidity advection. Average annual totals range from 1850 to 6300 mm year^{-1} along the altitudinal gradient. Occult precipitation frequencies of up to 85 % of the time have been observed in the research area, adding to the total amount of precipitation. Occult precipitation is generated when warm and moist air masses from the Amazon lowlands hit the Andes, leading to intense formation of clouds and long lasting light rain (Bendix et al. 2006b,a; Emck 2007; Rollenbeck 2010).

Rainfall increases with altitude (Bendix et al. 2008). Occult precipitation was estimated to add 5 % to the total precipitation at 1800–2000 m a.s.l. and it contributes about 35 % at the highest measurement station (3200 m a.s.l.).

3.2.2 Field data collection and analysis

NO_3^- sampling

Rainfall and occult precipitation amounts have been measured in three meteorological stations (MSs) installed along an altitudinal gradient (ECSF, TS1 and Antenas at 1960, 2660, and 3180 m a.s.l., respectively) and a fourth one 4 km downwind at a mountain pass (El Tiro) between the basin of Loja and the eastern slopes of the Andean main ridge (at 2870 m a.s.l.) (Fig. 3.1b).

Samples were collected on a weekly basis from 2005 to 2009. Rain samples were taken using UMS-RS 200 polyethylene rain samplers of 20 cm diameter. A fog sampling device suggested by Schemenauer and Cereceda (1994) was used to collect occult precipitation. Fog collectors have a size of 1 x 1 m and are composed of polypropylene nets with a 2 x 1 mm mesh width. They are set up perpendicular to the main wind direction and collect all type of deposition, like particles, aerosols, and gases (Fabian et al. 2005). For more details on rain and occult precipitation measurement techniques, calibration, and handling of the data refer to Fabian et al. (2005) and (Rollenbeck et al. 2007, 2011). The samples were measured for electrical conductivity and pH on site and then stored deep frozen until the chemical analyses.

Concentrations of NO_3^- ions in rain and occult precipitation water were analyzed by ion chromatography (Dionex DX-210). The major NO_3^- ions were taken as proxies of nitrogen inputs into the ecosystem. Time series of NO_3^- Volume Weighted Mean (VWM) ion concentrations in rain and occult precipitation water were created for the period 2005–2009 (refer to section 3.2.4) and general trends were examined.

Wind data

In addition to the measurement of nitrate inputs, wind speed and direction were recorded on an hourly basis at each MS. Then, hourly wind direction vectorial averages and wind speed means were calculated for each month of the year and for the whole observation period.

3.2.3 Modeling of NO_x transport

The modelling of NO_x transport is based on 10 days backward trajectories (3.2.3), two emission inventories (3.2.3), and a satellite dataset (3.2.3). The modelling outputs are NO_x daily transport values at coordinates 3.9°00 S and 79°00 W.

Emission inventories

An emission geodatabase was derived from different emission inventories for the period 2005–2009. The different emission inventories and their properties are presented in Table 3.1. We used the Global Fire Emission Database version 3 (GFEDv3) and the Regional Vehicle Emissions Inventory (SA-INV) to estimate NO_x emissions from biomass burning and urban and transportation emissions, respectively.

GFEDv3 estimates are made up of burned area data from satellite observations and a biogeochemical model (CASA-GFED) that approximates fuel loads and combustion completeness for each time-step (van der Werf et al. 2010). Since fires have a sporadic nature, the high temporal and spatial resolution of the GFEDv3 inventory is a key factor in the reproduction of the variability of emissions (Mu et al. 2011). However, it still underestimates the emissions in the tropics, where cloud cover and canopy closeness make the detection of fires a difficult task. Gaps in the satellite coverage are also an issue (Mu et al. 2011).

The SA-INV inventory (Alonso et al. 2010) is an enhanced version of the EDGAR (Emission Database for Global Atmospheric Research) and RETRO (REanalysis of the TROpospheric chemical composition over the past 40 years) global anthropogenic emission inventories. It incorporates regional information from municipal inventories, including mobile NO_x emissions from traffic in different South American countries. These improvements increased the accuracy of atmospheric chemistry simulations on a local and regional scale. Nonetheless, even if this represents an advance with respect to EDGAR and RETRO inventories, its principal disadvantage is that it does not reproduce the weekly and monthly variability of emissions, leading, among other things, to an overestimation of the latter.

Table 3.1: Principal attributes of the two emission inventories used in this study. NOx emitted from biomass burning and industrial activity, two important sources of atmospheric nitrogen, are accounted by these two inventories

	SA-INV [kg m^{-2} d^{-1}]	GFED [g m^{-2} d^{-1}]
Spatial resolution	0,5° x 0,5°	0,5° x 0,5°
Temporal resolution	Yearly	Daily
Trace gas species	NO_x	NO_x
Source of emission	Urban/industrial	Biomass burning

SCIAMACHY tropospheric NO_2 retrievals

The SCanning Imaging Absorption spectroMeter for Atmospheric CHartographY (SCIAMACHY) instrument onboard ESA's ENVISAT satellite measures back scattered, transmitted, and reflected light from Earth's atmosphere and surface in the UV and visible range, between 220 and 2380 nm. ENVISAT overflies the earth in a sun-synchronous orbit, with an Equator overpass time at 10:00 am LT. The spatial resolution of the retrieved images is 30 km (along track) x 60 km (across track). This leads to global coverage in six days if only nadir measurements are considered. For more information about SCIAMACHY refer to Richter (2004); Richter et al. (2005).

Tropospheric NO_2 from SCIAMACHY offers some additional advantages compared to modelling approaches like SA-INV and GFEDv3. SCIAMACHY provides real observational data of tropospheric NO_2 regarding all the emission sources, including natural NO_x production (e.g. Thunderstorms-produced NO_x), in a relative high temporal and spatial resolution.

Emisstraject: trajectory-emission integration tool

To explain periodical patterns and extreme nitrate deposition events observed in the time series, a tool (Emisstraject, Rollenbeck 2010) that models the transport of nitrogen oxides (NO_x) from upwind sources to our research area was developed. Emisstraject combines 10 days FLEXTRA (Stohl et al. 1995) backward wind trajectories with gridded emission/concentration data from inventories (GFEDv3 and SA-INV) and satellite products (SCIAMACHY NO_2). The program follows the path of the trajectories and integrates all emission values of the respective data set where temporal and spatial coincidence between air mass passage and emissions exist. At the end of each trajectory the total addition of the pixel values would represent an estimate of NO_x reaching the San Francisco River catchment at 4°00 S and 79°00 W.

The FLEXTRA model is based on wind fields from reanalysis data of the European Centre for Medium-range Weather Forecast (ECMWF). The model calculates trajectories

with a time resolution of three hours. However, for the purpose of this research a mean wind vector was calculated for each day. Additionally, a buffer of 25 km radius from the trajectory was assumed to account for uncertainties in accordance to the resolution of the underlying ECMWF global climate model.

To simulate wet scavenging and rain-out processes in the atmosphere, a decay function was integrated into the algorithm:

$$\mathrm{C}_t = \frac{\mathrm{C}_0}{\mathrm{e}^{\frac{t}{k}}} \tag{3.1}$$

where C_t is the NO_x concentration at time t in days, C_0 is the initial NO_x concentration value at the emission point, and k is the mean lifetime constant in days.

In this way, the NO_x concentration in the airmass will decrease exponentially depending on the value of the mean lifetime constant k, the time at which the NO_x quantity is reduced to $1/e$ = 0.367879441 times its initial value. Model runs were conducted using three, four, and six days mean lifetime. Higher values would represent dryer conditions along the trajectories with low wet scavenging rates. Lower values would mean more rain-out. We then chose the lifetime constant which most closely reflected the observed deposition values.

3.2.4 Data evaluation

Time-series of volume-weighted monthly mean NO_3^- concentrations were calculated for the observation period. Deposition values were calculated as the product of the volume weighted NO_3^- monthly-mean concentrations and the water input of that month. Total deposition was subsequently computed for each of the MSs regarding the deposition type (occult precipitation or rain). The time-series from the model outputs using different input datasets are presented in Fig. 3.2. The rather periodic fluctuations observed in the time-series of modeled NO_2 (SCIAMACHY NO_2) transport are echoed by those in the time-series of biomass burning NO_x (GFEDv3), while industrial NO_x (SA-INV) transport presents a quite different oscillation regime. The high transport values for both SCIAMACHY tropospheric NO_2 and GFEDv3 NO_x datasets most likely correspond to the increased fire activity during the biomass burning season in the Brazilian Amazon (August–October) (Andreae et al. 2004).

Since the previously mentioned datasets were not normally distributed even after logarithmic and square root transformations (Shapiro-Wilkinson test, $p < 0.05$), non parametric Spearman correlation analysis was applied to test for correlations between field observations (NO_3^- concentrations) and model outputs (NO_x transport).

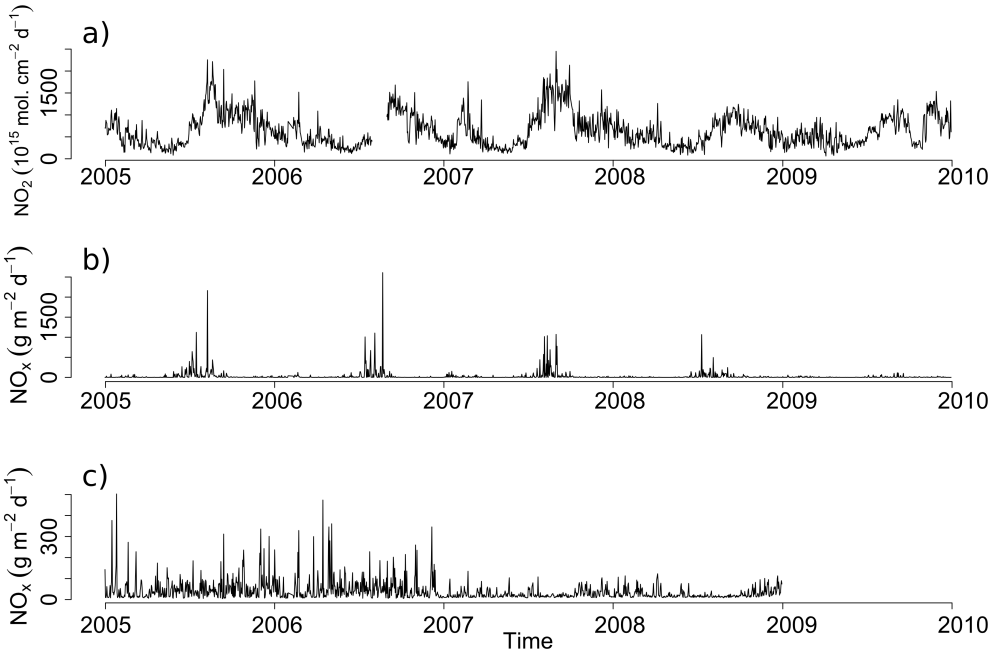

Figure 3.2: Time series of monthly NO_x transport at the Reserva Biológica San Francisco (RBSF) (3.9°00 S and 79°00 W) resulted from the Global Fire Emission Database (GFED), the regional vehicle emissions inventory (SA-INV), and the Scanning Imaging Absorption SpectroMeter for Atmospheric CHartographY (SCIAMACHY) data sets.

Wind data (speed and direction in degrees) was recorded hourly 2 m above ground level at the four MSs. The data were processed to build grid maps of prevailing hourly wind direction for each month. Information on the diurnal behavior of winds and wind patterns (local or synoptical) could help to explain the different correlation coefficients between transport model outputs and concentrations at the different MSs. Additionally, we computed the mean wind direction from NCEP/NCAR reanalysis data to calculate the deviation of wind direction at the MSs to this mean synoptic wind. If synoptic wind exposure is an important parameter affecting the deposition, this deviation should have an effect on the correlations. Because occult precipitation increases with wind speed, total nitrate deposition could increase too; hence, we calculated mean wind speed for each MS as well. If wind speed has an impact on the deposition, then high correlations should coincide with high wind speeds.

3.3 Results

3.3.1 Variability of deposition

The resulting rain and occult precipitation water inputs and related NO_3^- deposition are shown in Table 3.2. Total precipitation was found to increase with altitude, as well as

the proportion of occult precipitation water to the total precipitation amount. Occult precipitation contributed to only 5 % of the total precipitation at ECSF, 17 % at Antenas, and 36 % at El Tiro. The pH values were usually lower in occult precipitation samples and the electrical conductivity higher.

Table 3.2: Average annual precipitation (P)([mm]), pH, conductivity (eC[μ S cm^{-1}]), and NO_3^- deposition rates ([kg ha^{-1}]) at different elevations for the period 2005-2009. From top to bottom, the three first meteorological stations (MS) are those located along an altitudinal gradient, where Antenas is the uppermost one; El Tiro MS is located at a mountain pass 4 km upriver

MS	Altitude	P		pH		eC		NO_3^-	
		Rain	Occult p.	Rain	Occult p.	Rain	Occult p.	Rain	Occult p.
ECSF	1960	1742	92	5.4	4.9	4.2	12.4	1	0.1
		σ_x= 58.2	σ_x=5.6	σ_x=0.6	σ_x=0.7	σ_x=3.5	σ_x=12.9	σ_x=8.7	σ_x=0.2
TS1	2660	3453	415	5.4	5.3	4.0	5.5	2.4	0.4
		σ_x= 107.8	σ_x=15.5	σ_x=0.6	σ_x=0.4	σ_x=3	σ_x=4.5	σ_x=0.1	σ_x=0.4
Antenas	3180	5994	1259	5.3	5.5	3.5	12.4	3.5	9
		σ_x= 247.5	σ_x=42.7	σ_x=0.6	σ_x=4.1	σ_x=2.2	σ_x=12.4	σ_x=0.1	σ_x=1.1
El Tiro	2870	1700	968	5.4	4.7	5.4	18.1	1.6	6.5
		σ_x= 68.7	σ_x=42.9	σ_x=0.6	σ_x=10.8	σ_x=7.4	σ_x=20.3	σ_x=0.1	σ_x=2

In occult precipitation water we found a significant difference between NO_3^- concentrations at the mountain top (El Tiro and Antenas; Fig. 3.3) and those at the middle and lower slope (TS1 and ECSF, respectively). At higher altitudes the concentration was not only higher but also more scattered, with a higher number of extreme values. Opposed to this, NO_3^- concentrations at ECSF and TS1 were less dispersed, with most of the values centered around the median.

Because deposition is the product of precipitation and concentration, a gradient of mean deposition values of NO_3^- with height was observed for both precipitation types. In occult precipitation, NO_3^- inputs increase even more at the highest MSs of El Tiro and Antenas (Table 3.2), due to the combined effect of higher concentration and higher precipitation.

3.3.2 Links between distant upwind NO_x emission events and NO_3^- inputs

Correlation between NO_x transport and NO_3^- concentrations

Variation of NO_3^- concentrations in occult precipitation from El Tiro MS (2660 m a.s.l.) was well reproduced by the modeled time-series of NO_x transport (Fig. 3.4a). In rain, however, the fluctuations in NO_x transport did not match those of the NO_3^- concentrations measured at this station (Fig. 3.4b). On the contrary, at the lowest MS (ECSF) only the fluctuations of NO_3^- concentrations in rain water were well captured by the model outputs

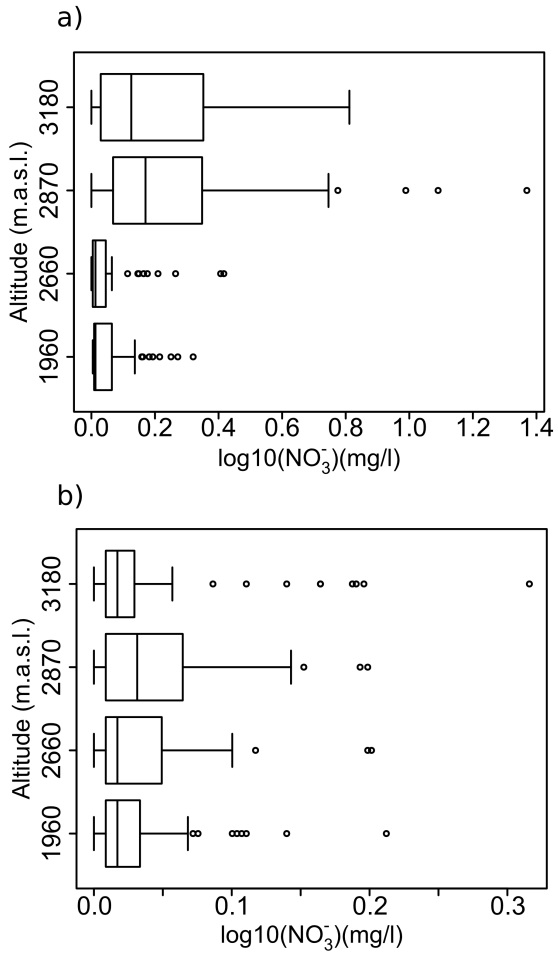

Figure 3.3: Tukey boxplots illustrating the NO_3^- concentrations in a) rain and b) occult precipitation at different altitudinal levels. From bottom to top, altitudes on the y axis represent data from ECSF, TS1, El Tiro and Antenas meteorological stations (MSs), respectively.

of NO_x transport (Fig. 3.4c and d).

Correlations between long-range transported NO_x and occult precipitation NO_3^- concentrations were significant at higher elevations only (mainly at El Tiro) (Table 3.3). For rain water NO_3^- inputs, the correlation coefficients of the lower MSs (TS1 and ECSF) are more significant than the upper MSs. NO_3^- peak concentrations were generally well represented by the simulated NO_x transport from biomass burning sources (GFEDv3), whose variations were similar to the transport from all continental sources (SCIAMACHY). No relations were found between nitrate concentrations in both occult precipitation and rain water samples and the long-range transport from urban NO_x sources (SA-INV).

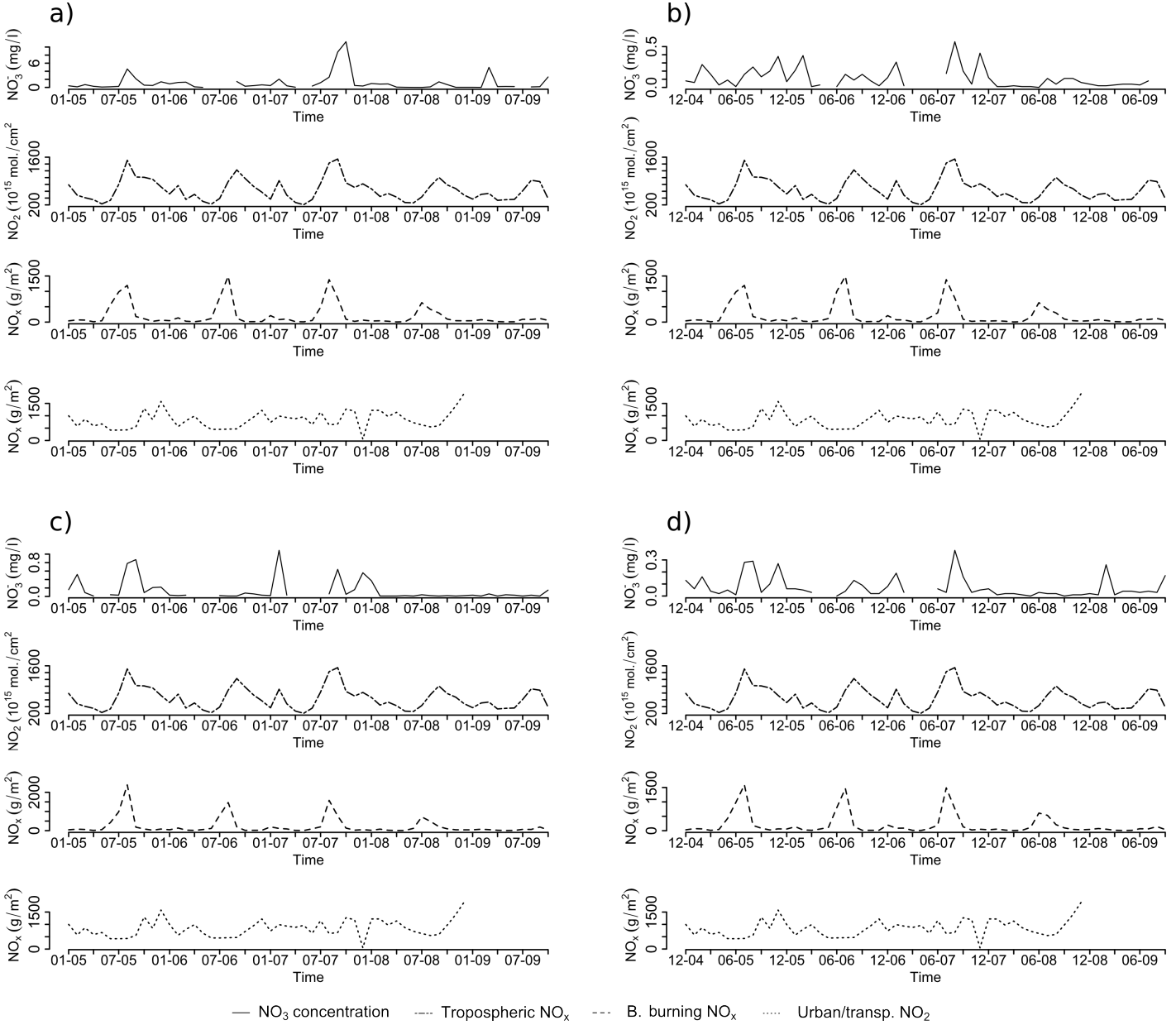

Figure 3.4: Time series comparing modeled NO_x transport to measured NO_3^- concentrations in occult precipitation (a,c) and rain water (b,d) for El Tiro (top charts) and ECSF (bottom charts) meteorological stations.

Wind exposure

The wind plots in Fig. 3.5 show prevailing wind direction 2 m above terrain surface, indicating two different wind systems and their interactions. The diurnal cycle of the valley breeze system is clearly visible at the ECSF station (Fig. 3.5a). In the noon/afternoon an up-slope/up-valley flow (NE/E) dominates, while cold air drainage flow from the slopes and down the valley (SW in the early morning hours) characterizes the nocturnal circulation system. The patterns at the TS1 MS are less clear because the station is located in the transition zone between the mountain breeze-systems and the influence of synoptic easterly directions of the higher parts (Fig. 3.5b). It completely changes at the Antenas MS, where almost permanent north-easterly directions prevail. North and north-westerly winds set up in the mean wind field uniquely in the drier month of November (Fig. 3.5c). An almost identical pattern is present at El Tiro but the change of the wind direction was not as clearly in the month of November (Fig. 3.5d).

Table 3.3: Correlation matrix between NO_x transmissions and NO_3^- concentrations in a) rain and b) occult precipitation samples from meteorological stations at the studied altitudinal gradient

	El Tiro NO_3^- mg l^{-1}	Antenas NO_3^- mg l^{-1}	TS1 NO_3^- mg l^{-1}	ECSF NO_3^- mg l^{-1}
a)				
GFED NO_x	0.41**	0.37	0.32***	0.32***
SCIAMACHY NO_2	0.37**	0.14	0.51***	0.32**
SA-INV NO_x	-0.07	0.00	-0.03	-0.11
b)				
GFED NO_x	0.26*	0.02	-0.11	0.02
SCIAMACHY NO_2	0.43**	0.51**	0.08	0.24**
SA-INV NO_x	0.05	0.13	0.20	-0.02

Note: *** $p < 0.001$, ** $p < 0.01$, * $p < 0.05$.

Concerning wind speeds, the two uppermost MSs (Antenas and El Tiro) registered the highest values (Fig. 3.5, Table 3.4). Surface mean wind-direction vectors at middle and uppermost MSs (El Tiro, TS1, and Antenas) presented the lowest deviations to mean synoptic wind vectors. Because slope face shapes the wind field, the deviation was lower for TS1 MS (2660 m a.s.l.) than for Antenas MS (3180 m a.s.l.).

Table 3.4: Surface wind direction deviation from synoptic wind field and mean surface wind speed for each MS. Wind direction deviation index is a value between 0 and 1 where 0 means the same wind direction as the synoptical wind field and 1 the opposite wind direction

	El Tiro	Antenas	TS1	ECSF
Deviation from synoptic wind (0-1)	0.08	0.13	0.1	0.56
Mean wind speed (m s^{-1})	6.82	5.46	0.8	0.97
	σ_x=4.3	σ_x=2.6	σ_x=0.7	σ_x=2.6

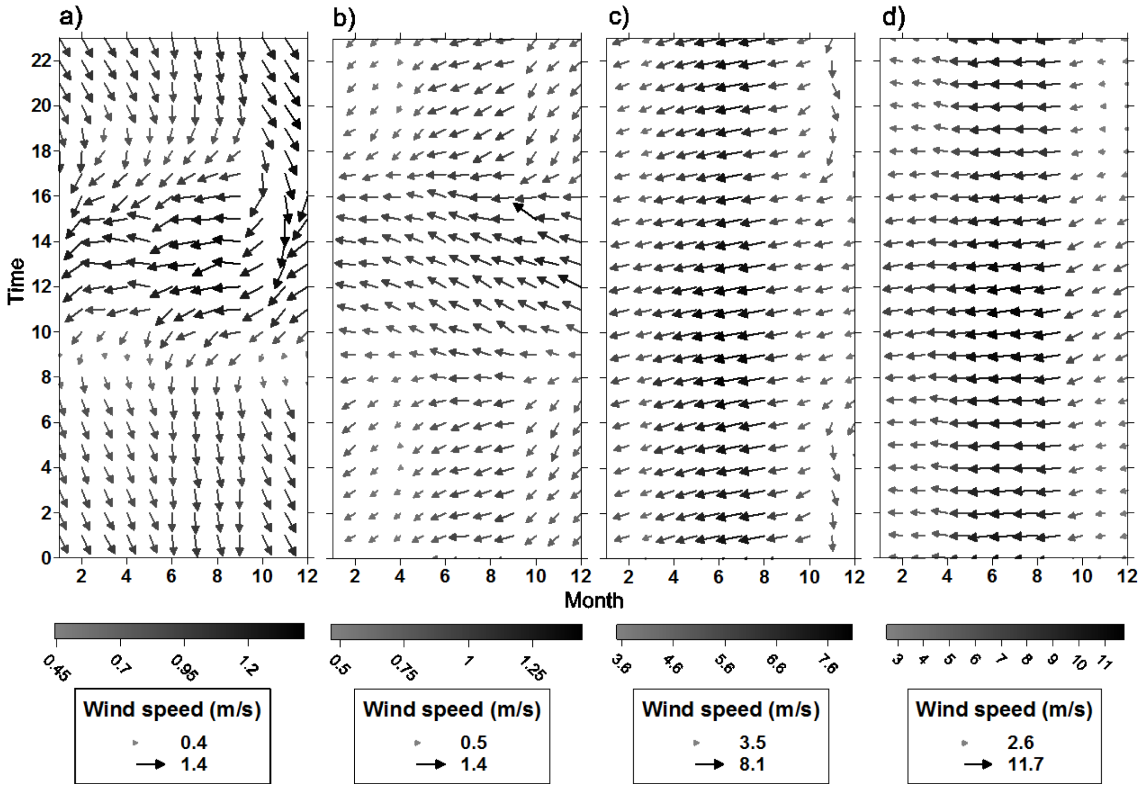

Figure 3.5: Vectorial wind direction averages for the period 2005-2009 at a) ECSF, b) TS1, c) Antenas and d) El Tiro meteorological stations (MSs). Arrows represent wind direction and their size and gray tone indicate wind speed for the daily and annual cycle.

3.4 Discussion

3.4.1 Nitrate inputs into the ecosystem

Topography is a major factor affecting the deposition at the study area. An overall increase in rain, occult precipitation, and NO_3^- input is observed with terrain height. This fact corresponds to the high frequency of orographic cap clouds on higher terrain caused by the strong easterlies (Bendix et al. 2006b,a, 2008). Total nitrate deposition is higher at the crests as well, where rain and especially occult precipitation inputs are greater. The fact that nitrate concentrations are much greater in occult precipitation than in rain, already observed by Lovett and Kinsman (1990) and Clark et al. (1998), contributes to the differences of deposition rates at the mountain tops and lower north facing slopes (lee side), where the occult precipitation frequency is low. Bulk nitrate deposition was in the middle range compared to depositions reported for similar ecosystems and in agreement with the depositions observed in previous studies at the RBSF (Table 3.5). Although deposition was not as high as those found in tropical Africa and in central and south-eastern Brazil (Table 3.5), they still must be considered very high for tropical mountain forests located in the vicinity of very few and weak local sources of nitrogen precursors. Together, occult precipitation and rain nitrate depositions can exceed the 10 kg N ha^{-1} yr^{-1} threshold, above

of which nitrogen additions are known to damage vegetation in some temperate ecosystems (Phoenix et al. 2006). Few studies have addressed atmospheric nitrate deposition in tropical forests from cloud and occult precipitation water. Comparing the deposition at the peak of the Cordillera del Consuelo (Antenas MS), where occult precipitation input is constant throughout the year, with the results from a tropical mountain forest in Puerto Rico (Asbury et al. 1994), yielded twofold greater nitrate inputs for our site in southeastern Ecuador. The exposed situation of the Cordillera del Consuelo and the long distance the air masses travel across polluted continental air layers are more than likely responsible for this difference (Fabian et al. 2005, 2009; Boy et al. 2008).

Table 3.5: Comparison of nitrate depositions in rain and occult precipitation from selected lowland and mountain tropical forests (modified after Boy et al. 2008)

	Occult p. NO_3^- (kg ha^1)	Bulk NO_3^- (kg ha^1)	Obs. period	Reference	Sampling
South Ecuador (RBSF)	0.1-9	1.0-3.5	2005-2009	This study	Weekly intervals
South Ecuador (RBSF)	0.2-11	1.8-3.1	2002-2006	Fabian et al. 2009	Weekly intervals
South Ecuador (RBSF)	-	2.6-2.9	1998-2003	Boy et al. 2008	Weekly intervals
Costa Rica	-	1.8-3.4	1992-1995	Eklund and McDowell 1997	Weekly intervals
Venezuela	-	1.7-4.2	1988-1999	Morales et al. 1998	Event-based
Central Amazon	-	7.1	1988-1990	Williams et al. 1997	Event-based
SE-Brazil	-	9.2	1999-2001	Da Rocha et al. 2005	Event-based
SE-Brazil	-	6.6-10.0	1991-1995	Mayer et al. 2000	Weekly intervals
Puerto Rico	4.1	5.3	1984-1985	Asbury et al. 1994	Event-based
Cameroon	-	8.6	1996-2000	Sigha-Nkamdjou et al. 2003	Event-based
Nigeria	-	19-45	May-Nov 1995	Muoghalu 2003	Event-based
Côte d'Ivoire	-	5.7	1995-2002	Yoboué et al. 2005	Event-based

3.4.2 Linking NO_x distant upwind emissions to NO_3^- deposition

NO_x transport from far upwind sources largely influences the NO_3^- concentrations in occult precipitation from MSs at crests. In rain water vertical differences in nitrate concentrations are smaller. The two different wind regimes at different altitudes likely contribute to the higher correlations for occult precipitation at higher elevations. Here, NO_x transport is associated with easterly airmasses approaching from the Amazon (Fig. 3.6b). In the valley, resuspended surface dust and road transportation emissions (Da Rocha et al. 2005) transported by the valley breeze system contribute to the deposition, thus weakening the correlation between synoptic transport and occult precipitation deposition (Fig. 3.6a).

Together with the lower wind speed, the much lower occult precipitation capture, could explain the weaker correlation coefficients to the transport from distant upwind sources of the deposition at the lower sites. Locally enriched occult precipitation and nitrate aerosol from fires and transportation are more prone to be caught by the fog collectors than advected clouds. Moreover, the low wind speeds and lower humidity at this site favors the gravitation of particulate matter directly into the collectors, altering the measurements. This is not the case at the uppermost MSs where strong winds are very constant and the humidity high. The standard rain gauges predominantly capture larger droplets that tend to cross all altitude levels in the atmosphere. On their path down to earth they integrate local and remote pollutants and blur the correlations to remote sources (Fig. 3.6a).

The results of the Spearman correlations indicate biomass burning as the most important anthropogenic source of nitrate for the RBSF, explaining most of the temporal variability of nitrate deposition at the study site. Fabian et al. (2009) gave a possible explanation to NO_3^- that was formed from precursors in the atmosphere, revealing its anthropogenic nature. Yet, it couldn't be distinguished between its urban or biomass burning origin. The results of this study confirm the interpretations of Fabian et al. (2005, 2009) and Boy et al. (2008) showing biomass burning as the most important source of nitrate inputs to the tropical mountain forest of south Ecuador, especially affecting wind exposed crests. Transported NO_x from urban/transportation emissions were not correlated to the deposition at the RBSF, probably because most of these emissions stem from populated areas at the east-coast of South America and were already washed out further east.

NO_3^- deposition at the mountain pass El Tiro has the strongest relationship with NO_x transported from distant upwind sources. Significant correlations between NO_3^- concentrations in occult precipitation and rain water and the transport model outputs for both biomass burning NO_x inventory (GFEDv3) and NO_2 satellite observations (SCIAMACHY)

support this argument. Consequently, we consider El Tiro MS to be the most suitable site for future monitoring of atmospheric deposition from far upwind sources.

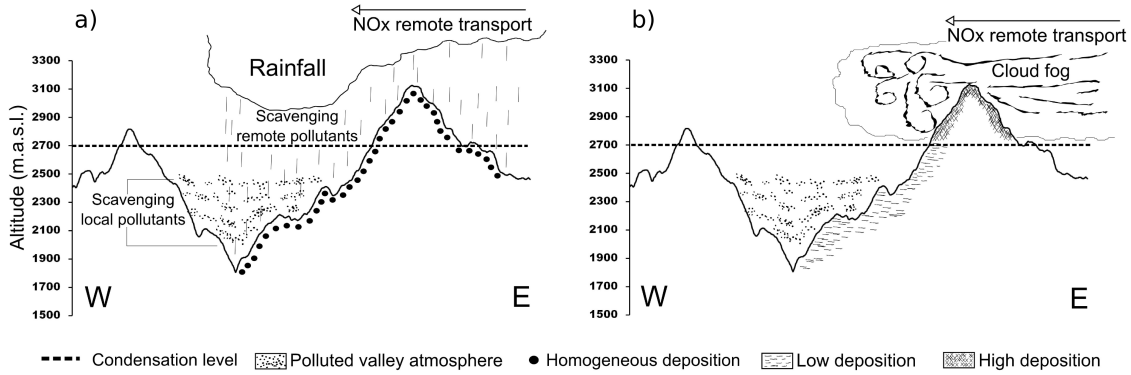

Figure 3.6: Conceptual sketch illustrating the two observed deposition regimes. E and W refer to east and west, respectively. The scale represents altitude in meters.

3.5 Conclusion

Our main goal in this study was to find out how nitrate deposition in occult precipitation and rain water varied in a height profile in the San Francisco River catchment during the period 2005-2009 and to elucidate the strength in the relationship between distant upwind emission events and the topographic variations of deposition.

We conclude that nitrate concentrations are higher in occult precipitation water and the deposition is more important at the crests where occult precipitation contribution to the total precipitation is largest.

For occult precipitation water a significant relationship with long-range atmospheric matter transport mainly occurs at higher elevations (mainly at El Tiro MS) where the landscape is exposed to free synoptic air flow. The correlation coefficients for rain water were more significant for the lower MSs (TS1 and ECSF), probably because rain drops are traversing the polluted air layer before being sampled.

Biomass burning was the most probable source explaining the variability of nitrate deposition at the RBSF. The proximity to the region where the majority of forest fires occur (Brazilian states of Mato Grosso, Rondonia, and Pará), and the synoptical wind pattern favor the transport of fire emissions. Urban emissions coming from the most populated and industrialized areas in Brazil are transported only episodically.

Further research will focus on the identification of other aerosol species sources, using

more accurate emission inventories and satellite data, as well as longer time-series of atmospheric matter inputs. In order to improve the results of the modelling dispersion modelling (FLEXPART) and data from local/regional weather model WRF (like high resolution wind fields) should be implemented into our modelling scheme.

Acknowledgements

We thank the German Academic Exchange Service (DAAD) for funding the PhD thesis of Sandro Makowski Giannoni (Ref. Number A/08/98222) and the German Research Foundation (DFG) for the funding of the work in the scope of the Research Unit RU816 (funding number: BE 1780/15-1). We are grateful to Katja Trachte, Michael Richter and Thorsten Peters for providing meteorological data and to Andreas Richter for providing the SCIAMACHY NO_2 data. We also thank the foundation Nature & Culture International (NCI) Loja and San Diego for logistic support. We finally thank the anonymous reviewer for the valuable comments, and Giulia Curatola Fernández for cartographic support and proof reading.

Bibliography

Alonso, M. F., Longo, K. M., Freitas, S. R., da Fonseca, R. M., Marécal, V., Pirre, M., Klenner, L. G., Mello da Fonseca, R., Marécal, V., Pirre, M., and Klenner, L. G.: An urban emissions inventory for South America and its application in numerical modeling of atmospheric chemical composition at local and regional scales, Atmos. Environ., 44, 5072–5083, doi:DOI:10.1016/j.atmosenv.2010.09.013, URL http://www.sciencedirect.com/science/article/B6VH3-5125R8F-3/2/1a18f95838b3777510913f11961c9490, 2010.

Andreae, M. O., Rosenfeld, D., Artaxo, P., Costa, A. A., Frank, G. P., Longo, K. M., and Silva-Dias, M. A. F.: Smoking rain clouds over the Amazon., Science, 303, 1337–42, doi:10.1126/science.1092779, URL http://www.ncbi.nlm.nih.gov/pubmed/14988556, 2004.

Asbury, C. E., McDowell, W. H., Trinidad-Pizarro, R., and Berrios, S.: Solute deposition from cloud water to the canopy of a puerto rican montane forest, Atmos. Environ., 28, 1773–1780, doi:10.1016/1352-2310(94)90139-2, URL http://linkinghub.elsevier.com/retrieve/pii/1352231094901392, 1994.

Beck, E., Makeschin, F., Haubrich, F., Richter, M., Bendix, J., and Valarezo, C.: The Ecosystem (Reserva Biológica San Francisco), in: Gradients in a tropical mountain ecosystem of Ecuador, edited by Beck, E., Bendix, J., Kottke, I., Makeschin, F., and Mosandl, R., chap. 1, pp. 1–14, Springer, URL http://www.springer.com/life+sciences/ecology/book/978-3-540-73525-0, 2008.

Bendix, J. and Beck, E.: Spatial aspects of ecosystem research in a biodiversity hot spot of southern Ecuador – an introduction, Erdkunde, 63, 305–308, doi:10.3112/erdkunde.2009.04.01, URL http://www.erdkunde.uni-bonn.de/archive/2009/spatial-aspects-of-ecosystem-research-in-a-biodiversity-hot-spot-of-southern-ecuador-an-introduction, 2009.

Bendix, J., Rollenbeck, R., Goettlicher, D., and Cermak, J.: Cloud occurrence and cloud properties in Ecuador, Clim. Res., 30, 133–147, doi:10.3354/cr030133, URL http://www.int-res.com/abstracts/cr/v30/n2/p133-147/, 2006a.

Bendix, J., Rollenbeck, R., and Reudenbach, C.: Diurnal patterns of rainfall in a tropical Andean valley of southern Ecuador as seen by a vertically pointing K-band Doppler radar, Int. J. Climatol., 26, 829–846, doi:10.1002/joc.1267, URL http://onlinelibrary.wiley.com/doi/10.1002/joc.1267/fullhttp://doi.wiley.com/10.1002/joc.1267, 2006b.

Bendix, J., Rollenbeck, R., Richter, M., Fabian, P., and Emck, P.: Climate, in: Gradients in a tropical mountain ecosystem of Ecuador, edited by Beck, E., Bendix, J., Kottke, I., Makeschin, F., and Mosandl, R., chap. 1, pp. 63–74, Springer Berlin / Heidelberg, ecological edn., URL http://dx.doi.org/10.1007/978-3-540-73526-7{\protect\T1\textbraceleft}{_}{\protect\T1\textbraceright}8, 2008.

Bobbink, R., Hicks, K., Galloway, J., Spranger, T., Alkemade, R., Ashmore, M., Bustamante, M., Cinderby, S., Davidson, E., Dentener, F., Emmett, B., Erisman, J. W., Fenn, M., Gilliam, F., Nordin, A., Pardo, L., and De Vries, W.: Global assessment of nitrogen deposition effects on terrestrial plant diversity: a synthesis, Ecol. Appl., 20, 30–59, doi:10.1890/08-1140.1, URL http://www.esajournals.org/doi/abs/10.1890/08-1140.1, 2010.

Boy, J., Rollenbeck, R., Valarezo, C., and Wilcke, W.: Amazonian biomass burning-derived acid and nutrient deposition in the north Andean montane forest of Ecuador, Global Biogeochem. Cycles, 22, GB4011, URL http://dx.doi.org/10.1029/2007GB003158, 2008.

Clark, K., Nadkarni, N., Schaefer, D., and Gholz, H.: Cloud water and precipitation chemistry in a tropical montane forest, Monteverde, Costa Rica, Atmos. Environ., 32, 1595–1603, URL http://www.sciencedirect.com/science/article/pii/S1352231097003841, 1998.

Da Rocha, G. O., Allen, A. G., and Cardoso, A. A.: Influence of agricultural biomass burning on aerosol size distribution and dry deposition in southeastern Brazil, doi:10.1021/ES048007U, 2005.

Eklund, T. and McDowell, W.: Seasonal variation of tropical precipitation chemistry: La Selva, Costa Rica, Atmos. Environ., 31, 3903–3910, URL http://www.sciencedirect.com/science/article/pii/S135223109700246X, 1997.

Emck, P.: A climatology of South Ecuador, Phd thesis, Fachbereich Geographie der Friedrich-Alexander-Universität Erlangen-Nürnberg, Germany, URL http://www.opus.ub.uni-erlangen.de/opus/volltexte/2007/656/, 2007.

Fabian, P., Kohlpaintner, M., and Rollenbeck, R.: Biomass burning in the Amazon–fertilizer for the mountaineous rain forest in Ecuador, Environ. Sci. Pollut. Res., 12, 290–296, URL http://dx.doi.org/10.1065/espr2005.07.272http://www.ncbi.nlm.nih.gov/pubmed/16206723, 2005.

Fabian, P., Rollenbeck, R., Spichtinger, N., Brothers, L., Dominguez, G., and Thiemens, M.: Sahara dust, ocean spray, volcanoes, biomass burning: pathways of nutrients into Andean rainforests, Adv. Geosci., 22, 85–94, doi:10.5194/adgeo-22-85-2009, URL http://www.adv-geosci.net/22/85/2009/, 2009.

Galloway, J. N., Dentener, F. J., Capone, D. G., Boyer, E. W., Howarth, R. W., Seitzinger, S. P., Asner, G. P., Cleveland, C. C., Green, P. A., Holland, E. A., Karl, D. M., Michaels, A. F., Porter, J. H., Townsend, A. R., and Vörosmarty, C. J.: Nitrogen cycles: Past, present, and future, Biogeochemistry, 70, 153–226, doi:10.1007/s10533-004-0370-0, URL http://dx.doi.org/10.1007/s10533-004-0370-0http://www.springerlink.com/openurl.asp?id=doi:10.1007/s10533-004-0370-0, 2004.

Gordon, C., Herrera, R., and Hutchinson, T.: Studies of fog events at two cloud forests near Caracas, Venezuela-II. Chemistry of fog, Atmos. Environ., 28, 323–337, URL http://www.sciencedirect.com/science/article/pii/1352231094901082, 1994a.

Gordon, C. A., Herrera, R., and Hutchinson, T. C.: Studies of fog events at two cloud forests near Caracas, Venezuela-I. Frequency and duration of fog, Atmos. Environ., 28, 317–322, doi:10.1016/1352-2310(94)90107-4, 1994b.

Homeier, J., Hertel, D., Camenzind, T., Cumbicus, N. L., Maraun, M., Martinson, G. O., Poma, L. N., Rillig, M. C., Sandmann, D., Scheu, S., Veldkamp, E., Wilcke, W., Wullaert, H., and Leuschner, C.: Tropical andean forests are highly susceptible to nutrient inputs–rapid effects of experimental N and P addition to an ecuadorian montane forest., PLoS One, 7, e47 128, doi:10.1371/journal.pone.0047128, URL http://www.pubmedcentral.nih.gov/articlerender.fcgi?artid=3468540{&}tool=pmcentrez{&}rendertype=abstract, 2012.

Koehler, B., Corre, M. D., Veldkamp, E., Wullaert, H., and Wright, S. J.: Immediate and long-term nitrogen oxide emissions from tropical forest soils exposed to elevated nitrogen input, Glob. Chang. Biol., 15, 2049–2066, doi:10.1111/j.1365-2486.2008.01826.x, URL http://doi.wiley.com/10.1111/j.1365-2486.2008.01826.x, 2009.

Lewis, S. L., Malhi, Y., and Phillips, O. L.: Fingerprinting the impacts of global change on tropical forests., Philos. Trans. R. Soc. Lond. B. Biol. Sci., 359, 437–62, doi:10.1098/rstb.2003.1432, URL http://www.pubmedcentral.nih.gov/articlerender.fcgi?artid=1693339{&}tool=pmcentrez{&}rendertype=abstract, 2004.

Lovett, G. and Kinsman, J.: Atmospheric pollutant deposition to high-elevation ecosystems, Atmos. Environ., 24, 2767–2786, URL http://www.sciencedirect.com/science/article/pii/096016869090164I, 1990.

Matson, P., Lohse, K. A., and Hall, S. J.: The globalization of nitrogen deposition: Consequences for terrestrial ecosystems, Ambio, 31, 113–119, URL http://www.jstor.org/stable/4315223, 2002.

Matson, P. a., McDowell, W. H., Townsend, A. R., and Vitousek, P. M.: The globalization of N deposition: Ecosystem consequences in tropical environments, Biogeochemistry, 46, 67–83, doi:10.1007/BF01007574, URL http://www.springerlink.com/index/10.1007/BF01007574, 1999.

Mayer, R., Liess, S., Lopes, M. I. M. S., and Kreutzer, K.: Atmospheric pollution in a tropical rain forest: effects of deposition upon biosphere and hydrosphere I. Concentrations of chemicals, Water. Air. Soil Pollut., 121, 79–92, doi:10.1023/A:1005249615589, URL http://link.springer.com/article/10.1023/A:1005201732427http://link.springer.com/article/10.1023/A:1005249615589, 2000.

McDowell, W. H., Ginés Sánchez, C., Asbury, C. E., and Ramos Pérez, C. R.: Influence of sea salt aerosols and long range transport on precipitation chemistry at El Verde, Puerto Rico, Atmos. Environ., 24A, 2813–2821, URL http://www.sciencedirect.com/science/article/pii/096016869090168M, 1990.

Morales, J., Bifano, C., and Escalona, A.: Atmospheric deposition of SO_4-S and (NH_4 + NO_3)-N at two rural sites in the western Maracaibo Lake basin, Venezuela, Atmos. Environ., 32, 3051–3058, URL http://www.sciencedirect.com/science/article/pii/S135223109700160X, 1998.

Mu, M., Randerson, J. T., van der Werf, G. R., Giglio, L., Kasibhatla, P., Morton, D., Collatz, G. J., DeFries, R. S., Hyer, E. J., Prins, E. M., Griffith, D. W. T., Wunch, D., Toon, G. C., Sherlock, V., and Wennberg, P. O.: Daily and 3-hourly variability in global fire emissions and consequences for atmospheric model predictions of carbon monoxide, Journal of Geophysical Research: Atmospheres, 116, n/a–n/a, doi:10.1029/2011JD016245, URL http://dx.doi.org/10.1029/2011JD016245, d24303, 2011.

Muoghalu, J.: Contributions of throughfall, stemflow and litterfall to nutrient cycling in a secondary lowland rain forest in Ile-Ife, Nigeria, J. Trop. For. Sci., 15, 399–410, URL http://scholar.google.com/scholar?hl=en{&}btnG=Search{&}q=intitle:Contributions+of+throughfall,

+stemflow+and+litterfall+to+nutrient+cycling+in+a+secondary+lowland+rain+forest+in+ILE-IFE,+Nigeria{#}0, 2003.

Phoenix, G. K., Hicks, K. W., Cinderby, S., Kuylenstierna, J. C. I., Stock, W. D., Dentener, F. J., Giller, K. E., Austin, A. T., Lefroy, R. D. B., Gimeno, B. S., Ashmore, M. R., and Ineson, P.: Atmospheric nitrogen deposition in world biodiversity hotspots: the need for a greater global perspective in assessing N deposition impacts, Glob. Chang. Biol., 12, 470–476, doi:10.1111/j.1365-2486.2006.01104.x, URL http://dx.doi.org/10.1111/j.1365-2486.2006.01104.x, 2006.

Richter, A.: Satellite measurements of NO_2 from international shipping emissions, Geophys. Res. Lett., 31, 4–7, doi:10.1029/2004GL020822, URL http://www.agu.org/pubs/crossref/2004/2004GL020822.shtml, 2004.

Richter, A., Burrows, J. P., Nüß, H., Granier, C., and Niemeier, U.: Increase in tropospheric nitrogen dioxide over China observed from space, Nature, 437, 129–132, doi:10.1038/nature04092, URL http://www.nature.com/doifinder/10.1038/nature04092, 2005.

Rollenbeck, R.: Global sources-local impacts: natural and anthropogenic sources of matter deposition in the Andes of Ecuador, Geo-öko, pp. 5–27, 2010.

Rollenbeck, R., Bendix, J., Fabian, P., Boy, J., Wilcke, W., Dalitz, H., Oesker, M., and Emck, P.: Comparison of different techniques for the measurement of precipitation in tropical montane rain forest regions, J. Atmos. Ocean. Technol., 24, 156–168, doi:10.1175/JTECH1970.1, URL http://journals.ametsoc.org/doi/abs/10.1175/JTECH1970.1, 2007.

Rollenbeck, R., Bendix, J., and Fabian, P.: Spatial and temporal dynamics of atmospheric water inputs in tropical mountain forests of South Ecuador, Hydrol. Process., 25, 344–352, doi:10.1002/hyp.7799, URL http://doi.wiley.com/10.1002/hyp.7799, 2011.

Schemenauer, R. S. and Cereceda, P.: A proposed standard fog collector for use in high-elevation regions, J. Appl. Meteorol., 33, 1313–1322, URL http://adsabs.harvard.edu/abs/1994JApMe..33.1313S, 1994.

Sigha-Nkamdjou, L., Galy-Lacaux, C., Pont, V., Richard, S., Sighomnou, D., and Lacaux, J.: Rainwater chemistry and wet deposition over the equatorial forested ecosystem of Zoétélé (Cameroon), J. Atmos. Chem., 46, 173–198, URL http://link.springer.com/article/10.1023/A:1026057413640, 2003.

Stohl, A., Wotawa, G., Seibert, P., and Kromp-Kolb, H.: Interpolation errors in wind fields as a function of spatial and temporal resolution and their impact on different types of kinematic trajectories, doi:10.1175/1520-0450(1995)034<2149:IEIWFA>2.0.CO;2, 1995.

Unger, M., Homeier, J., and Leuschner, C.: Effects of soil chemistry on tropical forest biomass and productivity at different elevations in the equatorial Andes, Oecologia, 170, 263–274, doi:10.1007/s00442-012-2295-y, URL http://link.springer.com/10.1007/s00442-012-2295-y, 2012.

Vallack, H. and Cinderby, S.: Emission inventories for SO2 and NOx in developing country regions in 1995 with projected emissions for 2025 according to two scenarios, Water. Air. Soil Pollut., 130, 217–222, URL http://www.springerlink.com/index/K8P3G04068343X3N.pdf, 2001.

van der Werf, G. R., Randerson, J. T., Giglio, L., Collatz, G. J., Mu, M., Kasibhatla, P. S., Morton, D. C., DeFries, R. S., Jin, Y., and van Leeuwen, T. T.: Global fire emissions and the contribution of deforestation, savanna, forest, agricultural, and peat fires (1997-2009), Atmos. Chem. Phys., 10, 11 707–11 735, doi:10.5194/acp-10-11707-2010, URL http://www.atmos-chem-phys.net/10/11707/2010/, 2010.

Williams, M. R., Fisher, T. R., and Melack, J. M.: Chemical composition and deposition of rain in the central Amazon, Brazil, Atmos. Environ., 31, 207–217, doi:10.1016/1352-2310(96)00166-5, URL http://www.sciencedirect.com/science/article/pii/1352231096001665http://www.sciencedirect.com/science/article/B6VH3-3SVHG1X-8/2/d033b026107388fe3f991cd9b492e31c, 1997.

Wolf, K., Veldkamp, E., Homeier, J., and Martinson, G. O.: Nitrogen availability links forest productivity, soil nitrous oxide and nitric oxide fluxes of a tropical montane forest in southern Ecuador, Global Biogeochem. Cycles, 25, GB4009, doi:10.1029/2010GB003876, URL http://www.agu.org/pubs/crossref/2011/2010GB003876.shtml, 2011.

Yoboué, V., Galy-Lacaux, C., Lacaux, J. P., and Silué, S.: Rainwater Chemistry and Wet Deposition over the Wet Savanna Ecosystem of Lamto (Côte d'Ivoire), J. Atmos. Chem., 52, 117–141, doi:10.1007/s10874-005-0281-z, URL http://link.springer.com/10.1007/s10874-005-0281-z, 2005.

Chapter 4

Natural or anthropogenic? On the origin of atmospheric sulfate deposition in the Andes of southeastern Ecuador

Sandro Makowski Giannoni, Rütger Rollenbeck, Katja Trachte and Jörg Bendix

ATMOSPHERIC CHEMISTRY AND PHYSICS

ATMOS. CHEM. PHYS., 14, 11297-11312, 2014

Received: 04 March 2014
Revised: 05 September 2014
Accepted: 15 September 2014
First published online: 28 October 2014
DOI: 10.5194/acp-14-11297-2014

Abstract

Atmospheric sulfur deposition above certain limits can represent a threat to tropical forests, causing nutrient imbalances and mobilizing toxic elements that impact biodiversity and forest productivity. Atmospheric sources of sulfur deposited by precipitation have been roughly identified in only a few lowland tropical forests. Even scarcer are studies of this type in tropical mountain forests, many of them mega-diversity hotspots and especially vulnerable to acidic deposition. In these places, the topographic complexity and related streamflow conditions affect the origin, type, and intensity of deposition. Furthermore, in regions with a variety of natural and anthropogenic sulfur sources, like active volcanoes and biomass burning, no source emission data has been used for determining the contribution of each source to the deposition. The main goal of the current study is to evaluate sulfate (SO_4^-) deposition by rain and occult precipitation at two topographic locations in a tropical mountain forest of southern Ecuador, and to trace back the deposition to possible emission sources applying back-trajectory modelling. To link upwind natural (volcanic) and anthropogenic (urban/industrial and biomass-burning) sulfur emissions and observed sulfate deposition, we employed state-of-the-art inventory and satellite data, including volcanic passive degassing as well. We conclude that biomass-burning sources generally dominate sulfate deposition at the evaluated sites. Minor sulfate transport occurs during the shifting of the predominant winds to the north and west. Occult precipitation sulfate deposition and likely rain sulfate deposition are mainly linked to biomass-burning emissions from the Amazon lowlands. Volcanic and anthropogenic emissions from the north and west contribute to occult precipitation sulfate deposition at the mountain crest Cerro del Consuelo meteorological station and to rain-deposited sulfate at the upriver mountain pass El Tiro meteorological station.

4.1 Introduction

Sulfur enters the atmosphere principally as sulfur dioxide (SO_2), an air pollutant with a lifetime of about 1 to 2 days, before it is normally deposited or oxidized into sulfate (SO_4^-). After oxidation, lifetime increases to 3 or more days, depending on the state of the atmosphere and the injection height. Because of its longer lifetime, sulfate can be spread over greater distances. In high concentrations, sulfate decreases the pH of precipitation to levels that represent a threat to health and ecosystems. This phenomenon called "acid rain" has been discussed in the past, particularly in the industrialized countries of Europe and North America where adverse effects were found to be more serious for health than for ecosystems (Menz and Seip 2004).

In tropical ecosystems, only a few studies are available despite the fact that they are mostly characterized by an interference-prone biogeochemical cycle and nutrient limitation (Elser et al. 2007; Wullaert 2010), and hence particularly sensitive to acid deposition (Boy et al. 2008; Delmelle et al. 2002; Kuylenstierna et al. 2001). Kuylenstierna et al. (2001), for example, revealed that acidification from atmospheric sulfur could represent a threat to tropical ecosystems in developing countries. Acidification of soil due to persistent increases in sulfate inputs could lead to nutrient imbalances and changes in ecosystem diversity and productivity (Greaver et al. 2012; Phoenix et al. 2006). It can also mobilize many potentially toxic elements that promote soil degradation and erosion in some areas. Acid and toxic elements can leach out of the soil by rain and go into groundwater and nearby water bodies (Ljung et al. 2009). Considering these adverse effects of acidic deposition in land ecosystems, serious impacts can be expected, especially in highly biodiverse and disturbance-sensitive forest ecosystems. The probability that undisturbed tropical forests suffer from these detrimental impacts increases if we bear in mind that emissions and related deposition in developing countries, where most of megadiverse tropical forests are found, are rapidly intensifying and that 50–80 % of the fraction of deposition on land falls on natural vegetation (Dentener et al. 2006).

Regarding the sources of deposition, SO_2 is emitted from different natural and anthropogenic processes. Volcanoes are considered the most important natural sources representing around 26–35 % of total global emissions (Graf et al. 1997; Stevenson et al. 2003). The most important anthropogenic sources are fossil fuel combustion for energy production, transportation, and industrial activities in big cities and their surroundings, and biomass burning from deforestation, land clearing, and bush fires (Lee et al. 2011; Smith et al. 2011). The contribution of each to the total SO_2 emissions may vary depending on the region and its developmental state (industrial or industrializing countries). However, in some tropical regions (e.g., Ecuador) volcanic emissions and biomass burning might

contribute larger amounts as a consequence of the density of active volcanoes (Carn et al. 2008) and an accelerated land use change mostly characterized by deforestation for creating arable land (Crutzen and Andreae 1990; Rudel et al. 2005).

On a local to regional scale, detailed knowledge on pollutant deposition from rain and cloud water in specific regions, its sources, and its smaller-scale spatial variability, particularly in complex terrain as that of the Andes, is still scarce. To date, only few studies on atmospheric acidic deposition exist for tropical ecosystems and those including a characterization of source emissions are very rare.

Precipitation chemistry surveys in some montane but mainly lowland tropical forests of Costa Rica, Venezuela, Puerto Rico, Cameroon, and Brazil have characterized nutrient and pollutant deposition by analyzing ionic concentrations, sulfate among others, and in situ meteorological parameters. In Venezuela and Cameroon, Morales et al. (1998); Sigha-Nkamdjou et al. (2003) indicated the relative importance of local sources, such as biogenic sulfur oxidation by swamps and lakes, to sulfate deposition. However, industrial emissions were indicated as the most important source of sulfate deposition in Venezuela. The opposite was found by Eklund and McDowell (1997) and Gordon et al. (1994) in Costa Rica and Puerto Rico, respectively, where no significant pollution footprints where found in the samples of the two studied tropical mountain forests. The same was noticed by Pauliquevis et al. (2012) in the central Amazon of Brazil, where high sulfate loads in rainwater likely stem from the oxidation of sulfur compounds from the Atlantic Ocean.

In areas with an important number of active volcanoes like Indonesia, Costa Rica, and Nicaragua, volcanic emissions were given special attention as contributors of acidic sulfate deposition in the surrounding areas and downwind of the emitting craters (Pfeffer et al. 2006; Langmann and Graf 2003; Delmelle et al. 2001, 2002). For central Africa and tropical South America, however, emissions from burning forests, savannas, and agricultural fields were claimed to be the principal source of atmospheric pollution (Hansen et al. 2013; Rissler et al. 2006; van der Werf et al. 2010) and reactive sulfur deposition in the downwind regions (Diehl et al. 2012; Fabian et al. 2005).

With regard to the mega-diverse tropical mountain rain forest in the southeastern Ecuadorian Andes (Bendix and Beck 2009), biomass burning in the Amazon has been hitherto identified as the principal source of atmospheric sulfate deposition (Beiderwieden et al. 2005; Boy et al. 2008; Fabian et al. 2005, 2009; Rollenbeck et al. 2011). However, volcanic and biomass-burning emissions were included by roughly estimated data. Given the dense concentration of active volcanoes in Ecuador, where as much as 95 % of emissions can stem from non-eruptive degassing, and considering the difference in

emissions between burned areas depending on land use type, it is of utmost importance to include data on source emissions as accurate as possible to characterize air mass pollution history leading to the deposition. Furthermore, preliminary work on nitrogen deposition has shown that crest areas considerably differ in their behavior from valley sites (Makowski Giannoni et al. 2013). Hence, a comprehensive deposition analysis must not only investigate sinks and source intensities but should also study different topographic positions.

Consequently, the main aim of the current study is (1) to determine sulfate deposition at two different topographic positions in the mountain rain forest of southern Ecuador and (2) to trace back the deposition to different natural and anthropogenic emission sources applying back-trajectory modelling. To link the spatiotemporal patterns of upwind natural (volcanoes) and anthropogenic (urban/industrial and biomass-burning) sulfur emissions to sulfate deposition at site, we used the latest state-of-the-art inventories and satellite data and also considered volcanic passive degassing.

4.2 Geographical setting

The Reserva Biológica San Francisco (RBSF) (4°00 S and 79°00 W) is located in a remote area at the outer edge of the Amazon, on the eastern slopes of the southern Ecuadorian Andes, between the humid Amazon plains and the dryer inter-Andean valleys. The RBSF lies within the small San Francisco River catchment between the capital cities of Loja and Zamora (Fig. 4.1). Since 2002, the protected forest and the pastures outside of the reserve have been the subject of investigations from two successive multidisciplinary research groups funded by the German Research Council (DFG) (Bendix et al. 2013; Beck et al. 2008). The terrain height of the area is lower compared to the northern and southern Andes and its topography more complex, as the system of few parallel mountain ranges gives way to a net of small valleys and *cordilleras* (Rollenbeck et al. 2011).

There are only a few sources of pollution in the vicinity of the RBSF. The cities of Loja ($\sim$ 214 855 inhabitants, 10 km to the west; INE 2010) and Zamora ($\sim$ 25 510 inhabitants, 14 km southeast; INE 2010) are quite small and without any notable industrial activity. Between October and December, a relative dry season, slash-and-burn techniques are a common practice in local pasture management which quite often runs out of control, burning adjacent areas of forest (Bendix et al. 2008b; Curatola Fernández et al. 2013; Hartig and Beck 2003).

The synoptic winds at the upper levels of the *cordillera* consist of tropical easterly trades over more than 70 % of the year. Northeasterlies prevail between January and

March while southeasterlies dominate between June and September. The remaining 30 % of the year corresponds with the westerlies and northerlies, mainly occurring between the end of October and December (Bendix et al. 2008a; Emck 2007).

Precipitation varies, mainly depending on the migration of the Intertropical Convergence Zone (ITCZ) and the variation in the direction of the tropical easterlies. The associated humidity advection dominates the amount of atmospheric water entering the ecosystem. The total annual average of rainfall (rainfall and occult precipitation) range from 1850 to 6300 mm year^{-1} along an altitudinal gradient of between 1960 and 3180 m a.s.l. Occult precipitation (OP) frequencies of up to 85 % of the year occur particularly in the more elevated parts of the research area, when warm and humid air masses from the Amazon lowlands hit the Andes, leading to intense condensation and immersion in clouds (Bendix et al. 2006a,b; Emck 2007; Rollenbeck 2010).

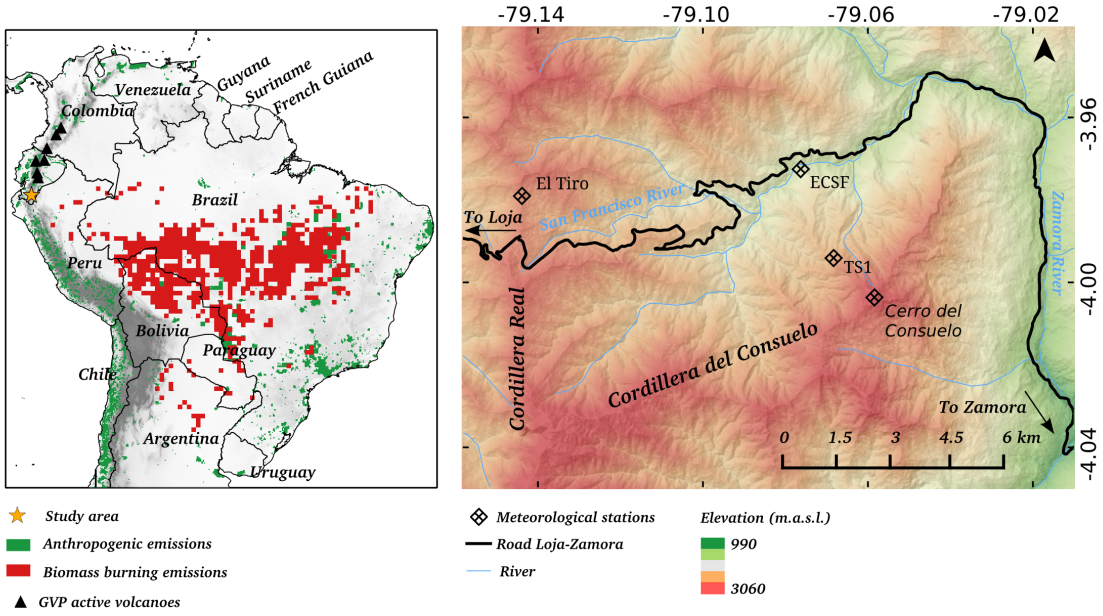

Figure 4.1: Study area. The left map shows possible anthropogenic and biomass-burning SO_2 sources in tropical South America and the location of active volcanoes in Ecuador and Colombia. The right map depicts the study area in the River San Francisco catchment and the location of the meteorological stations (MSs) involved in the study.

4.3 Data and methods

In the present study, we discuss the variation of sulfate concentration/deposition in precipitation in a 5-year period (2005–2009) at two meteorological stations (MSs). Higher locations are more vulnerable to higher deposition (Makowski Giannoni et al. 2013), hence the selection of the two highest MSs in the RBSF for this study. Because of the

strong winds at the locations of sampling, we will refer to all types of light precipitation, from wind-driven drizzle down to fog and cloud droplets as OP.

For studying source–receptor relationships, we brought together measurements of sulfate concentrations in rain and OP samples with back-trajectory transport modelling using satellite and emission inventories as inputs. The modelling of SO_2 transport, hereinafter referred to as "SO_2 transport", results in SO_2 daily concentration values at the target coordinates which match the observation sites.

The following section (4.3.1–4.3.2) is devoted to a detailed description of the data and methods used. Section 4.3.2 mentions and discusses the techniques employed to unveil the relationships between in situ observations and transport to the observation sites.

4.3.1 Data

Sulfate in rain and OP

We measured rainfall and OP at two MSs: one installed on the highest surrounding peak (Cerro del Consuelo, 3180 m a.s.l.) and the other one on an upriver mountain pass (El Tiro, 2870 m a.s.l.), separating the basin of Loja in the west from the eastern slopes of the Andean mountain range (Fig. 4.1).

The collection of samples was conducted on a weekly basis between 2005 and 2009. Rain was sampled using UMS-RS 200 polyethylene rain samplers of 20 cm diameter. Standard fog collectors (Schemenauer and Cereceda 1994) were used to sample OP. With a size of 1 $\times$ 1 m and composed of polypropylene nets with a 2 $\times$ 1 mm mesh width, they were set up at 90° with respect to the main wind direction and collected all types of deposition, such as particles, aerosols, and gases (Fabian et al. 2005).

We did not use wet-only collectors, so dry deposition likely adds to the total deposition. For the fog collectors, Schemenauer et al. (1995) estimated the contribution of dry deposition to the total deposition to be less than 5 % for temperate mountain forests of North America. Because of the very humid conditions at our study site (high frequency of cloud immersion, around 85 % of the time, Bendix et al. 2008a) and the dense vegetation cover, which implies no sources for turbulent generation of local aerosol, dry deposition's contribution is most probably negligible for fog collectors (very probably less than that found by Schemenauer et al. 1995) and rain gauges. Considering that one of our goals is to evaluate sulfate inputs into the ecosystem, the catching efficiency from collectors in relation to trees is also an important parameter. For this, Schemenauer and Cereceda (1994) found good agreements between the collection rates of different tree species

and the standard fog collectors that we used in this study. For further details on field measurement techniques, calibration, and handling of the data, the reader is referred to Fabian et al. (2005) and (Rollenbeck et al. 2011, 2007). On the day of collection, electrical conductivity (WTW-LF 90) and pH (Methron 73065/682) of the samples were measured on site. Then, the samples were stored deep frozen until chemical analyses were carried out.

Ion chromatography (Dionex DX-210) was used to measure concentrations of sulfate ions in rain and OP water. The sulfate ions were taken as proxies of sulfur inputs into the ecosystem. Finally, time series of sulfate volume-weighted monthly mean (VWMM) concentrations and total deposition rates inrain and OP water were created for the period 2005–2009.

SO_2 source data

We used three recent emission inventories and one satellite data set as emission inputs to simulate the SO_2 transport to our study area: (a) one for anthropogenic emissions (EDGARv4, Janssens-Maenhout et al. 2012), (b) one for biomass-burning emissions (Global Fire Emissions Database (GFED) v3,Mu et al. 2011), and (c) one for emissions from volcanic degassing and explosive eruptions (Aerocom, Diehl et al. 2012). The ozone monitoring instrument (OMI) SO_2 data accounts mostly for SO_2 emissions from volcanoes, including passive degassing, but very strong anthropogenic pollution events are also detected by the sensor (Carn et al. 2008, 2007).

a. The emissions in EDGARv4 are calculated using a technology-based emission factor approach which includes country-specific emissions when these are available. Emissions are allocated spatially on $0.1 \times 0.1^\circ$ grid cells for point, line, and area sources built upon geographic data sets such as the location of energy and manufacturing facilities, road networks, and population density. In version 4, EDGAR delivers annual emission estimates from 1970 to 2008, which represents an improvement compared to former static inventories. For more information readers may visit the EDGAR website (`http://edgar.jrc.ec.europa.eu/index.php`).

b. For biomass-burning SO_2 estimates, we used the GFEDv3 inventory. The compilation of this inventory was based on a biogeochemical model (CASA-GFED) that approximates fuel loads and combustion completeness for each time step, and burned area data from satellite observations (van der Werf et al. 2010). Considering that fires are very often sporadic and transient, the high temporal and spatial resolution appear very advantageous when dealing with the variation of emissions in space and time. Some issues which might reduce the regional quality are the underestimation of emissions in the tropics because of cloud cover and canopy closeness, and gaps in the satellite coverage.

c. As part of the Aerocom global emission inventories, a daily resolved volcanic SO_2 emission data set was generated for the time period 1979–2009, including all volcanoes with historic eruptions listed in the Global Volcanism Program (`http://www.volcano.si.edu/`). Since volcanic emissions are in some cases occasional, the high temporal resolution of the inventory is indispensable for capturing the variability in the emission rates. Emissions for 1167 volcanoes considered to be active were compiled. The emissions originating from passive and quiescent degassing are also taken into account. The default SO_2 estimates are based on the volcanic sulfur index (VSI). In cases where data from the total ozone mapping spectrometer (TOMS), OMI, or the correlation spectrometer (COSPEC) were available, the respective values were replaced by emissions calculated from these observations. In other cases the default values were replaced by more precise estimations from the literature. For more information on the Aerocom volcanic SO_2 inventory, readers are referred to Diehl et al. (2012) and the Aerocom website (`http://aerocom.met.no/emissions.html`).

The OMI on board the polar-orbiting AURA satellite is a nadir solar backscatter spectrometer with a spatial footprint of 13 $\times$ 24 km that covers the earth's surface in 1 day. The instrument's UV-2 channel, which is used for the SO_2 retrievals, has a mean spectral resolution of 0.45 nm. Both its spatial and spectral resolution and its daily global coverage allow for a SO_2 retrieval-based monitoring of low emission sources like volcanic passive degassing and smelter plumes which was not possible with older instruments like TOMS or Global Ozone Monitoring Experiment (GOME) . OMI SO_2 data has already been successfully applied for daily monitoring of volcanic degassing in Ecuador (Carn et al. 2008) and the detection of SO_2 emissions from Peruvian copper smelters (Carn et al. 2007). Although the OMI instrument cannot distinguish between anthropogenic and volcanic SO_2 when co-occurring in close vicinity, Carn et al. (2007) concluded that anthropogenic sources in the coastal plains of Ecuador would only contribute less than 1 % to the total amount measured by OMI. In the current study, we used subsets of the OMI data replicating the same geographical domain defined by (Carn et al. 2008) for Ecuadorian volcanic emissions. The region selected is not affected by the South Atlantic anomaly, an artifact impacting the retrievals of a big area in central and southern South America (Lee et al. 2011); this means that OMI retrievals are reliable in the selected domain. The concentration retrieved by OMI was assumed to represent mainly the Ecuadorian volcanic emissions' contribution to the atmospheric SO_2 concentrations. Given its small geographic domain, the OMI data is set to account for regional emissions from Ecuador and southern Colombia.

4.3.2 Methods

Trajectory modelling

To link potential SO_2 source regions with the sulfate concentration measurements at our study site, a tool was developed which models the transport of SO_2 from upwind sources (biomass-burning, anthropogenic, and volcanic emissions) to our receptor area. The tool follows the path of the wind trajectories and adds the emission amounts from the pixels that prove spatial and temporal coincidence until a target point, which corresponds with the coordinates of the RBSF. No chemical or physical transformations are included in the modelling scheme. Scavenging and rainout processes are accounted for by a decay function integrated into the algorithm. For more details on the tool refer to Rollenbeck (2010) and Makowski Giannoni et al. (2013).

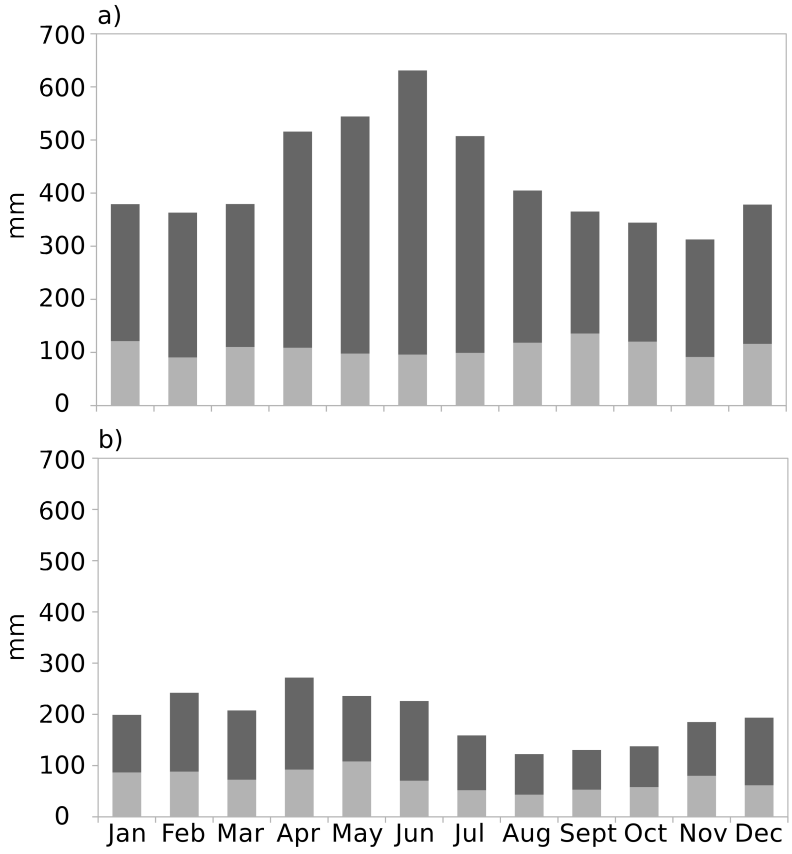

Figure 4.2: Rain (dark grey) and occult precipitation (OP) (light grey) monthly means for a) Cerro del Consuelo and b) El Tiro meteorological stations (MSs).

Observation and model data processing and evaluation

To calculate best estimates of precipitation (rain and OP), we used a method similar to the one used in the Goddard Institute for Space Studies Surface Temperature Analysis (GISTEMP, Hansen et al. 2010). Nearby MSs were used to evaluate unrealistic values and

to fill in data gaps of the MSs that we used in this study.

Time series of volume-weighted conductivity and pH monthly means were compiled and summary statistics such as median, median absolute deviation (MAD), and minimum and maximum values were calculated. For sulfate concentrations in both types of precipitation, VWMM were also calculated and time series covering the whole observation period were built. Here, we identified the time span in which peak values or regular phenomena took place, as well as long-term trends. All time series were then compared to check for acidification of the samples when highly loaded with sulfate ions.

Additionally, we calculated and analyzed annual mean deposition rates for El Tiro and Cerro del Consuelo MSs as having a measure of sulfate input variability per unit area, which is important for assessing potential impacts on ecosystems by a nutrient manipulation experiment (NUMEX, Homeier et al. 2012).

Table 4.1: pH and conductivity summary statistics in occult precipitation (OP) and rain samples from El Tiro and Cerro del Consuelo meteorological stations (MSs)

	El Tiro		Cerro del Consuelo	
	OP	Rain	OP	Rain
Median pH	4.8	5.4	5	5.3
	MAD = 0.37	MAD = 0.51	MAD = 0.29	MAD = 0.36
Min–max pH	2.4–5.8	3.7–6.7	1.8–6.2	3–6.1
Median conductivity ($S\,m^{-1}$)	10.9	3.7	2.6	8.1
	MAD = 6.4	MAD = 1.6	MAD = 1	MAD = 6.8
Min–max conductivity ($S\,m^{-1}$)	2.3–110.3	1.4–45.4	1.4–12.4	1.7–72

For source–receptor analysis, the daily transport model outputs were first aggregated according to the dates of sample collection in the field, in order to achieve comparable values for time series compilation and correlation analysis. We calculated the mean weekly values to compensate for irregular time intervals between the collection of samples. We then used these new values to calculate SO_2 transport monthly averages and to compile transport time series from the different emission sources represented by the emission inventories and satellite data. Before proceeding with statistical analysis, all the data was transformed to a logarithmic scale to approach normality. We then carried out a Pearson correlation analysis to test for correlations between field observations (VWMM sulfate concentrations) and model outputs (SO_2 transport); we used VWMM and not deposition values to avoid extra uncertainty added by new variables present in the deposition calculations. Finally, visual analysis of coincidences between transport and VWMM concentration time series was performed, taking into account events which could influence the transport of sulfate and its deposition into our study area.

In addition to the bivariate correlation analysis, we applied a factor analysis with varimax rotation to test for variance explanation from groups of variables.

4.4 Results

4.4.1 Emission sources and annual deposition

The highest precipitation and OP inputs were registered from April to July at Cerro del Consuelo MS (Fig. 4.2a), and in February and from April to June at El Tiro MS (Fig. 4.2b). A short dry season took place between September and November. Rain quantity varied significantly between dry and wet periods while OP inputs remained quite constant at around 100 mm for both MSs over the whole observation period.

The calculated volume-weighted monthly pH values in samples from Cerro del Consuelo MS yielded median values of 5.3 and 5 with a median absolute deviation (MAD) of 0.36 and 0.29 in rain and OP, respectively (Table 4.1). The water samples in both types of precipitation input tended to be acidic with some extreme values going as low as 1.86 in OP samples and 3 in rain samples. Occult precipitation sulfate concentration presented a negative and weak, but significant, correlation with pH values (Pearson, $r = -0.34$, $p < 0.05$). Conductivity values ranged between 1.4 and 72 S m^{-1}, with median values of 2.6 and 8.1 S m^{-1} in OP and rain, respectively. The bulk of the data ranged, nevertheless, between 1.4 and 14.3 S m^{-1}. Conductivity is a proxy of ion concentrations in water and thus, high conductivity values coincide with episodes of rain and OP water droplets with high ion loads.

In samples from El Tiro MS, pH volume-weighted values were in the acidic area of the spectrum too, with median values of 5.4 and 4.8 and MAD of 0.51 and 0.37 in rain and OP, respectively (Table 4.1). There was a strong negative correlation between sulfate concentration in OP and pH (Pearson, $r = -0.64$, $p < 0.001$), and a weaker one for sulfate concentration in rain (Pearson, $r = -0.34$, $p < 0.05$). Median conductivity values were generally higher when compared to those at Cerro del Consuelo MS. They yielded a median of 10.9 and 3.7 S m^{-1} in OP and rain, respectively. As opposed to what we observed at Cerro del Consuelo MS, conductivity was much higher in OP than in rain at El Tiro MS, meaning a strong ion load; values ranged between 1.4 and 110.3 S m^{-1}.

Figure 4.3 shows the annual sulfate deposition by rain and OP at (a) Cerro del Consuelo and b) El Tiro MSs. The deposition was generally higher for the Cerro del Consuelo MS for both types of precipitation. The only exception was the year 2009 where the OP deposition at El Tiro MS increased significantly in comparison to a decrease at

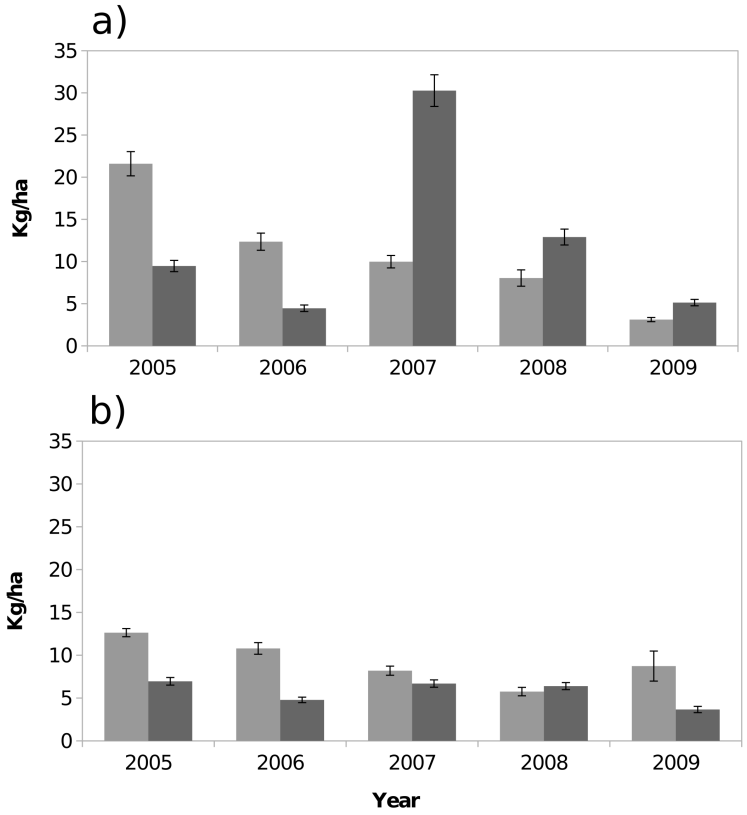

Figure 4.3: Total yearly sulfate (SO_4^-) deposition at a) Cerro del Consuelo and **b)** El Tiro meteorological stations (MSs). Dark grey bars represent deposition by rain and light grey bars, deposition by occult precipitation (OP).

Cerro del Consuelo MS. The highest amount of sulfate was deposited by rain in 2007 at the Cerro del Consuelo MS. Lowest burden was observed in rain samples from El Tiro MS in 2009. The figure shows that El Tiro MS was experiencing higher annual deposition rates by OP over nearly all years, pointing to a more advective environment. In contrary, Cerro del Consuelo MS was characterized by changing deposition maxima between rain and OP over time.

A tendency towards lower OP sulfate deposition (light grey bars) was observed in Fig. 4.3, with an upturn in 2009 for El Tiro MS. Deposition by rain (dark grey bars) was more oscillating, especially in the quantities deposited at Cerro del Consuelo MS. After 2008, a negative tendency in rain deposition became clearer.

Concerning the emissions, Fig. 4.4 depicts 5-year average maps of emissions for every data set used for simulating transport. From a rather local perspective, emissions from volcanoes appeared to be intense mainly close to the most active volcanoes: Sangay, Tungurahua, and Reventador (Fig. 4.4a). Emissions from big cities were only evident for the metropolitan region of Guayaquil and Quito. Still, much of the air above the region of

Guayaquil and the coast of Ecuador seems to have been contaminated with SO_2 emissions from volcanoes, which plumes were transported principally to the west and southwest and cover part of the ocean next to the southern coast of the country.The strong emissions east of Reventador most probably originate from deforestation activities. The high emission pixels at the same location in the biomass-burning data set (Fig. 4.4c) support this argument.

Figure 4.4b shows volcanic emissions from eruptions and passive degassing. Once again, Sangay, Tungurahua, and Reventador belong to the volcanoes that contribute the most to emissions in Ecuador. In Colombia, the Nevado del Huila and Galeras volcanoes are the strongest SO_2 emitters. For biomass burning, the main region is located in the Brazilian and Bolivian Amazon (Fig. 4.4c). The Venezuelan savanna in the northeast is another important biomass-burning region. The majority of potential anthropogenic sources (industrial, urban, and transportation) are located in the north of our study area (Fig. 4.4d). This occurs because of the extreme scarcity of significant sources in the east and because no air masses arriving to our study area originate and pass over the sources from the south.

4.4.2 Linking emissions to deposition

Correlation analyses

A first test, using a cross-correlation technique, is required to unveil the dependence of the transport data sets. This is shown in Table 4.2. Only moderate correlations for El Tiro and somewhat higher correlations for Cerro del Consuelo were revealed by this analysis. As expected, volcanic and anthropogenic source concentrations correlate well, while only low (partly negative) correlations between biomass-burning and anthropogenic and volcanic pollutant transport is visible. This means that there is some overlap in the data sets related to volcanic and anthropogenic emissions. The negative correlation between anthropogenic and biomass-burning emissions could indicate that their transport depends on changing wind directions (east for biomass-burning, north and west for anthropogenic) which means that the anthropogenic sources affecting the area are located more in the western and northern sectors.

To connect sinks with sources, correlation analysis between atmospheric SO_2 concentrations in the pixel representing the location of the observation site, derived by back-trajectory modelling, and the measured sulfate concentrations was conducted. Pearson's correlation coefficients calculated for sulfate concentration and SO_2 transport are presented in Table 4.3. It is observed that, even if significant, the correlations between source and sink data are generally low.

For the Cerro del Consuelo crest site, it is interesting to see that more evident correlations occur between OP and volcanic emissions. Because OMI includes volcanic emissions, it shows the second highest correlation coefficient for OP. The link to biomass burning seems to be generally weak at this altitude and topographical location of the *cordillera*.

Table 4.2: Cross-correlation of calculated SO_2 concentration time series over El Tiro and Cerro del Consuelo SO_2 transport pixels using the different emission data sets

	Biomass-burning (GFED SO_2)	Regional volcanic and strong anthropogenic (OMI SO_2)	Volcanic (Aerocom SO_2)	Anthropogenic (EDGAR SO_2)
(a) Pixel El Tiro				
Biomass-burning (GFED SO_2)	1			
Regional volcanic and strong anthropogenic (OMI SO_2)	0.01	1		
Volcanic (Aerocom SO_2)	0.14	0.42^{***}	1	
Anthropogenic (EDGAR SO_2) (EDGAR SO_2)	-0.29^{*}	0.52^{***}	0.66^{***}	1
b) Pixel Cerro del C.				
Biomass-burning (GFED SO_2) (GFED SO_2)	1			
Regional volcanic and strong anthropogenic (OMI SO_2)	0-0.13	1		
Volcanic (Aerocom SO_2)	0.13	0.60^{***}	1	
Anthropogenic (EDGAR SO_2)	0-0.35^{**}	0.69^{***}	0.76^{***}	1

Note: *** $p < 0.001$, ** $p < 0.01$, * $p < 0.05$.

The situation changes for the up-valley El Tiro MS, where the highest correlations occur between rain concentrations and anthropogenic sources and between OP concentrations and biomass-burning sources.

Even if the correlation coefficients are low, they show interesting tendencies. For the El Tiro site, volcanic and anthropogenic emissions are more clearly related to rain concentrations while the opposite is true for biomass-burning emissions, which is more strongly related to OP concentrations. OMI shows a mixed behavior because it includes volcanic as well as regional anthropogenic emissions as shown in Table 4.2 and Fig. 4.4.

Rather low correlation coefficients imply that no unique source can totally explain the oscillations in the concentrations. Furthermore, correlation coefficients are blurred because

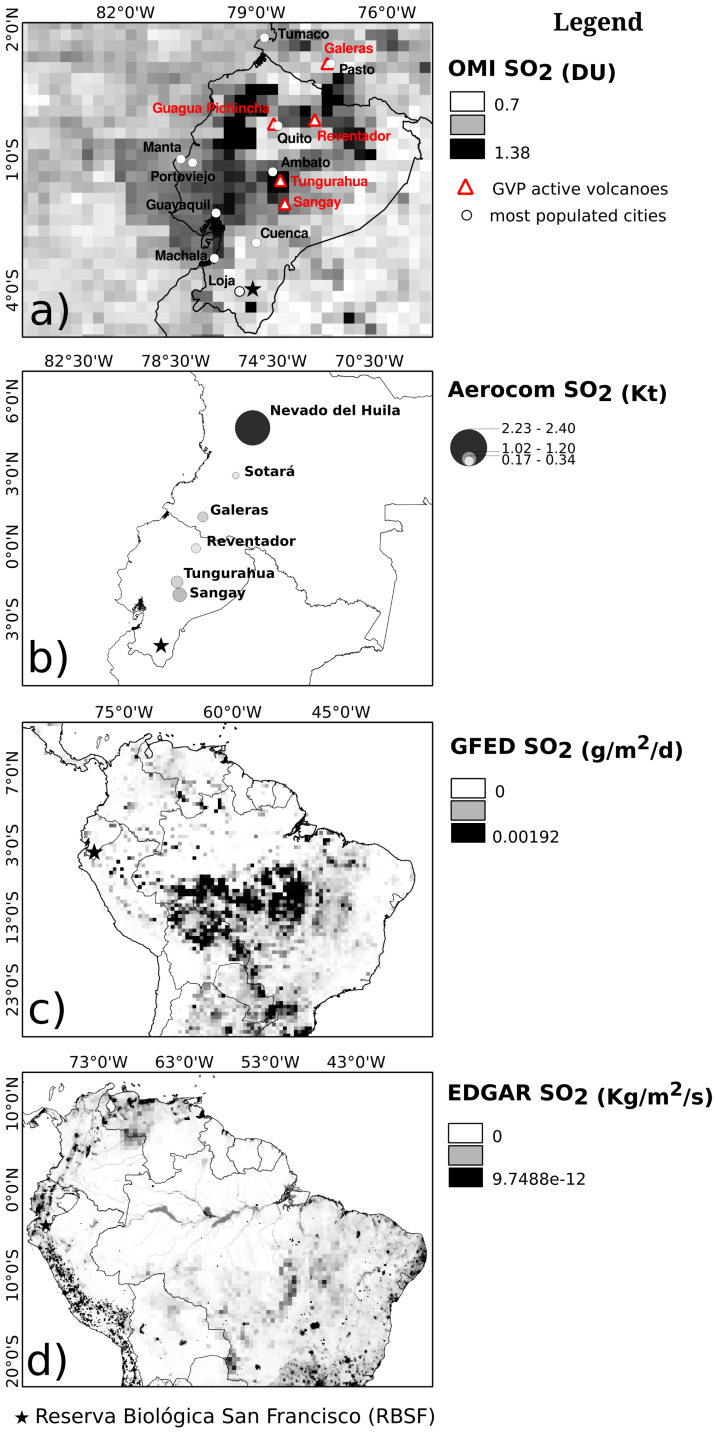

Figure 4.4: Average 2005–2009 source-dependent emission maps for a) volcanic and strong anthropogenic regional emissions, **b)** volcanic eruptive and passive degassing, c) biomass-burning, and d) anthropogenic emissions.

peaks are extreme values, which represent scatter. The concentration time series are a sum curve of all transport values. By exploring time series of sink and transport from sources, the next section sheds some light on what groups of transport variables explain the most of the variability in the concentration variables.

Analysis of monthly time series

Table 4.3: Cross-correlation matrix for SO_2 transport concentrations above El Tiro and Cerro del Consuelo pixels and sulfate concentrations from meteorological stations (MSs) at these two sites, located on an upriver mountain pass and on the highest catchment peak, respectively. Variables in bold represent measured sulfate (SO_4^-) concentrations and non-bold variables SO_2 transport. The acronym OP stands for occult precipitation

	Biomass-burning (GFED SO_2)	Regional volcanic and strong anthropogenic (OMI SO_2)	Volcanic (Aerocom SO_2)	Anthropogenic (EDGAR SO_2)
OP SO_4^- (El Tiro)	0.43^{***}	0.40^{**}	0.18	0.19
Rain SO_4^- (El Tiro)	0.08	0.33^{*}	0.39^{**}	0.46^{***}
OP SO_4^- (C. del Consuelo)	0.27	0.43^{**}	0.52^{***}	0.37^{**}
Rain SO_4^- (C. del Consuelo)	0.21	0.09	0.12	0.14

Note: *** $p < 0.001$, ** $p < 0.01$, * $p < 0.05$.

Figure 4.5 shows the time series of SO_2 transport (concentrations at the pixels above the study site) and the respective sulfate concentrations observed at the sites. We observed that mainly depending on emission state and air mass history, emission peaks resulted in concentration peaks of different intensity. One general finding is that the peak concentrations in biomass-burning transport were ~ 56 times higher than those of the other sources. Besides this there was a slight tendency of increasing emissions from anthropogenic, regional, and even volcanic sources in the observation period. At the same time, emissions due to biomass burning decreased, particularly in the last years of the study period (2008 and 2009) which is consistent with deforestation statistics in Brazil (Hansen et al. 2013; Rodrigues-Ramos et al. 2011; Torres et al. 2010).

Regarding the relationship between wind direction and the link between sources and sinks, it is obvious that during easterly airstreams coinciding with the Amazon biomass-burning season from August to October (dark grey bars) (Andreae et al. 2004), biomass emission peaks caused concentration peaks. Contrary to this, during wind conditions from the northern and western sector (light grey), peaks in volcanic activity and anthropogenic emissions in central/northern Ecuador is clearly related to concentration peaks.

El Tiro MS had higher sulfate loads in fog than in rain. A decrease following the reduction in biomass burning was observed in the OP sulfate concentration time series from 2007 to 2008, with a violent upturn at the end of the biomass-burning season of 2009

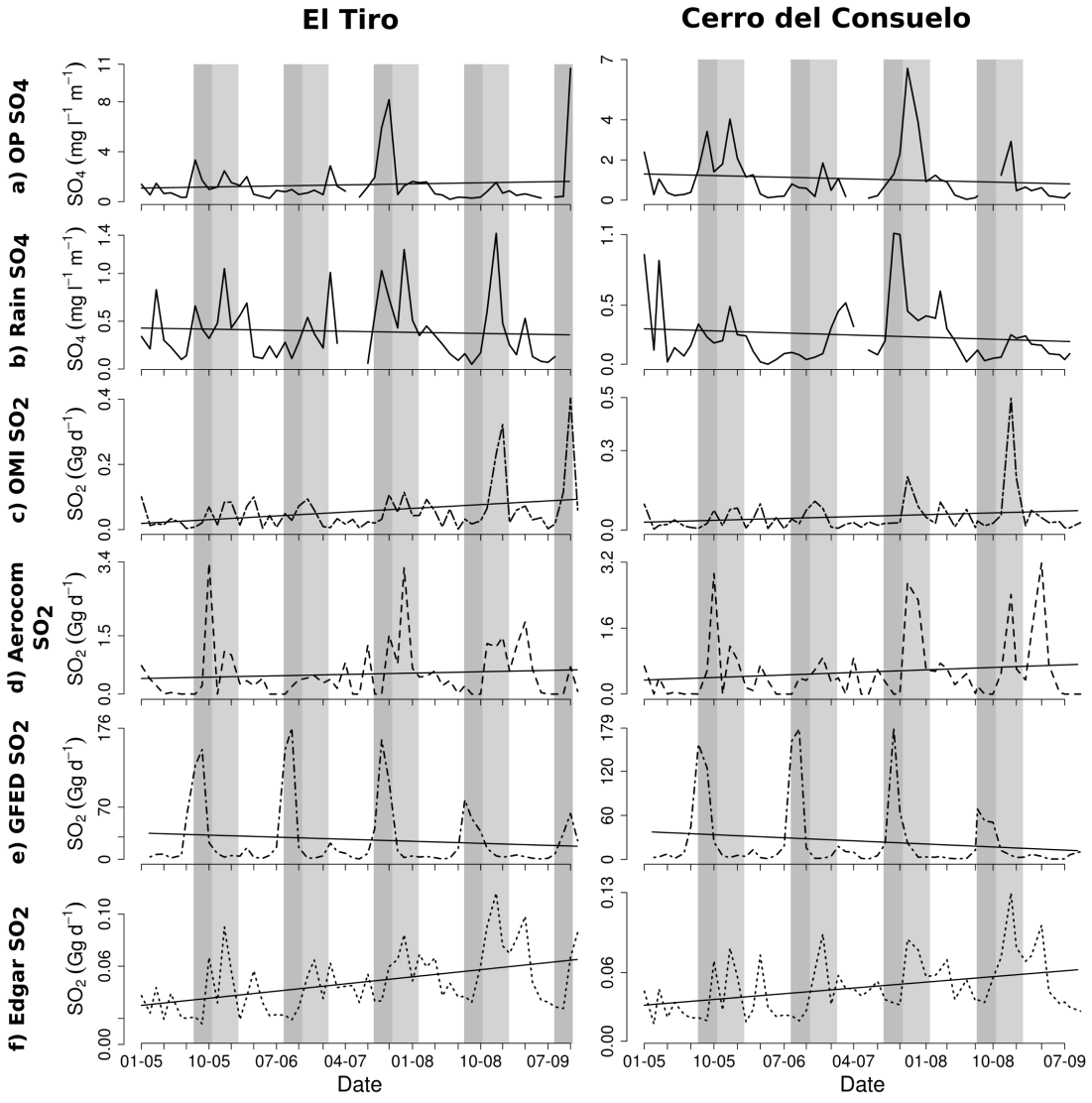

Figure 4.5: Time series comparing SO_2 transport from c) volcanic and strong anthropogenic regional emissions (OMI), d) volcanic emissions (Aerocom), e) biomass-burning emissions (GFED), and f) anthropogenic emissions (EDGAR), to measured sulfate concentrations in a) occult precipitation (OP) and b) rainwater from Cerro del Consuelo (right panel) and El Tiro (left panel) meteorological stations (MSs). The black straight line represents the line of best fit. Dark grey bars depict the Amazonian biomass-burning season (easterly wind direction) and light grey bars, the shift of the incoming air masses towards a northerly/northwesterly/westerly direction. Note the different scaling of the y axes.

(Fig. 4.5a) for which we have not found any explanation yet; this last peak is responsible for the light positive tendency of the curve. Rain sulfate time series (Fig. 4.5b) presented a small negative tendency over the observed period (2005–2009).

In OP, only one peak in the biomass-burning time series (July 2008) seemed to dominate the resulting concentrations. Volcanic transport did not play a role. In rain, biomass-burning and volcanic transport peaks were both reflected in the concentration time series, with a stronger coincidence with volcanic emissions. Anthropogenic sources and rainwater sulfate concentrations showed the same peak coincidences at El Tiro MS during northerly winds (particularly in 2005 and 2008). However, volcanic transport was quantitatively higher than that from anthropogenic sources, which means that it likely contributes more to the deposition.

At the uppermost and more-exposed Cerro del Consuelo MS we observe a different situation, namely a very small negative tendency in the sulfate concentrations in both OP (Fig. 4.5a) and rain (Fig. 4.5b). Occult precipitation sulfate concentrations are also higher than in rain here. In this case, the negative tendency of the biomass-burning SO_2 transport with the highest transport (Fig. 4.5e) seems to dominate the concentration's temporal development irrespective of the type of precipitation. Biomass-burning peaks affect only rain concentrations, except for one emission peak in August 2005, which affects both OP and rain concentrations (this is more or less the same for El Tiro MS). Interestingly, volcanic transport peaks (Fig. 4.5d) mostly affect OP concentrations. This is definitely different from El Tiro MS, where no influence in OP concentrations was noticed. EDGAR anthropogenic transport (Fig. 4.5f) is nonetheless also reflected in OP concentrations, but again here the transport was quantitatively lower.

Between March and May of 2005 to 2007, small peaks in the biomass-burning SO_2 transport time series can be seen which very likely correspond with the emissions of the Venezuelan savanna's biomass-burning season as observed by Hamburger et al. (2013). Apparently, this biomass-burning emission source has no significant resonance in the deposition at our study site. In 2008 and 2009 the peaks almost disappear, again coinciding with the anomalous biomass-burning season these 2 years (Torres et al. 2010).

Factor analysis

Table 4.4 presents the results from factor analysis applied to observational and modeled data. A main outcome is that the three first factors explain more than 80 % of the variance for both El Tiro and Cerro del Consuelo MSs.

For the Cerro del Consuelo MS, the eigenvectors show that biomass-burning SO_2

transport (GFED) was related to the sulfate concentrations in rain since both were loaded to the factors 2 and 3. The rest were more closely related to sulfate concentrations in OP, with loadings to factors 1, 4, and 5. The commonalities also show that factor 2 was dominated by biomass-burning SO_2 (GFED) and rain sulfate concentrations. Factor 1 shows important loadings of OP sulfate concentrations and SO_2 transport from all other source data sets (OMI, Aerocom, and EDGAR).

At the El Tiro MS, the relationship was inverse; biomass-burning SO_2 modeled transport and OP sulfate concentrations were more closely related, both of them contributing to factor 2. Loadings from rain sulfate concentrations and all other source data sets contributed to factor 1, and therefore they lay close in the multidimensional space. This is stressed by the commonalities, where both the variance of OP sulfate concentrations and biomass-burning SO_2 transport contributed mainly to factor 2, and rain sulfate concentrations and the SO_2 transport from the rest of emission sources to factor 1.

4.5 Discussion

In this study, we concerned ourselves with the identification of important natural and anthropogenic sources contributing to atmospheric sulfate deposition in the tropical mountain forests of southeastern Ecuador. Special attention was given to the contribution of natural volcanic emissions, given that the study site is located in a region with a very high density of active volcanoes (Carn et al. 2008).

Based on fire pixels, emission inventories, and back-trajectories, several previous studies (Fabian et al. 2009, 2005; Rollenbeck 2010; Rollenbeck et al. 2006) have pinpointed biomass burning as the principal source of atmospheric sulfate. These did not use, however, either data on explosive emissions or passive degassing, which represents a considerable part of the total volcanic emissions (Carn et al. 2008). Because of this fact, we have concluded that the contribution of volcanoes to the sulfate deposition in the area may have being underestimated.

Contrary to what we expected, we found that, quantitatively, volcanic emission sources did not play a substantial role, even if they were more important than anthropogenic emissions. Biomass-burning sources were indeed substantially dominant for two reasons: first, because easterlies are strong and constant, which is translated into preponderant air mass transport from the east (Bendix et al. 2008b), where the main biomass-burning region is located; second, because biomass-burning emissions in the Brazilian Amazon are strong and the burns cover a very large surface area (Giglio et al. 2010; Prins and Menzel 1992), making it more likely for the emissions to be advected.

Table 4.4: Eigenvectors and commonalities from factor analysis with varimax rotation, where a) shows the results of the data aggregated according to Cerro del Consuelo meteorological station (MS) sample collection dates and b) those for El Tiro MS

(a)	Eigenvectors					
	Factor 1	Factor 2	Factor 3	Factor 4	Factor 5	Factor 6
GFED SO_2	0.14	0.61	0.69	0.12	0.28	0.12
OMI SO_2	−0.48	−0.08	0.27	0.65	−0.40	−0.31
Aerocom SO_2	−0.51	−0.07	0.16	−0.44	0.46	−0.55
EDGAR SO_2	−0.53	−0.21	−0.02	0.17	0.39	0.70
Cerro del C. OP SO_4^-	−0.42	0.41	−0.005	−0.5	−0.58	0.25
Cerro del C. rain SO_4^-	−0.16	0.63	−0.64	0.30	0.23	−0.16
	Commonalities					
GFED SO_2	6 %	55 %	35 %	1 %	3 %	0 %
OMI SO_2	66 %	1 %	5 %	19 %	6 %	1 %
Aerocom SO_2	76 %	1 %	2 %	9 %	8 %	5 %
EDGAR SO_2	79 %	6 %	0 %	1 %	6 %	8 %
Cerro del C. OP SO_4^-	50 %	25 %	0 %	11 %	13 %	1 %
Cerro del C. rain SO_4^-	7 %	56 %	30 %	4 %	2 %	0 %
(b)	Eigenvectors					
GFED SO_2	0.04	0.69	0.24	0.51	0.45	0.01
OMI SO_2	−0.47	0.1	−0.68	0	0.24	0.50
Aerocom SO_2	−0.47	−0.25	0.25	0.64	−0.46	0.17
EDGAR SO_2	−0.5	−0.33	0.02	0.03	0.52	0.60
El Tiro OP SO_4^-	−0.34	0.56	−0.22	−0.18	−0.5	−0.48
El Tiro rain SO_4^-	−0.44	0.16	0.61	0.08	−0.53	0.34
	Commonalities					
GFED SO_2	0 %	75 %	4 %	14 %	7 %	0 %
OMI SO_2	56 %	1 %	34 %	0 %	2 %	7 %
Aerocom SO_2	56 %	10 %	5 %	22 %	7 %	1 %
EDGAR SO_2	64 %	17 %	0 %	0 %	9 %	10 %
El Tiro OP SO_4^-	30 %	50 %	4 %	2 %	8 %	6 %
El Tiro rain SO_4^-	50 %	4 %	28 %	15 %	0 %	3 %

Transport from the north and west occurred only for short periods and the sources of SO_2 did not cover such a big surface as biomass burning in the Brazilian Amazon did (Fig. 4.4c). However, no single emission sources explained the variability in the deposition, rather it was the sum of individual contributions, always depending on the type of precipitation and the topographic features of the site where samples where gathered.

The correlation analysis of SO_2 transport and sulfate concentrations resulted in some significant but not so strong correlations. Furthermore, the comparison of time series revealed that no single transport curve completely matches either OP or rain concentrations. The different source-related transport curves coincided only in specific time periods with the concentration curves, producing OP and/or rain deposition depending on the location of the MS. This is clarified in the following subsections and a graphical interpretation is given in Fig. 4.6.

4.5.1 Easterly transport

The correlation between El Tiro MS and biomass-burning transport was significant but weak only for OP samples. This relationship was supported by factor analysis.

In the period from August to October, the tropical easterlies still blow strongly and persistently and overlap with the occurrence of the biomass-burning season in the Amazon basin. Sulfur emissions, primarily from the Brazilian Amazon, are transported towards the west until they encounter the first foothills and *cordilleras* of the Andean mountain range, where intense scavenging of pollutants takes place. The connection to the emissions in the Amazon basin is mainly noticed in OP sulfate concentrations from El Tiro MS (dark grey bars in Fig. 4.5a, e). Here, concentration peaks coincide with SO_2 transport. Biomass-burning emissions have a mean low injection height into the atmosphere (max. 3 km, but only a very thin haze, while the main heating at 850 hPa has a mean injection height of 1.5 km, Davidi et al. 2009), which means that the pollution is transported in the lower valley upwards with the up-valley winds and hits the fog collectors at El Tiro (2660 m a.s.l.).

The same easterly air masses hit the mountain on top of which the Cerro del Consuelo MS is located, and are adiabatically uplifted producing intense rainfall and OP mainly windward but also on the summit. The fog collector is not located directly on the windward hillside, exposed to ascending air masses, so water with high ion loads is apparently mostly collected by the rain gauges, as shown by time series and factor analysis. However, measurements from fog collectors and rain gauges overlap here more frequently than at El Tiro, making the separation between rain and OP more difficult. The result is that the rain and OP differentiation is fuzzy, which blurs the correlations between concentrations and transport. Hence, the biomass-burning signal is relatively low here.

4.5.2 Northerly and westerly transport

Volcanic and anthropogenic transport were significantly correlated to sulfate concentrations from El Tiro MS rain samples and OP samples from Cerro del Consuelo MS. The same was also reflected in the results of the factor analysis.

Between October and January, as northerlies set in, the volcanic SO_2 transport time series coincide with those of sulfate concentrations from the MSs, especially regarding sulfate in rain, from El Tiro MS, and in OP from Cerro del Consuelo MS. The greater recurrence of coincidences with the rain time series at El Tiro MS is explained by its location at a mountain pass which links the eastern slopes and the inter-Andean valley of Loja. The two parallel east-to-west mountain ranges mark the boundaries of the San

Francisco Valley. As already mentioned (section 4.5.1), they shape the wind field, leading advected polluted air masses to come from the east or west, like biomass-burning transport, to impact the vegetation and the east–west oriented fog collectors on the mountain pass. Clouds advected from the north and northwest (likely charged with SO_2 ions) are partially blocked by the delimiting mountain range to the north. Hence, only rain gauges can collect sulfate scavenged from these clouds as rain drops traverse the atmosphere on their way to the ground.

Between 20 and 50 % of wind trajectories reach the RBSF from the north, passing over areas of active volcanoes. Volcanoes in the Andes lie at altitudes that in most cases exceed 4000 m a.s.l., so even emissions from degassing can contaminate high clouds in the lower troposphere (Stuefer et al. 2013; Diehl et al. 2012). During these months there is also an incremental increase in the transport of anthropogenic SO_2, most likely in response to air masses passing over emission sources from Ecuadorian and possibly Colombian cities. Anthropogenic sources in the Andes north of the RBSF also lie at high altitudes and, as recent studies have reported for Europe, this type of emissions can also reach higher atmospheric levels than previously assumed (Bieser et al. 2011). This would make anthropogenic plumes from Ecuadorian big cities in the Andes likely to reach higher clouds in the atmosphere as well. Therefore, northerly air masses charged with volcanic sulfate particles, and to a lesser extent anthropogenic particles, directly strike the mountain where

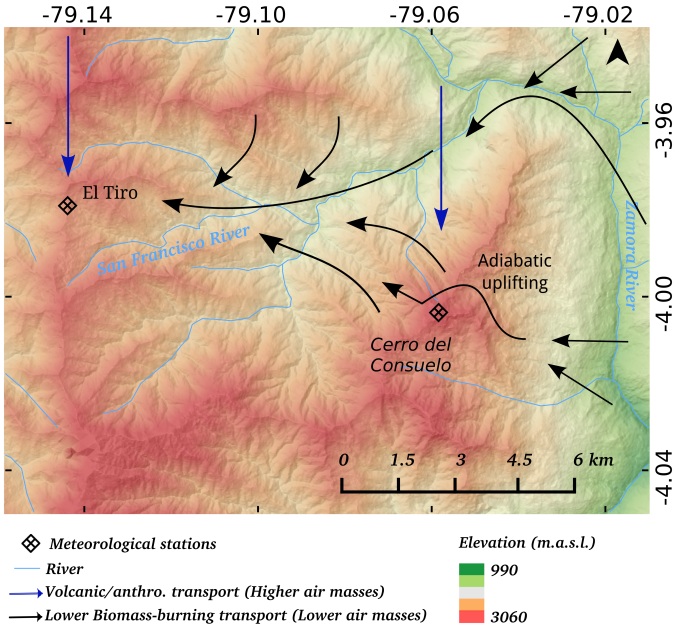

Figure 4.6: Representation of the deposition regimes observed in the study area. The blue arrows represent volcanic and anthropogenic transport from the north and northwest creating rain deposition at El Tiro meteorological station (MS) and occult precipitation (OP) deposition at Cerro del Consuelo MS. The black arrows represent biomass-burning transport from the east causing OP deposition at El Tiro MS and mainly rain deposition at Cerro del Consuelo MS.

the Cerro del Consuelo fog collector is located, on the windward (north-facing slopes) side. Occult precipitation water is here a major part of precipitation (41 % of rainfall; Bendix et al. 2008b). In addition, it is located at 3200 m a.s.l., probably more exposed to pollutants transported through higher atmospheric levels than El Tiro MS. Multicollinearity found between volcanic, anthropogenic, and regional (Ecuadorian) transport data sets reinforces this hypothesis (Table 4.2).

4.6 Conclusions

We conclude that biomass-burning sources dominate the sulfate deposition as a result of strong and persistent easterly sulfate transport of emissions from large burned areas of Amazon forests and from anthropogenic sources replacing the forests (pastures and croplands). These take place during the main Amazon biomass-burning season between August and October. Between October and December, the main wind direction shifts to the north and west, transporting volcanic and anthropogenic sulfate to our study site. The transport from these sources is, nonetheless, much less compared to biomass burning.

We found two different deposition regimes at the evaluated topographic sites. The up-valley mountain pass El Tiro is located on the eastern side of the ridge and is characterized by a more advective environment with dominating OP deposition from low tropospheric fire-polluted air masses from the Amazon lowlands. Sulfate from volcanic and anthropogenic emissions are episodically transported through a higher atmospheric level from the north and, as there is no cloud immersion during these wind directions, sulfate can be only deposited by rain.

At the highest mountain crest of the study area, Cerro del Consuelo, the situation is less homogeneous and less clear. Deposition was dominated by OP until 2007, when it started to be dominated by rain. Sulfate deposition by OP is likely linked to volcanic and anthropogenic sources in the north as a consequence of its higher location and its orientation. The higher atmospheric transport reaches Cerro del Consuelo MS from all wind directions and thus contaminates the cloud fog, resulting in OP deposition. According to the cross-correlation results, biomass burning has no significant relationship with this site's deposition. The overlapping of rain gauge and fog collector measurements made the differentiation of deposition types difficult. However, time series and factor analyses show a likely contribution of human-induced fires in the lowlands to sulfate deposition by rain at Cerro del Consuelo MS. The higher conductivity of the rain samples point to the likely higher contamination of the rain samples as well.

In general, this study revealed that even if volcanic emission are proximate and

numerous, they do not dominate the sulfate deposition at the RBSF. The shape and size of the sources, as well as the consistency of the winds, are important parameters that determined the dominance of biomass-burning emissions in the deposition at the study site. However, the importance of topography is also stressed as important parameter in determining the type and quantity of deposition in areas with complex terrain.

Author contributions

J. Bendix, R. Rollenbeck, and S. Makowski Giannoni designed the experiments and S. Makowski Giannoni carried them out.R. Rollenbeck developed the trajectory model code and S. Makowski Giannoni performed the simulations. S. Makowski Giannoni and K. Trachte collected, processed, and adapted the satellite data and emission inventories to the format requested for model runs. S. Makowski Giannoni analyzed the data and prepared the manuscript with contributions from all co-authors.

Acknowledgements

We thank the German Academic Exchange Service (DAAD) for funding the PhD thesis of S. Makowski Giannoni (Ref. no. A/08/98222) and the German Research Foundation (DFG) for the funding of the work in the scope of the Research Unit RU816 (funding no. BE 1780/15-1). We are grateful to Giulia F. Curatola Fernández, Lukas Lehnert, Nicolas Caspari, and Maik Dobermann for their valuable help. We also thank the foundation Nature & Culture International (NCI) Loja and San Diego for logistic support. We finally thank L. Zhang, and the two anonymous referees for their valuable comments and corrections.

Edited by: L. Zhang

Bibliography

Resultados del censo de población y vivienda, Tech. rep., Instituto Nacional de Estadística y Censos (INEC), URL http://www.ecuadorencifras.gob.ec/wp-content/descargas/Manu-lateral/Resultados-provinciales/, 2010.

Andreae, M. O., Rosenfeld, D., Artaxo, P., Costa, A. A., Frank, G. P., Longo, K. M., and Silva-Dias, M. A. F.: Smoking rain clouds over the Amazon., Science, 303, 1337–42, doi:10.1126/science.1092779, URL http://www.ncbi.nlm.nih.gov/pubmed/14988556, 2004.

Beck, E., Makeschin, F., Haubrich, F., Richter, M., Bendix, J., and Valarezo, C.: The Ecosystem (Reserva Biológica San Francisco), in: Gradients in a tropical mountain ecosystem of Ecuador, edited by Beck, E., Bendix, J., Kottke, I., Makeschin, F., and Mosandl, R., chap. 1, pp. 1–14, Springer, URL http://www.springer.com/life+sciences/ecology/book/978-3-540-73525-0, 2008.

Beiderwieden, E., Wrzesinsky, T., and Klemm, O.: Chemical characterization of fog and rain water collected at the eastern Andes cordillera, Hydrol. Earth Syst. Sci., 9, 185–191, doi:10.5194/hess-9-185-2005, URL http://www.hydrol-earth-syst-sci.net/9/185/2005/, 2005.

Bendix, J. and Beck, E.: Spatial aspects of ecosystem research in a biodiversity hot spot of southern Ecuador – an introduction, Erdkunde, 63, 305–308, doi:10.3112/erdkunde.2009.04.01, URL http://www.erdkunde.uni-bonn.de/archive/2009/spatial-aspects-of-ecosystem-research-in-a-biodiversity-hot-spot-of-southern-ecuador-an-introduction, 2009.

Bendix, J., Rollenbeck, R., Goettlicher, D., and Cermak, J.: Cloud occurrence and cloud properties in Ecuador, Clim. Res., 30, 133–147, doi:10.3354/cr030133, URL http://www.int-res.com/abstracts/cr/v30/n2/p133-147/, 2006a.

Bendix, J., Rollenbeck, R., and Reudenbach, C.: Diurnal patterns of rainfall in a tropical Andean valley of southern Ecuador as seen by a vertically pointing K-band Doppler radar, Int. J. Climatol., 26, 829–846, doi:10.1002/joc.1267, URL http://onlinelibrary.wiley.com/doi/10.1002/joc.1267/fullhttp://doi.wiley.com/10.1002/joc.1267, 2006b.

Bendix, J., Rollenbeck, R., Göttlicher, D., Nauß, T., Fabian, P., Goettlicher, D., Nauss, T., and Fabian, P.: Seasonality and diurnal pattern of very low clouds in a deeply incised valley of the eastern tropical Andes (South Ecuador) as observed by a cost-effective

webcam system, Meteorol. Appl., 15, 281–291, doi:10.1002/met, URL http://onlinelibrary.wiley.com/doi/10.1002/met.72/abstract, 2008a.

Bendix, J., Rollenbeck, R., Richter, M., Fabian, P., and Emck, P.: Climate, in: Gradients in a tropical mountain ecosystem of Ecuador, edited by Beck, E., Bendix, J., Kottke, I., Makeschin, F., and Mosandl, R., chap. 1, pp. 63–74, Springer Berlin / Heidelberg, ecological edn., URL http://dx.doi.org/10.1007/978-3-540-73526-7{\protect\T1\textbraceleft}{_}{\protect\T1\textbraceright}8, 2008b.

Bendix, J., Beck, E., Bräuning, A., Makeschin, F., Mosandl, R., Scheu, S., and Wilcke, W., eds.: Ecosystem services, biodiversity and environmental change in a tropical mountain ecosystem of South Ecuador, vol. 221 of *Ecological Studies*, Springer Berlin / Heidelberg, doi:10.1007/978-3-642-38137-9, URL http://link.springer.com/10.1007/978-3-642-38137-9, 2013.

Bieser, J., Aulinger, A., Matthias, V., Quante, M., and Denier van der Gon, H. A. C.: Vertical emission profiles for Europe based on plume rise calculations, Environ. Pollut., 159, 2935–2946, doi:10.1016/j.envpol.2011.04.030, URL http://www.ncbi.nlm.nih.gov/pubmed/21561695, 2011.

Boy, J., Rollenbeck, R., Valarezo, C., and Wilcke, W.: Amazonian biomass burning-derived acid and nutrient deposition in the north Andean montane forest of Ecuador, Global Biogeochem. Cycles, 22, GB4011, URL http://dx.doi.org/10.1029/2007GB003158, 2008.

Carn, S. A., Krueger, A. J., Krotkov, N. A., Yang, K., and Levelt, P. F.: Sulfur dioxide emissions from Peruvian copper smelters detected by the Ozone Monitoring Instrument, Geophys. Res. Lett., 34, doi:10.1029/2006GL029020, URL http://www.agu.org/pubs/crossref/2007/2006GL029020.shtml, 2007.

Carn, S. A., Krueger, A. J., Arellano, S., Krotkov, N. A., and Yang, K.: Daily monitoring of Ecuadorian volcanic degassing from space, J. Volcanol. Geotherm. Res., 176, 141–150, doi:DOI:10.1016/j.jvolgeores.2008.01.029, URL http://www.sciencedirect.com/science/article/B6VCS-4S0205V-1/2/2fe6d1fb29c1168746aed55392f8981a, 2008.

Crutzen, P. J. and Andreae, M. O.: Biomass burning in the tropics: impact on atmospheric chemistry and biogeochemical cycles., Science, 250, 1669–78, doi:10.1126/science.250.4988.1669, URL http://www.ncbi.nlm.nih.gov/pubmed/17734705, 1990.

Curatola Fernández, G. F., Silva, B., Gawlik, J., Thies, B., and Bendix, J.: Bracken fern frond status classification in the Andes of southern Ecuador: combining multispectral satellite data and field spectroscopy, Int. J. Remote Sens., 34, 7020–7037, doi:10.1080/01431161.2013.813091, URL http://www.tandfonline.com/doi/abs/10.1080/01431161.2013.813091, 2013.

Davidi, A., Koren, I., and Remer, L.: Direct measurements of the effect of biomass burning over the Amazon on the atmospheric temperature profile, Atmos. Chem. Phys., 9, 8211–8221, doi:10.5194/acp-9-8211-2009, URL http://www.atmos-chem-phys.net/9/8211/2009/acp-9-8211-2009.html, 2009.

Delmelle, P., Stix, J., Bourque, C. P.-A., Baxter, P. J., Garcia-Alvarez, J., and Barquero, J.: Dry deposition and heavy acid loading in the vicinity of masaya volcano, a major sulfur and chlorine source in Nicaragua, Environ. Sci. Technol., 35, 1289–1293, doi:10.1021/es000153m, URL http://dx.doi.org/10.1021/es000153m, 2001.

Delmelle, P., Stix, J., Baxter, P. J., and Garcia-Alvarez, J.: Atmospheric dispersion, environmental effects and potential health hazard associated with the low-altitude gas plume of Masaya volcano, Nicaragua, Bull. Volcanol., 64, 423–434, doi:10.1007/s00445-002-0221-6, URL http://link.springer.com/10.1007/s00445-002-0221-6http://link.springer.com/article/10.1007/s00445-002-0221-6, 2002.

Dentener, F., Drevet, J., Lamarque, J. F., Bey, I., Eickhout, B., Fiore, A. M., Hauglustaine, D., Horowitz, L. W., Krol, M., Kulshrestha, U. C., Lawrence, M., Galy-Lacaux, C., Rast, S., Shindell, D., Stevenson, D., Van Noije, T., Atherton, C., Bell, N., Bergman, D., Butler, T., Cofala, J., Collins, B., Doherty, R., Ellingsen, K., Galloway, J., Gauss, M., Montanaro, V., Müller, J. F., Pitari, G., Rodriguez, J., Sanderson, M., Solmon, F., Strahan, S., Schultz, M., Sudo, K., Szopa, S., and Wild, O.: Nitrogen and sulfur deposition on regional and global scales: a multimodel evaluation, Global Biogeochem. Cycles, 20, GB4003, doi:10.1029/2005GB002672, URL http://dx.doi.org/10.1029/2005GB002672http://www.agu.org/pubs/crossref/2006/2005GB002672.shtml, 2006.

Diehl, T., Heil, A., Chin, M., Pan, X., Streets, D., Schultz, M., and Kinne, S.: Anthropogenic, biomass burning, and volcanic emissions of black carbon, organic carbon, and SO_2 from 1980 to 2010 for hindcast model experiments, Atmos. Chem. Phys. Discuss., 12, 24 895–24 954, doi:10.5194/acpd-12-24895-2012, URL http://www.atmos-chem-phys-discuss.net/12/24895/2012/, 2012.

Eklund, T. and McDowell, W.: Seasonal variation of tropical precipitation chemistry: La Selva, Costa Rica, Atmos. Environ., 31, 3903–3910, URL http://www.

sciencedirect.com/science/article/pii/S135223109700246X, 1997.

Elser, J. J., Bracken, M. E. S., Cleland, E. E., Gruner, D. S., Harpole, W. S., Hillebrand, H., Ngai, J. T., Seabloom, E. W., Shurin, J. B., and Smith, J. E.: Global analysis of nitrogen and phosphorus limitation of primary producers in freshwater, marine, and terrestrial ecosystems, Ecol. Lett., 10, 1135–42, doi:10.1111/j.1461-0248.2007.01113.x, URL http://www.ncbi.nlm.nih.gov/pubmed/17922835, 2007.

Emck, P.: A climatology of South Ecuador, Phd thesis, Fachbereich Geographie der Friedrich-Alexander-Universität Erlangen-Nürnberg, Germany, URL http://www.opus.ub.uni-erlangen.de/opus/volltexte/2007/656/, 2007.

Fabian, P., Kohlpaintner, M., and Rollenbeck, R.: Biomass burning in the Amazon–fertilizer for the mountaineous rain forest in Ecuador, Environ. Sci. Pollut. Res., 12, 290–296, URL http://dx.doi.org/10.1065/espr2005.07.272http://www.ncbi.nlm.nih.gov/pubmed/16206723, 2005.

Fabian, P., Rollenbeck, R., Spichtinger, N., Brothers, L., Dominguez, G., and Thiemens, M.: Sahara dust, ocean spray, volcanoes, biomass burning: pathways of nutrients into Andean rainforests, Adv. Geosci., 22, 85–94, doi:10.5194/adgeo-22-85-2009, URL http://www.adv-geosci.net/22/85/2009/, 2009.

Giglio, L., Randerson, J. T., van der Werf, G. R., Kasibhatla, P. S., Collatz, G. J., Morton, D. C., and DeFries, R. S.: Assessing variability and long-term trends in burned area by merging multiple satellite fire products, Biogeosciences, 7, 1171–1186, doi:10.5194/bg-7-1171-2010, URL http://www.biogeosciences.net/7/1171/2010/, 2010.

Gordon, C., Herrera, R., and Hutchinson, T.: Studies of fog events at two cloud forests near Caracas, Venezuela-II. Chemistry of fog, Atmos. Environ., 28, 323–337, URL http://www.sciencedirect.com/science/article/pii/1352231094901082, 1994.

Graf, H.-F., Feichter, J., and Langmann, B.: Volcanic sulfur emissions: Estimates of source strength and its contribution to the global sulfate distribution, J. Geophys. Res., 102, 10 727, doi:10.1029/96JD03265, URL http://doi.wiley.com/10.1029/96JD03265, 1997.

Greaver, T. L., Sullivan, T. J., Herrick, J. D., Barber, M. C., Baron, J. S., Cosby, B. J., Deerhake, M. E., Dennis, R. L., Dubois, J.-J. B., Goodale, C. L., Herlihy, A. T., Lawrence, G. B., Liu, L., Lynch, J. A., and Novak, K. J.: Ecological effects of nitrogen and sulfur air pollution in the US: what do we know?, Front. Ecol. Environ.,

10, 365–372, doi:10.1890/110049, URL http://www.esajournals.org/doi/abs/10.1890/110049, 2012.

Hamburger, T., Matisāns, M., Tunved, P., Ström, J., Calderon, S., Hoffmann, P., Hochschild, G., Gross, J., Schmeissner, T., Wiedensohler, A., and Krejci, R.: Long-term in situ observations of biomass burning aerosol at a high altitude station in Venezuela – sources, impacts and interannual variability, Atmos. Chem. Phys., 13, 9837–9853, doi:10.5194/acp-13-9837-2013, URL http://www.atmos-chem-phys.net/13/9837/2013/, 2013.

Hansen, J., Ruedy, R., Sato, M., and Lo, K.: Global surface temperature change, Rev. Geophys., 48, RG4004, doi:10.1029/2010RG000345, URL http://www.agu.org/pubs/crossref/2010/2010rg000345.shtml, 2010.

Hansen, M. C., Potapov, P. V., Moore, R., Hancher, M., Turubanova, S. a., Tyukavina, A., Thau, D., Stehman, S. V., Goetz, S. J., Loveland, T. R., Kommareddy, A., Egorov, A., Chini, L., Justice, C. O., and Townshend, J. R. G.: High-resolution global maps of 21st-century forest cover change, Science, 342, 850–853, doi:10.1126/science.1244693, URL http://www.ncbi.nlm.nih.gov/pubmed/24233722, 2013.

Hartig, K. and Beck, E.: The bracken fern (*Pteridium arachnoideum* (Kaulf.) Maxon) dilemma in the Andes of Southern Ecuador, Ecotropica, 9, 3–13, 2003.

Homeier, J., Hertel, D., Camenzind, T., Cumbicus, N. L., Maraun, M., Martinson, G. O., Poma, L. N., Rillig, M. C., Sandmann, D., Scheu, S., Veldkamp, E., Wilcke, W., Wullaert, H., and Leuschner, C.: Tropical andean forests are highly susceptible to nutrient inputs–rapid effects of experimental N and P addition to an ecuadorian montane forest., PLoS One, 7, e47 128, doi:10.1371/journal.pone.0047128, URL http://www.pubmedcentral.nih.gov/articlerender.fcgi?artid=3468540{&}tool=pmcentrez{&}rendertype=abstract, 2012.

Janssens-Maenhout, G., Dentener, F., van Aardenne, J., Monni, S., Pagliari, V., Orlandini, L., Klimont, Z., Kurokawa, J.-i., Akimoto, H., Ohara, T., Wankmüller, R., Battye, B., Grano, D., Zuber, A., and Keating, T.: EDGAR-HTAP: a harmonized gridded air pollution emission dataset based on national inventories, Tech. rep., Joint Research Centre, Institute for Environment and Sustainability, Ispra, Italy, doi:10.2788/14102, URL http://www.jrc.ec.europa.eu/ftp://139.191.1.85/pub/maenhout/HTAP/EDGAR-HTAP{_}report/LBNA25229ENN.pdf, 2012.

Kuylenstierna, J. C. I., Rodhe, H., Cinderby, S., and Hicks, K.: Acidification in developing countries: ecosystem sensitivity and the critical load approach on a global scale, Ambio, 30, 20–28, doi:10.1579/0044-7447-30.1.

20, URL http://www.bioone.org/doi/pdf/10.1579/0044-7447-30.1.20http://dx.doi.org/10.1579/0044-7447-30.1.20, 2001.

Langmann, B. and Graf, H. F.: Indonesian smoke aerosols from peat fires and the contribution from volcanic sulfur emissions, Geophys. Res. Lett., 30, 1547, doi:10.1029/2002GL016646, URL http://doi.wiley.com/10.1029/2002GL016646, 2003.

Lee, C., Martin, R. V., van Donkelaar, A., Lee, H., Dickerson, R. R., Hains, J. C., Krotkov, N., Richter, A., Vinnikov, K., and Schwab, J. J.: SO_2 emissions and lifetimes: estimates from inverse modeling using in situ and global, space-based (SCIAMACHY and OMI) observations, J. Geophys. Res., 116, D06 304, URL http://dx.doi.org/10.1029/2010JD014758, 2011.

Ljung, K., Maley, F., Cook, A., and Weinstein, P.: Acid sulfate soils and human health–A Millennium Ecosystem Assessment, Environ. Int., 35, 1234–1242, doi:10.1016/j.envint.2009.07.002, URL http://www.sciencedirect.com/science/article/pii/S0160412009001500, 2009.

Makowski Giannoni, S., Rollenbeck, R., Fabian, P., and Bendix, J.: Complex topography influences atmospheric nitrate deposition in a neotropical mountain rainforest, Atmos. Environ., 79, 385–394, doi:10.1016/j.atmosenv.2013.06.023, URL http://www.sciencedirect.com/science/article/pii/S1352231013004780http://linkinghub.elsevier.com/retrieve/pii/S1352231013004780, 2013.

Menz, F. C. and Seip, H. M.: Acid rain in Europe and the United States: an update, Environ. Sci. Policy, 7, 253–265, doi:10.1016/j.envsci.2004.05.005, URL http://www.sciencedirect.com/science/article/pii/S1462901104000590, 2004.

Morales, J., Bifano, C., and Escalona, A.: Atmospheric deposition of SO_4-S and (NH_4 + NO_3)-N at two rural sites in the western Maracaibo Lake basin, Venezuela, Atmos. Environ., 32, 3051–3058, URL http://www.sciencedirect.com/science/article/pii/S135223109700160X, 1998.

Mu, M., Randerson, J. T., van der Werf, G. R., Giglio, L., Kasibhatla, P., Morton, D., Collatz, G. J., DeFries, R. S., Hyer, E. J., Prins, E. M., Griffith, D. W. T., Wunch, D., Toon, G. C., Sherlock, V., and Wennberg, P. O.: Daily and 3-hourly variability in global fire emissions and consequences for atmospheric model predictions of carbon monoxide, Journal of Geophysical Research: Atmospheres, 116, n/a–n/a, doi:10.1029/2011JD016245, URL http://dx.doi.org/10.1029/2011JD016245, d24303, 2011.

Pauliquevis, T., Lara, L. L., Antunes, M. L., and Artaxo, P.: Aerosol and precipitation chemistry measurements in a remote site in Central Amazonia: the role of biogenic contribution, Atmos. Chem. Phys., 12, 4987–5015, doi:10.5194/acp-12-4987-2012, URL http://www.atmos-chem-phys.net/12/4987/2012/acp-12-4987-2012.html, 2012.

Pfeffer, M., Langmann, B., and Graf, H.-F.: Atmospheric transport and deposition of Indonesian volcanic emissions, Atmos. Chem. Phys., 6, 2525–2537, doi:10.5194/acp-6-2525-2006, URL http://www.atmos-chem-phys.net/6/2525/2006/, 2006.

Phoenix, G. K., Hicks, K. W., Cinderby, S., Kuylenstierna, J. C. I., Stock, W. D., Dentener, F. J., Giller, K. E., Austin, A. T., Lefroy, R. D. B., Gimeno, B. S., Ashmore, M. R., and Ineson, P.: Atmospheric nitrogen deposition in world biodiversity hotspots: the need for a greater global perspective in assessing N deposition impacts, Glob. Chang. Biol., 12, 470–476, doi:10.1111/j.1365-2486.2006.01104.x, URL http://dx.doi.org/10.1111/j.1365-2486.2006.01104.x, 2006.

Prins, E. M. and Menzel, W. P.: Geostationary satellite detection of bio mass burning in South America, Int. J. Remote Sens., 13, 2783–2799, doi:10.1080/01431169208904081, URL http://dx.doi.org/10.1080/01431169208904081, 1992.

Rissler, J., Vestin, A., Swietlicki, E., Fisch, G., Zhou, J., Artaxo, P., and Andreae, M. O.: Size distribution and hygroscopic properties of aerosol particles from dry-season biomass burning in Amazonia, Atmos. Chem. Phys., 6, 471–491, doi:10.5194/acp-6-471-2006, URL http://www.atmos-chem-phys.net/6/471/2006/acp-6-471-2006.html, 2006.

Rodrigues-Ramos, A. B., Prado do Nascimento, E. R., and Oliveira, M. J.: Temporada de incêndios florestais no Brasil em 2010: análise de série histórica de 2005 a 2010 e as influências das chuvas e do desmatamento na quantidade dos focos de calor, in: Simpósio Brasileiro de Sensoriamento Remoto, pp. 7902–7909, Curitiba, URL http://www.dsr.inpe.br/sbsr2011/files/p1414.pdf, 2011.

Rollenbeck, R.: Global sources-local impacts: natural and anthropogenic sources of matter deposition in the Andes of Ecuador, Geo-öko, pp. 5–27, 2010.

Rollenbeck, R., Fabian, P., and Bendix, J.: Precipitation dynamics and chemical properties in tropical mountain forests of Ecuador, Adv. Geosci., 6, 73–76, doi:10.5194/adgeo-6-73-2006, URL http://www.adv-geosci.net/6/73/2006/, 2006.

Rollenbeck, R., Bendix, J., Fabian, P., Boy, J., Wilcke, W., Dalitz, H., Oesker, M., and Emck, P.: Comparison of different techniques for the measurement of precipi-

tation in tropical montane rain forest regions, J. Atmos. Ocean. Technol., 24, 156–168, doi:10.1175/JTECH1970.1, URL http://journals.ametsoc.org/doi/abs/10.1175/JTECH1970.1, 2007.

Rollenbeck, R., Bendix, J., and Fabian, P.: Spatial and temporal dynamics of atmospheric water inputs in tropical mountain forests of South Ecuador, Hydrol. Process., 25, 344–352, doi:10.1002/hyp.7799, URL http://doi.wiley.com/10.1002/hyp.7799, 2011.

Rudel, T. K., Coomes, O. T., Moran, E., Achard, F., Angelsen, A., Xu, J., and Lambin, E.: Forest transitions: towards a global understanding of land use change, Glob. Environ. Chang., 15, 23–31, doi:10.1016/j.gloenvcha.2004.11.001, URL http://www.sciencedirect.com/science/article/pii/S0959378004000809, 2005.

Schemenauer, R., Banic, C., and Urquizo, N.: High elevation fog and precipitation chemistry in southern Quebec, Canada, Atmos. Environ., 29, 2235–2252, URL http://www.sciencedirect.com/science/article/pii/135223109500153P, 1995.

Schemenauer, R. S. and Cereceda, P.: A proposed standard fog collector for use in high-elevation regions, J. Appl. Meteorol., 33, 1313–1322, URL http://adsabs.harvard.edu/abs/1994JApMe..33.1313S, 1994.

Sigha-Nkamdjou, L., Galy-Lacaux, C., Pont, V., Richard, S., Sighomnou, D., and Lacaux, J.: Rainwater chemistry and wet deposition over the equatorial forested ecosystem of Zoétélé (Cameroon), J. Atmos. Chem., 46, 173–198, URL http://link.springer.com/article/10.1023/A:1026057413640, 2003.

Smith, S. J., van Aardenne, J., Klimont, Z., Andres, R. J., Volke, A., and Delgado Arias, S.: Anthropogenic sulfur dioxide emissions: 1850-2005, Atmos. Chem. Phys., 11, 1101–1116, doi:10.5194/acp-11-1101-2011, URL http://www.atmos-chem-phys.net/11/1101/2011/, 2011.

Stevenson, D. S., Johnson, C. E., Collins, W. J., and Derwent, R. G.: The tropospheric sulphur cycle and the role of volcanic SO2, Geol. Soc. London, Spec. Publ., 213, 295–305, doi:10.1144/GSL.SP.2003.213.01.18, URL http://sp.lyellcollection.org/cgi/doi/10.1144/GSL.SP.2003.213.01.18, 2003.

Stuefer, M., Freitas, S. R., Grell, G., Webley, P., Peckham, S., McKeen, S. A., and Egan, S. D.: Inclusion of ash and SO_2 emissions from volcanic eruptions in WRF-Chem: development and some applications, Geoscientific Model Development, 6, 457–468,

doi:10.5194/gmd-6-457-2013, URL http://www.geosci-model-dev.net/6/457/2013/, 2013.

Torres, O., Chen, Z., Jethva, H., Ahn, C., Freitas, S. R., and Bhartia, P. K.: OMI and MODIS observations of the anomalous 2008-2009 southern hemisphere biomass burning seasons, Atmos. Chem. Phys., 10, 3505–3513, doi:10.5194/acp-10-3505-2010, URL http://www.atmos-chem-phys.net/10/3505/2010/, 2010.

van der Werf, G. R., Randerson, J. T., Giglio, L., Collatz, G. J., Mu, M., Kasibhatla, P. S., Morton, D. C., DeFries, R. S., Jin, Y., and van Leeuwen, T. T.: Global fire emissions and the contribution of deforestation, savanna, forest, agricultural, and peat fires (1997-2009), Atmos. Chem. Phys., 10, 11 707–11 735, doi:10.5194/acp-10-11707-2010, URL http://www.atmos-chem-phys.net/10/11707/2010/, 2010.

Wullaert, H.: Response of nutrient cycles of an old-growth montane forest in Ecuador to experimental low-level nutrient amendments, Phd thesis, Fachbereich Chemie, Pharmazie und Geowissenschaften der Johannes Gutenberg-Universität Mainz, Germany, URL http://ubm.opus.hbz-nrw.de/volltexte/2010/2312/, 2010.

Chapter 5

Atmospheric salt deposition in a tropical mountain rain forest at the eastern Andean slopes of South Ecuador - Pacific or Atlantic origin?

Sandro Makowski Giannoni, Katja Trachte, Rütger Rollenbeck, Lukas Lehnert, Julia Fuchs, and Jörg Bendix

ATMOSPHERIC CHEMISTRY AND PHYSICS

Received: 17 June 2015
Revised: 29 June 2016
Accepted: 13 July 2016
Published: 12 August 2016

Abstract

Sea salt (NaCl) has recently been proven to be of the utmost importance for ecosystem functioning in Amazon lowland forests because of its impact on herbivory, litter decomposition and, thus, carbon cycling. Sea salt deposition should generally decline as distance from its marine source increases. For the Amazon, a negative east–west gradient of sea salt availability is assumed as a consequence of the barrier effect of the Andes Mountains for Pacific air masses. However, this generalized pattern may not hold for the tropical mountain rainforest in the Andes of southern Ecuador. To analyse sea salt availability, we investigated the deposition of sodium (Na^+) and chloride (Cl^-), which are good proxies of sea spray aerosol. Because of the complexity of the terrain and related cloud and rain formation processes, sea salt deposition was analysed from both, rain and occult precipitation (OP) along an altitudinal gradient over a period between 2004 and 2009. To assess the influence of easterly and westerly air masses on the deposition of sodium and chloride over southern Ecuador, sea salt aerosol concentration data from the Monitoring Atmospheric Composition and Climate (MACC) reanalysis data set and back-trajectory statistical methods were combined. Our results, based on deposition time series, show a clear difference in the temporal variation of sodium and chloride concentration and Na^+ / Cl^- ratio in relation to height and exposure to winds. At higher elevations, sodium and chloride present a higher seasonality and the Na^+ / Cl^- ratio is closer to that of sea salt. Medium- to long-range sea salt transport exhibited a similar seasonality, which shows the link between our measurements at high elevations and the sea salt synoptic transport. Although the influence of the easterlies was predominant regarding the atmospheric circulation, the statistical analysis of trajectories and hybrid receptor models revealed a stronger impact of the north equatorial Atlantic, Caribbean, and Pacific sea salt sources on the atmospheric sea salt concentration in southern Ecuador. The highest concentration in rain and cloud water was found between September and February when air masses originated from the north equatorial Atlantic, the Caribbean Sea and the equatorial Pacific. Together, these sources accounted for around 82.4 % of the sea salt budget over southern Ecuador.

5.1 Introduction

Poor substrate and intense leaching by precipitation make tropical forests particularly prone to nutrient deficiency. While phosphorus is mainly considered a limitation to net primary productivity (NPP) in lowland Amazonian tropical forests, phosphorus and nitrogen co-limit growth in the tropical mountain rainforests, as in southern Ecuador (Homeier et al. 2012; Koehler et al. 2009; Tanner et al. 1998; Vitousek 1984; Wolf et al. 2011; Wullaert 2010). Because of a worldwide increase in nitrogen and phosphorus emissions and a pronounced increase in emissions from developing countries, where the majority of tropical forests are located, atmospheric deposition in these countries has gained attention (Dentener et al. 2006; Galloway et al. 2008; Phoenix et al. 2006).

In several tropical and temperate forests, human intervention in the nitrogen and phosphorus cycles have has been documented (Mahowald et al. 2005; Matson et al. 2002; Phoenix et al. 2006; Tipping et al. 2014; Yu et al. 2015). Because nutrient availability regulates ecosystem processes and functions, the changes currently affecting the nitrogen and phosphorus budgets are expected to have wide-reaching impacts in forest ecosystem structure and diversity (Bobbink et al. 2010; Homeier et al. 2012; Matson et al. 2014; Peñuelas et al. 2013; Pett-Ridge 2009; Wang et al. 2014; Wilcke et al. 2013). The role of sea salt availability has very recently gained attentions, as it has been found to condition the behaviour of herbivores, in addition to affecting carbon cycling and organic matter decomposition in tropical ecosystems (Dudley et al. 2012; Kaspari et al. 2008, 2009; Powell et al. 2009; Voigt et al. 2008). At the western rim of the Amazon forest, in Peru, Ecuador, and Colombia, there is evidence that herbivorous and frugivorous birds and mammals visit mineral licks to compensate for low sodium concentration in plant and fruit tissues (Lee et al. 2009; Lizcano and Cavelier 2004; Powell et al. 2009; Voigt et al. 2008). Furthermore, some taxa of arthropod have reportedly begun practicing geophagy to deal with salt scarcity in plants (Kaspari et al. 2008). Yet, despite its pantropical importance, salt availability has hitherto been overlooked in most biogeographic and biogeochemical studies (Dudley et al. 2012).

By far, the most important source of continental sea salt depositions are the oceans. Sea salt scarcity in Amazonian rainwater increases along a gradient from the Atlantic coast towards the Andean range, which acts as a natural orographic barrier to the west. The concentration of both sodium and chloride in rainwater diminishes significantly with increasing distance from the Atlantic Ocean (Talbot et al. 1990). Additionally, the ratio between both concentrations inverts from $Cl^- > Na^+$ close to the ocean to $Cl^- < Na^+$ far from the ocean (Tardy et al. 2005). Consequently, tropical mountain forests on the eastern slopes of the Andes and tropical lowland forests at the western edge of the Amazon are

expected to suffer from sea salt deprivation, whereas forests closer to the Atlantic coast are subject to large sea salt deposition (Dudley et al. 2012).

The tropical mountain forests at the eastern Andean slopes in southern Ecuador may likely represent an exception of this generalized pattern because of their location in the Huancabamba depression, an area where the Andes rarely exceed 3600 m in altitude. This allows the transport of Pacific air masses rich in sea salt. As a result, the mountain forest might benefit not only from sea salt transported by easterly air masses from the Atlantic but also by sea salt originating from Pacific air masses. Depending on the strength of the contribution to sodium and chloride deposition originating from the Pacific, the combined input from Atlantic and Pacific sources could result in a greater sodium and chloride availability than that found for the lowland forests on the western rim of the Amazon (Dudley et al. 2012).

However, little research has investigated the deposition of atmospheric sodium and chloride in the tropical forests of the southern Ecuadorian Andes. Furthermore, any such research has yet to identify their sources. In this context, an investigation of the deposition by occult precipitation (OP) is particularly important, because OP comprises an extremely high proportion of total precipitation in tropical mountain forests. OP is the water supplied to soil or vegetation by light drizzle, wind-driven, rain and fog and/or clouds that conventional rain gauges cannot measure. An exception is the work of Fabian et al. (2009), who estimated the origin of the local sea salt deposition by visual interpretation of single back trajectories. To our knowledge, neither a comprehensive quantitative investigation on sea salt sources nor any estimates of their contribution to the atmospheric deposition have been conducted yet.

As a consequence of the knowledge gaps regarding the sea salt sources of deposition in the Andes of southeastern Ecuador, the aims of this study are as follows: (1) to characterize sodium and chloride atmospheric deposition by rain and OP along an altitudinal gradient and at different topographic locations in a tropical mountain rainforest site; (2) to identify potential Pacific, Atlantic, and continental geographic sources of sea salt concentration over the Andes of southern Ecuador by applying back-trajectory statistical techniques and reanalysis data of atmospheric composition; and (3) to estimate the contribution of each source area to the atmospheric sea salt concentration in the Andes of southern Ecuador.

5.2 Study area

The study area is located at the northwestern edge of the Amazon basin ($4°00'$ S, $79°05'$ W), at the southeastern Andes of Ecuador, approximately a 100 km straight line distance away

from the Pacific coast and around 2000 km from the closest part of the Atlantic coast (Fig. 5.1). The study area contains the San Francisco valley, deeply incised into the eastern slope of the main Andes range. Since 2002, two successive multidisciplinary research programs have investigated the Reserva Biológica San Francisco (RBSF), located on the northern slopes of the valley and some areas outside of the reserve (Beck et al. 2008; Bendix et al. 2013).

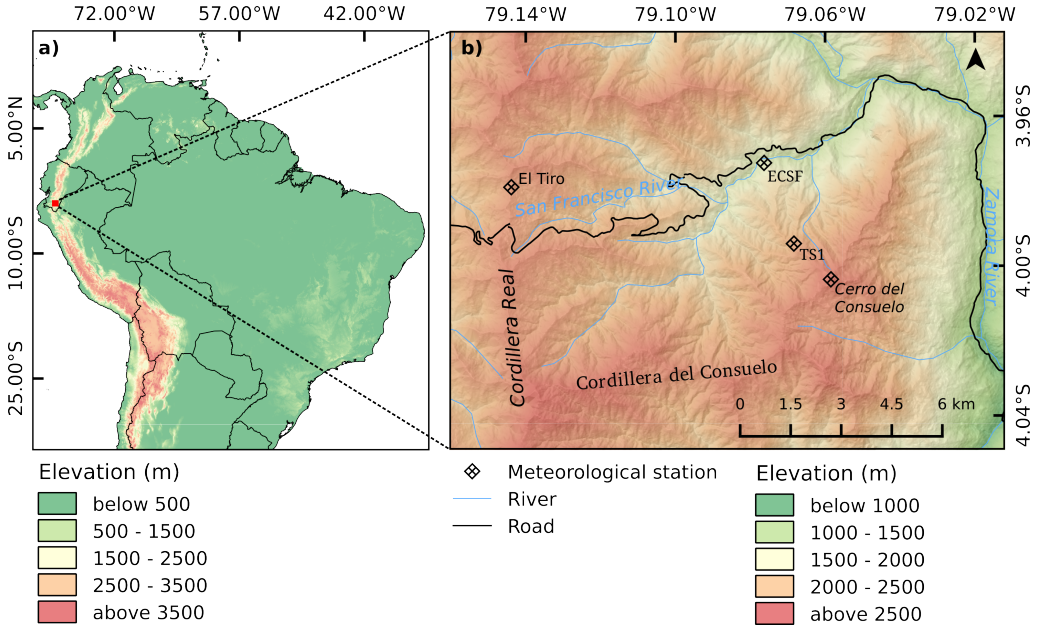

Figure 5.1: Map of the study area. a) Location of the study area in the Huancabamba depression of the Andes in South America. b) Detailed map of the rain and OP sampling sites installed in the study area.

The Andes in this area are characterized by lower elevations and higher geomorphological complexity compared to other parts of the mountain chain in northern Ecuador, Peru, and Colombia. Since studies have shown that exposure and altitude affect deposition patterns (Griffith et al. 2015; Kirchner et al. 2014; Lovett and Kinsman 1990; Makowski Giannoni et al. 2013), a precondition for the study of sea salt deposition is to collect measurements along a large altitudinal gradient and at different slope exposures.

The climate of the catchment is mainly determined by the constant tropical easterlies. However, the trade winds are weakened each year between November and March, and westerly wind bursts occur locally because of the low altitude of the mountains. Those westerly winds are transporting Pacific air masses into the study area (see Fig. 5.1, Bendix et al. 2008a; Emck 2007). Precipitation responds to the displacement of the intertropical convergence zone (ITCZ) and the intensity of the tropical easterlies. The highest rainfall occurs between June and August, when the easterly winds predominate, carrying humid air masses from the lowlands of the Amazon. The topography forces the humid air upwards

leading to high rainfall totals, especially in the higher parts of the mountains, and the peaks' immersion into the clouds, resulting in OP (Bendix et al. 2006, 2008b; Richter et al. 2013; Rollenbeck et al. 2011). In the period from 2004 to 2009, average rainfall varied from 1500 to 6500 mm per year between 1960 and 3180 m. In the highest regions, OP contributes up to 35 % of total precipitation (Rollenbeck et al. 2011). A short dry season occurs between November and March when Pacific air masses are transported to the area by occasional westerlies. Such air masses occur less than 20 % of the time (Richter et al. 2013) and are accompanied by convective activity.

5.3 Data and methods

The methodology is comprised of two components. First, we analyse local salt (sodium and chloride) concentrations by assessing the sodium and chloride concentrations in samples of rain and OP along an altitudinal gradient. To do so, we use a statistical approach due to the complexity of the terrain. Second, we attempt to derive the source of the salt. The second part focuses on describing the transport pathways associated with the general atmospheric circulation patterns to detect potential source areas of sea salt. Our goal is to draw connections between the contributions each respective atmospheric sea salt source has on our study area. Back-trajectory analysis was used to achieve this goal.

5.3.1 Sample collection, materials, and data

Three meteorological stations (MSs) were installed on the north-facing slopes of the San Francisco valley along an altitudinal transect ranging from 1960 to 3180 m in elevation. A fourth station (El Tiro, 2725 m) was installed at a mountain pass about 4 km up the valley on the Cordillera Real (Fig. 5.1).

Rain and OP samples were collected at each station between 2004 and 2009. While rain water was collected in totaling gauges (UMS 200, made of polyethylene to warrant chemical inertia), OP was collected in 1 m^2 mesh grid fog collectors designed according to Schemenauer and Cereceda's proposal (Schemenauer and Cereceda 1994). Details about rain and fog measurement techniques, calibration, and data handling are described in Rollenbeck et al. (2007), Fabian et al. (2009), and Rollenbeck et al. (2011).

Rain and OP samples were collected at almost regular weekly intervals. The samples were filtered and immediately stored in frozen state, before being sent to the laboratory for ion analyses. All samples were analysed at the University of Munich's Weihenstephan Center (TUM-WZW) for major ions (K^+, Na^+, $NH_4{}^+$, Ca^{2+}, Mg^{2+}, Cl^-, $SO_4{}^{2-}$, $NO_3{}^-$). Cations were analysed according to the inductivity-coupled plasma method (Perkin

Elmer Optima 3000), while ion chromatography (Dionex DX-210) was used for anions. The detection limits are 0.1 and 0.2 mg L^{-1} for sodium and chloride, respectively.

The sea salt mixing ratio of the Monitoring Atmospheric Composition and Climate (MACC) reanalysis data set was used as a proxy for the sea salt concentration in the atmosphere, with a horizontal resolution of 0.75° by 0.75° (Inness et al. 2013). In this data set, the concentration of sea salt generated by wind stress on the ocean surface was determined based on a source function developed by Guelle et al. (2001) and Schulz et al. (2004), accounting for sedimentation as well as wet and dry deposition processes. The sea salt concentration was integrated for three size bins (0.03-0.5, 0.5-5.0, and 5.0-20.0 μm) and calculated for 60 vertical model levels with the upper model limit at 0.1 hPa (Benedetti et al. 2009; Morcrette et al. 2009). To our knowledge, this is the only available global sea salt concentration data that span the period covered in this study. Furthermore, this reanalysis data set has performed well when compared to measured satellite and ground-based data (Benedetti et al. 2009).

5.3.2 Statistical evaluation of sodium and chloride ion concentration in rain and OP

Since sea spray aerosol consists mainly of chloride and sodium (Millero 2014), we used the ion concentration of both elements in rain and OP as proxies of sea salt atmospheric inputs into the ecosystem. Because sodium is a conservative ion in sea salt aerosol, it is often used as a reference for sea salt concentration in precipitation chemistry and atmospheric chemistry modelling studies (Jaeglé et al. 2011; Keene et al. 1986; Pozzer et al. 2012; Tardy et al. 2005; Vet et al. 2014). Chloride is more unstable, as it photochemically reacts with other atmospheric ions (e.g. sulfur and nitrogen species), and it is depleted as a function of time spent in the atmosphere (Keene et al. 1986).

Weekly sodium and chloride concentrations in water samples from rain and OP were weighted with the total weekly precipitation volume to calculate volume-weighted monthly mean concentrations (VWMMs). With the calculated VWMMs we compiled monthly time series of sea salt concentration for a 6-year time series from 2004 to 2009, which represented the temporal variation in the concentration at each altitudinal level of the study area. To identify differences in the distribution of sodium and chloride concentrations between the sites, we created boxplots of total concentration over the 6-year evaluated period at each altitudinal level. Additionally, we computed total volume-weighted means (VWMs) to compare our observations with those from other studies.

We analysed the relationship to other ions (K^+, NH_4^+, Ca^{2+}, Mg^{2+}, SO_4^{2-}, NO_3^-)

using a principal factor analysis (PFA) to locate common transport histories and the likely origin of sodium and chloride. Before conducting the PFA, the data were normalized and scaled to achieve comparable distributions.

In coastal continental areas, the Na^+ / Cl^- molar ratio is typically that of sea salt (Keene et al. 1986). This ratio was calculated using the measurements from each altitude and serves as an indicator of the origin of both sodium and chloride concentration in precipitation. The ratio changes as a function of distance from the ocean, as chloride is photochemically depleted in the atmosphere.

Finally, to asses a likely impact of anabatic flows on the sodium and chloride budget, we calculated wind direction relative frequency plots.

5.3.3 Back-trajectory and source–receptor analysis

The HYSPLIT model was used to generate back trajectories of air masses encompassing 10 days with a resolution of 1 day (Draxler and Hess 1998). Modeling was done using the openair package (Carslaw and Ropkins 2012) for R statistical language. The wind fields were derived from the ERA-Interim reanalysis (Dee et al. 2011) with a grid resolution of 0.75° by 0.75°. All trajectories had their origins at the San Francisco River catchment in southern Ecuador. The MACC reanalysis sea salt concentration data were set as proxy of sea salt concentration in the atmosphere for air-mass transport analysis by back-trajectory techniques. To test the link between the MACC sea salt concentration and the sodium and chloride concentrations actually measured in rain and OP, both were linearly correlated. Pearson's product–moment correlation coefficients were calculated between the concentration at the two uppermost MSs (El Tiro and Cerro del Consuelo) and the MACC sea salt concentration (see Table 5.1). Based on the correlation coefficients, the MACC data set at 700 hPa and the medium particle size ($0.5 - 5.0$ μm) was chosen as the input parameter for further examination by back-trajectory analysis, because it yielded the highest correlation coefficient and significance level.

Given the spatial resolution of the data set (0.75° by 0.75°), the outcome of this analysis can only provide evidence of synoptic transport pathways and source–receptor relationships for medium- to long-distance sources for an area of approximately 80 by 80 km^2 in the southern Ecuadorian Andes. Local-scale transport is not represented by the used trajectory models.

We first aimed to identify the potential geographic origin of the sea salt concentration over this wider area covering our receptor site in southern Ecuador. For this particular

Table 5.1: Results from the correlation analysis between sea salt monthly mean concentration from the MACC reanalysis data and Na^+ and Cl^- monthly mean concentration samples from El Tiro and Cerro del Consuelo meteorological stations. Correlations were tested for the various elevations within the MACC data set

	MACC1 (0.03–0.5 μm)			MACC2 (0.5–5 μm)			MACC3 (5–20 μm)		
	Cl^-	Na^+	Mean	Cl^-	Na^+	Mean	Cl^-	Na^+	Mean
Cerro del Consuelo									
700 hPa	0-.36**	0.35**	0.18	0.52***	0.52***	0.40***	0.48***	0.47***	0.52***
600 hPa	0.31**	0.26*	0.1	0.50***	0.47***	0.39**	0.36**	0.30*	0.40***
500 hPa	0.27*	0.19	0.03	0.47***	0.36**	0.30*	0.22	0.13	0.28*
400 hPa	0.24*	0.19	0.03	0.37**	0.27*	0.23	0.08	0.02	0.17
300 hPa	0.11	0.02	−0.05	0.25*	0.16	0.23	0.01	−0.05	0.14
200 hPa	0.22	0.09	0.03	0.30*	0.18	0.25*	−0.02	−0.04	0.08
El Tiro									
700 hPa	0.34**	0.18	0.18	0.41***	0.17	0.2	0.32**	0.05	0.16
600 hPa	0.37**	0.22	0.2	0.40***	0.14	0.18	0.19	−0.08	0.07
500 hPa	0.33**	0.18	0.16	0.31**	0.05	0.09	0.02	−0.15	−0.04
400 hPa	0.24*	0.14	0.12	0.14	−0.02	0	−0.14	−0.16	−0.12
300 hPa	0.14	0.15	0.1	−0.01	−0.08	−0.05	−0.21	−0.15	−0.13
200 hPa	0.15	0.15	0.19	−0.01	−0.12	0.01	−0.17	0.01	−0.04

Note: * $p < 0.05$, ** $p < 0.01$, *** $p < 0.001$.

purpose we used source–receptor modelling, as it has been successfully applied to determine likely geographic origins of pollutants and aerosols (e.g. Fleming et al. 2012; Hsu et al. 2003; Powell et al. 2009; Riuttanen et al. 2013; Robinson et al. 2011). Here, two different hybrid receptor models were used for comparison: the potential source contribution function (PSCF) and the adjusted concentration-weighted trajectory (CWT) running on a grid that covers the domain of the 2192 generated trajectories between 2004 and 2009. Given the high seasonality of synoptic air mass transport, we calculated the models on a seasonal basis (Bendix et al. 2008a; Emck 2007).

The PSCF (Malm et al. 1986; Pekney et al. 2006; Zeng and Hopke 1989) calculates the probability that a source of aerosol or pollutant observed at the ground measurement site is located at a specific cell in the geographic space and is defined by

$$\mathrm{PSCF}_{ij} = \frac{m_{ij}}{n_{ij}}, \tag{5.1}$$

where n_{ij} is the number of trajectory points that passed through cell (i, j) and m_{ij} is the number of times that trajectory points passing through the cell (i,j), and correspond to a high sea salt concentration (above an arbitrary threshold) at the time of the trajectory's arrival at the receptor site. The function is based on the premise that, if a source is located at that specific location, the air masses represented by the trajectory passing through the collocated cell are likely to collect and transport the material along the trajectory until the receptor site. In this study, we defined two concentration thresholds: the 75th percentile for moderate-to-high concentration and the 90th percentile for high concentration.

The adjusted CWT function uses a grid domain to calculate a grid-wise logarithmic mean concentration of an aerosol or pollutant (Seibert et al. 1994) and is defined by

$$\ln\left(\overline{C}_{ij}\right) = \frac{1}{\sum_{k=1}^{N} t_{ij}} \sum_{k=1}^{N} \ln\left(\overline{C}_{k}\right) t_{ijk}, \tag{5.2}$$

where i and j are the grid indices, k the trajectory index, N the total number of trajectories, $\overline{C}_k$ the pollutant concentration measured upon arrival of trajectory k, and t_{ijk} the residence time of trajectory k in grid cell (i, j). In this method, a weighted concentration is assigned to each pixel in the domain. This concentration is the average of the sample concentrations at a given receptor that have associated trajectories crossing the respective cell.

In a second step, we assessed the contribution of the main transport pathways of sea salt to the observed concentration over southern Ecuador. For this purpose, we integrated the MACC sea salt data to the back-trajectory cluster analysis. As for the source–receptor modelling approach, cluster analysis was applied on a seasonal basis to group similar air mass histories. This revealed general circulation patterns and, subsequently, enabled to post-process concentration data in relation to cluster origin and pathways. A partitioning algorithm based on spherical k means was used to define the appropriate number of trajectory clusters, as well as prior knowledge of the main wind systems affecting the receptor site. We tested different k values and chose the maximum number of cluster objects (i.e. back trajectories) that most closely reproduced the known conditions. The cosine distance was used as measure of similarity/dissimilarity between different trajectories. Afterwards, the frequency of trajectories represented by each cluster was determined.

To estimate the contribution of the different seasonal transport pathways to the observed sea salt concentration, the single trajectories belonging to each cluster object (cluster mean trajectory) were related to the sea salt concentration in the nearest neighbouring pixel within the study area. In this way, the contribution of each cluster object to the sea salt concentration above the study site could be statistically evaluated. Likewise, to analyse sources and sinks of sea salt along the cluster mean trajectories, we extracted the mean seasonal concentration values from the MACC data pixels (from 2004 to 2009) that matched the cluster mean trajectories in location, time, and height. Seasonal sea salt concentrations maps were calculated to further interpret the concentration along the cluster mean trajectories. For this, the MACC sea salt data were vertically integrated between 875 hPa (the minimum height of the trajectory clusters) and 500 hPa (maximum height).

Additionally, based on findings by Akagi et al. (2011) showing that burning biomass is a contributor to chloride emissions, the Copernicus atmosphere monitoring system's (CAMS) global fire assimilation system (GFAS) (Kaiser et al. 2012) was used to create seasonal maps of NO_x biomass burning fluxes over South America. To estimate the Na^+ and Cl^- contribution from the biomass-burning aerosol mass, we calculated the Na^+ and Cl^- mass ratio to NO_x based on emission factors from Ferek et al. (1998). In this way, seasonal fractions of biomass-burning Na and Cl relative to sea salt were calculated.

5.4 Results

5.4.1 Sodium and chloride concentration

Our study area is characterized by the complex topography of the Andes (see Fig. 5.1). Hence, temporal variation and distribution is of interest in our study of sodium and chloride concentrations in rain and OP at different altitudes and topographical locations.

Figure 5.2 (left column) depicts the time series of sodium and chloride concentrations at different altitudes. Cerro del Consuelo MS, situated at 3180 m, demonstrated the clearest temporal pattern in concentration, where the highest peaks occurred almost regularly between September and February (Fig. 5.2a). The highest concentrations of sodium were recorded at Cerro del Consuelo and El Tiro (2825 m) (Fig. 5.2a and b). Contrarily, chloride concentration peaks in OP were highest at the lowest MS, Estación Científica San Francisco (ECSF) (Fig. 5.2d).

To compare the respective distributions, the boxplots in Fig. 5.2 (right column) show the concentration of sodium and chloride for both rain and OP at every MS. Overall, no essential variations between the concentration at each MS could be observed except for chloride in OP and rainwater at ECSF (Fig. 5.2d), where reported values were much higher than those measured at other elevations. Regarding ion concentration in sodium and chloride species, a clear difference could be observed with chloride concentration in the interquartile range extending between 0.22 and 0.51 mg L^{-1}, and sodium concentration extending between 0.06 and 0.20 mg L^{-1}.

In rainwater samples, the concentrations of chloride were considerably higher than those of sodium at each MS. A larger range and higher extreme values were observed in the chloride concentration. Differences in sodium concentrations between MSs at different altitudes were negligible. The concentrations showed a slight increase at transect 1 (TS1) (median of 0.14 mg L^{-1}) and El Tiro (median of 0.13 mg L^{-1}) and decreased again at the highest station, Cerro del Consuelo (median of 0.07 mg L^{-1}). Compared to the rain

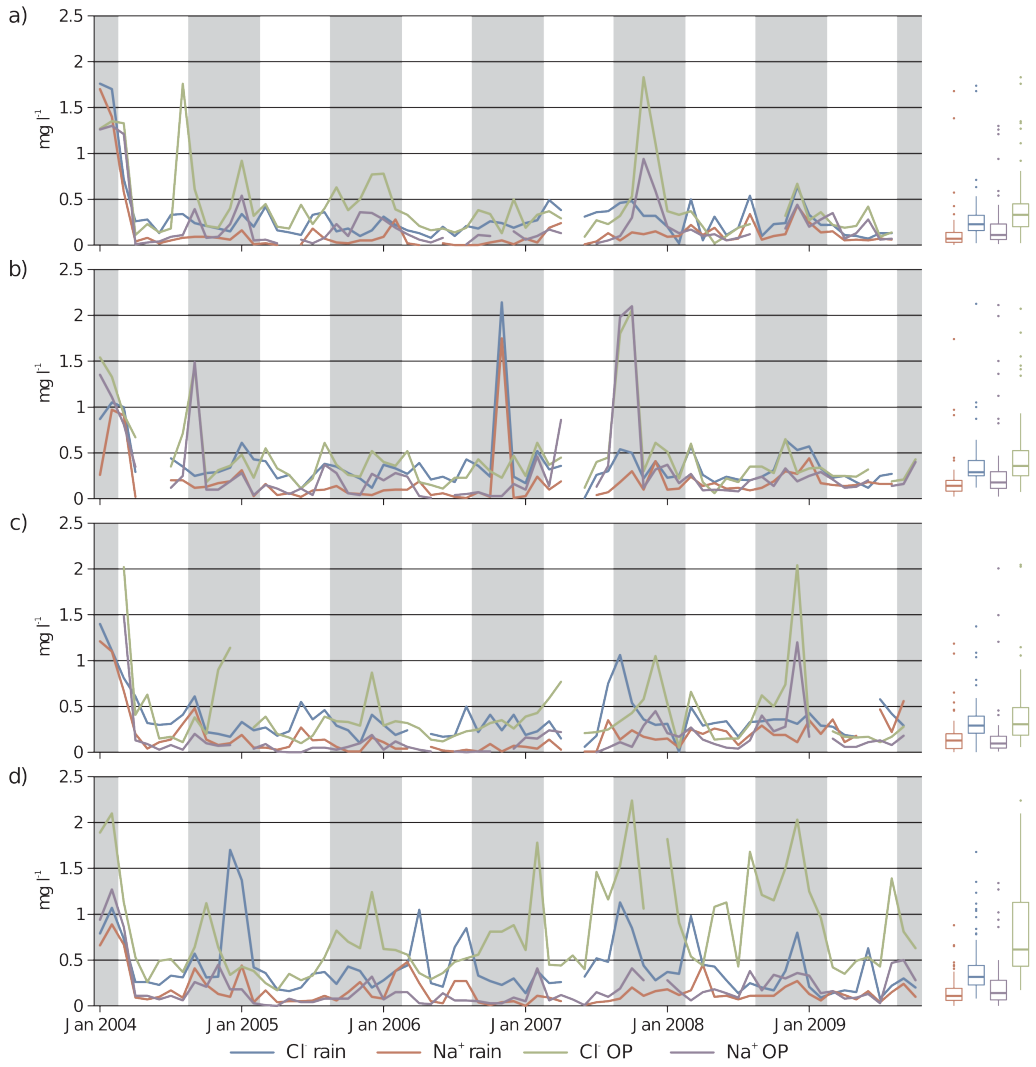

Figure 5.2: Time series of Na^+ and Cl^- VWMM concentration in rain and OP. These samples come from MSs at different altitudes and topographical locations: a) Cerro del Consuelo (3180 m), b) El Tiro (2825 m), c) TS1 (2660 m), and d) ECSF (1960 m). The shaded areas cover 6-month periods from September to February. The boxplots in the right column show the distribution of each time series: boxes symbolize the lower and upper quartile of the data, vertical lines show ranges of observed concentration, and points are outliers.

samples, OP contained a higher mean concentration of sodium and chloride but also a greater range in its distribution (Fig. 5.2, left column). The concentration of chloride was also considerably higher than that of sodium, with the highest mean concentration (median of 0.62 mg L^{-1}) at the lowest MS, ECSF. Sodium concentration peaked at El Tiro (0.17 mg L^{-1}). At TS1, the mean concentration was lowest (median Na^+ 0.09 mg L^{-1} and Cl^- 0.3 mg L^{-1}) increased once again at the highest elevations, El Tiro and Cerro del Consuelo (median Na^+ between 0.11 and 0.17 mg L^{-1} and Cl^- between 0.33 and 0.35 mg L^{-1}).

A PFA of every major ion concentration was conducted to gain insights into the origin of sea salt inputs for each MS (Table 5.2). This analysis indicated four

Table 5.2: Loadings from PFA with varimax rotation of major ions in rain and OP samples from Cerro del Consuelo, El Tiro, TS1, and ECSF meteorological stations

	Rain				OP			
	Factor 1	Factor 2	Factor 3	Factor 4	Factor 1	Factor 2	Factor 3	Factor 4
Cerro del Consuelo								
NH_4^+	0.05	0.14	0.81	0.00	0.88	0.09	0.15	0.08
Ca^{2+}	0.05	0.08	−0.04	0.73	0.17	0.30	0.60	0.60
Cl^-	0.88	0.44	0.06	−0.15	0.23	0.81	0.13	0.35
Mg^{2+}	0.04	−0.21	0.70	−0.06	0.17	0.20	0.86	0.14
NO_3^-	0.27	0.91	0.00	0.19	0.87	0.27	−0.02	0.42
K^+	0.85	0.06	−0.02	0.28	0.84	0.24	0.25	0.09
Na^+	0.88	0.37	0.19	−0.00	0.19	0.83	0.24	0.05
SO_4^{2-}	0.49	0.64	−0.15	−0.03	0.54	0.30	0.34	0.64
El Tiro								
NH_4^+	−0.07	−0.06	0.64	0.03	0.82	0.34	0.28	0.22
Ca^{2+}	−0.02	0.11	0.03	0.40	0.34	0.29	0.68	0.09
Cl^-	0.98	0.09	−0.11	−0.11	0.31	0.90	0.25	0.01
Mg^{2+}	0.05	−0.04	0.87	−0.03	0.48	0.38	0.52	0.38
NO_3^-	−0.06	0.80	−0.18	0.20	0.81	0.38	0.38	0.08
K^+	0.15	0.42	0.35	−0.38	0.85	0.30	0.39	0.02
Na^+	0.97	0.04	0.08	0.01	0.33	0.87	0.31	0.16
SO_4^{2-}	0.13	0.84	−0.00	0.08	0.61	0.32	0.63	−0.02
TS1								
NH_4^+	−0.04	0.05	0.59	0.27	0.03	0.12	0.09	0.68
Ca^{2+}	−0.06	−0.16	−0.02	0.04	0.67	0.23	0.37	0.21
Cl^-	0.36	0.89	−0.15	0.04	0.89	0.37	0.16	−0.00
Mg^{2+}	−0.22	−0.09	0.78	0.04	0.45	−0.15	0.55	0.46
NO_3^-	0.91	0.14	−0.20	0.27	0.22	0.89	0.00	0.18
K^+	0.15	0.08	0.34	0.67	0.57	0.42	0.58	0.18
Na^+	-0.04	0.89	−0.00	0.33	0.91	0.35	0.19	0.07
SO_4^{2-}	0.83	0.29	−0.11	−0.06	0.41	0.80	0.13	0.00
ECSF								
NH_4^+	0.01	0.78	0.11	−0.10	0.34	0.42	0.39	0.43
Ca^{2+}	0.23	0.01	0.02	0.03	−0.04	0.03	0.07	0.50
Cl^-	0.49	−0.23	0.04	0.30	0.31	0.77	0.34	0.32
Mg^{2+}	-0.10	0.54	−0.59	0.09	0.05	0.33	0.73	0.23
NO_3^-	−0.00	0.22	0.75	0.31	0.80	0.07	0.01	0.01
K^+	0.65	−0.02	−0.10	0.03	0.52	0.37	0.64	0.04
Na^+	0.80	0.02	0.15	0.22	0.13	0.79	0.25	−0.02
SO_4^{2-}	0.24	−0.07	0.17	0.73	0.77	0.29	0.27	−0.03

components that explain the majority of the variability in the data set. The load of sodium and chloride had a considerable bearing on either factor 1 or 2, depending on the altitude and location of the MS, and the precipitation type. These two factors explained at least 29 % of the variability in the system (Table 5.2). Sodium and chloride explained the greatest variability in the system's rain samples, except for TS1 (2660 m).

At Cerro del Consuelo, sodium, chloride, and potassium dominated the variability in rain, given that they loaded to factor 1. In OP samples, biomass-burning compounds such as nitrate, sulfate, and ammonium had a stronger signal, loading to factor 1. Factor 2 was

loaded by sodium and chloride only. No other compounds loaded to this factor, meaning that sodium and chloride most likely originated in sea salt from Atlantic and Pacific air masses.

At El Tiro, sea salt sources were exclusively present in factor 1 for rain and factor 2 for OP, similar to Cerro del Consuelo. As for Cerro del Consuelo, sea salt explained most of the variance in rain, followed by biomass-burning compounds. The opposite was true for OP, where biomass-burning compounds dominated, followed by sea salt.

The situation at TS1 was more complex than at Cerro del Consuelo and El Tiro, given the combined influence of the local mountain-valley breeze system and the synoptic system. In rain, biomass-burning compounds dominated the variability, with significant loadings on factor 1. Factor 2 was only loaded with sodium and chloride. In OP, factor 1 represented sea salt and crustal material, as sodium, chloride, and calcium loaded to this factor.

In the rain samples at ECSF, sodium and chloride loaded to factor 1 together with K^+. In the OP samples nitrate, $SO_4{}^-$, and K^+ dominated the variability loading to factor 1, while sodium and chloride loaded to factor 2.

Figure 5.3a shows the Na^+ / Cl^- molar ratio calculated in data from OP and rain water samples collected at each MS along the altitudinal gradient studied. The typical molar Na^+ / Cl^- ratio in precipitation for areas close to the sea is 0.86 (dotted line in the figure), according to Keene et al. (1986). The International Co-operative Programme on Assessment and Monitoring of Air Pollution Effects on Forests (ICP) recommends an acceptable range of values between 0.5 and 1.5 molar units (Clarke et al. 2010) (dashed line in Fig. 5.3). Outliers were likely due to samples with concentrations too close to the detection limits. When approaching the lower limits of the concentration, the ratio becomes more unstable and tends towards more extreme values.

The highest stations show a stronger marine influence, particularly in OP. The ratio fluctuates within the acceptable range and is mostly close to the standard value of sea salt in precipitation from coastal areas. This influence diminishes as the altitude decreases, especially for OP. Median ratios of 0.7, 0.8, 0.5, and 0.3 for Cerro del Consuelo, El Tiro, TS1, and ECSF, respectively, also reflect a greater influence of sea salt at higher altitudes.

A somewhat stronger seasonal behaviour was identified at the two highest stations (grey columns show the period from September to February, with the highest frequency of intrusion by the easterlies). Figure 5.3b depicts the frequency of trajectories on a yearly basis. In the first 3 years (2004–2006) the occurrence of westerlies was more frequent and

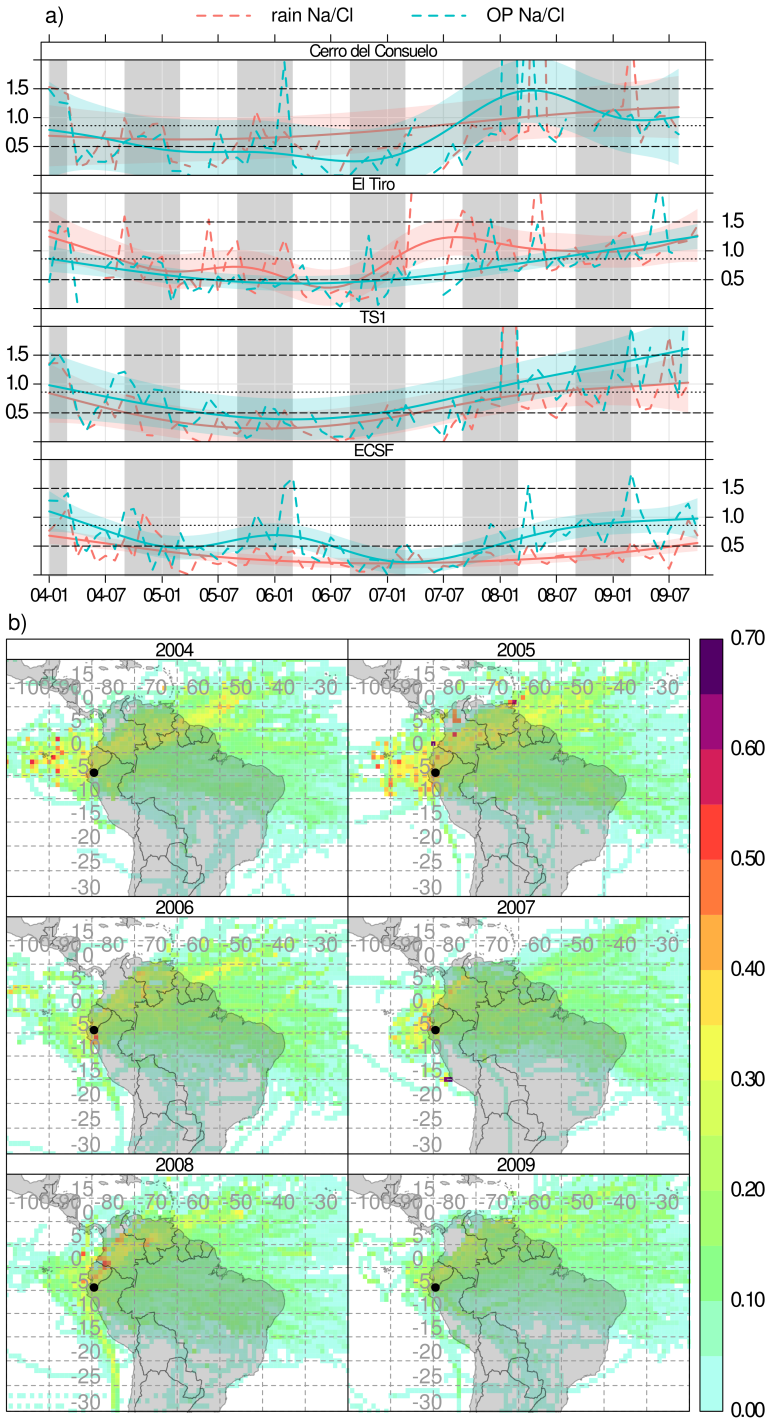

Figure 5.3: a) Time series of monthly Na^+ / Cl^- molar ratios for the four MSs along the altitudinal gradient. Smooth lines are fitted as solid lines and the 95 % confidence interval is shown by the shaded area. b) Yearly CWT sea salt source maps for southern Ecuador.

at the same time the Na^+ / Cl^- ratio was close to that of fresh sea water (local Pacific influence). During 2007–2009, when easterlies were more frequent, the Na^+ / Cl^- ratio increased due to the increasing influence of distant Atlantic sources (chloride is depleted during transport) and the likely contribution of forest and agricultural fires (Reid et al.

2004; Akagi et al. 2011).

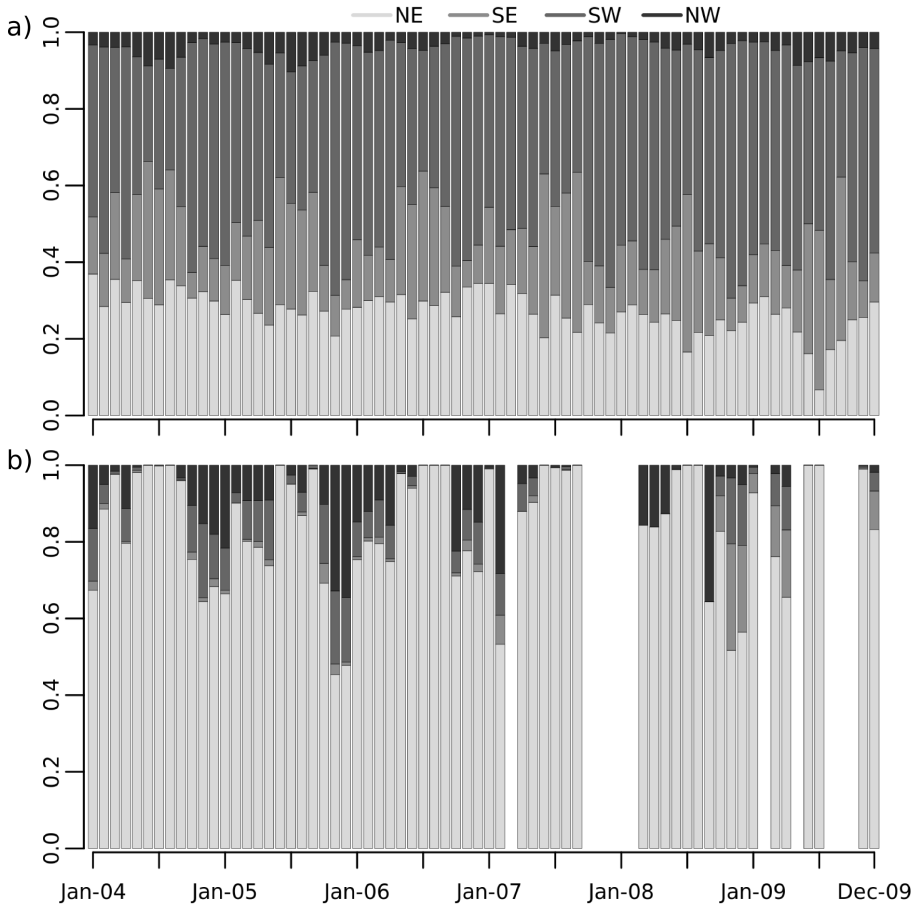

Figure 5.4: Monthly wind sector relative frequency (%) for meteorological stations a) ECSF and b) Cerro del Consuelo.

Locally driven winds, such as thermally induced anabatic winds, can contribute to the transport of local sodium and chloride from the valley to the upper parts of the catchment. In a previous study, however, Makowski Giannoni et al. (2013) showed that anabatic winds do not impact MSs located on mountain tops, where synoptic winds predominate. Figure 5.4a and b show relative frequencies of the wind direction at ECSF and Cerro del Consuelo, respectively. At the lower altitudes (ECSF) a typical mountain-valley breeze circulation system exists, while at the crest (Cerro del Consuelo) north-easterly wind directions predominated.

5.4.2 Spatial allocation of sources and general transport pathways

In the previous section, we analysed the temporal and altitudinal variation of sodium and chloride concentrations in deposition driven by rain and OP. This section addresses the remaining question of where the sodium and chloride source areas are located geographically.

The synoptic wind system over South America is driven by strong seasonal circulation patterns. Because the air mass transport to the receptor site is directly linked to the seasonal cycle of the large-scale circulation system (Bendix et al. 2008a; Emck 2007) and thus, sources of sea salt concentration and their intensity may vary with the seasons, we examined seasonal patterns present in the sources and dominant air mass trajectory clusters.

We first evaluated potential contributory sources to sea salt concentration at the receptor site for each season. For this purpose, the two hybrid receptor models were used as shown in Fig. 5.5. In accordance with a sensitivity analysis done with back trajectories starting at different altitudes, these functions were applied to 3180 m, the altitude of the MS Cerro del Consuelo, on top of the highest peak in the catchment. Trajectories starting at lower altitudes have greater uncertainty because local flows are driven by the complex topography and cannot be reproduced. Those starting at higher altitudes provided no further information as they have coincidental source areas.

Figure 5.5 shows the spatial distribution of potential sources calculated by the PSCF (a, b) and the CWT (c), for DJF, MAM, JJA, and SON at 3180 m starting height at the receptor. When we compare the spatial distribution of sources between the two models (PSCF and CWT), similar locations in the Atlantic and Pacific oceans are indicated. The highest likelihood (concentrations above $5e^{-9}$ for Fig. 5.5a and b and above $5e^{-9}$ for Fig. 5.5c) is an equatorial Pacific location, which points to stronger sources of sea salt in that region contributing to the high concentration at the receptor site.

Strong sources of sea salt are expected from either the Pacific or the Atlantic. To judge from the high probability that the concentration stems from the oceans, the results of the PSCF (90th percentile concentration threshold, Fig. 5.5b) and the CWT (Fig. 5.5c) performed best in discriminating between potential geographic sources that contributed to moderate and high sea salt concentrations over southern Ecuador. In contrast, when using the 75th percentile as the concentration threshold (Fig. 5.5a) the PSCF only detected the transport pathways for sea salt irrespective of the intensity of the source contribution to the concentration.

Seasonal source contributions that had the greatest impact, i.e. responsible for high sea salt concentrations at the receptor site, occurred between September and February (September, October, and November (SON) and December, January, and February (DJF)). During SON, the equatorial Pacific was the dominant source, while in DJF both the Pacific and Atlantic sources contributed to the concentration. Yet, the Pacific sources still appeared stronger, as indicated by the large number of high values in that area.

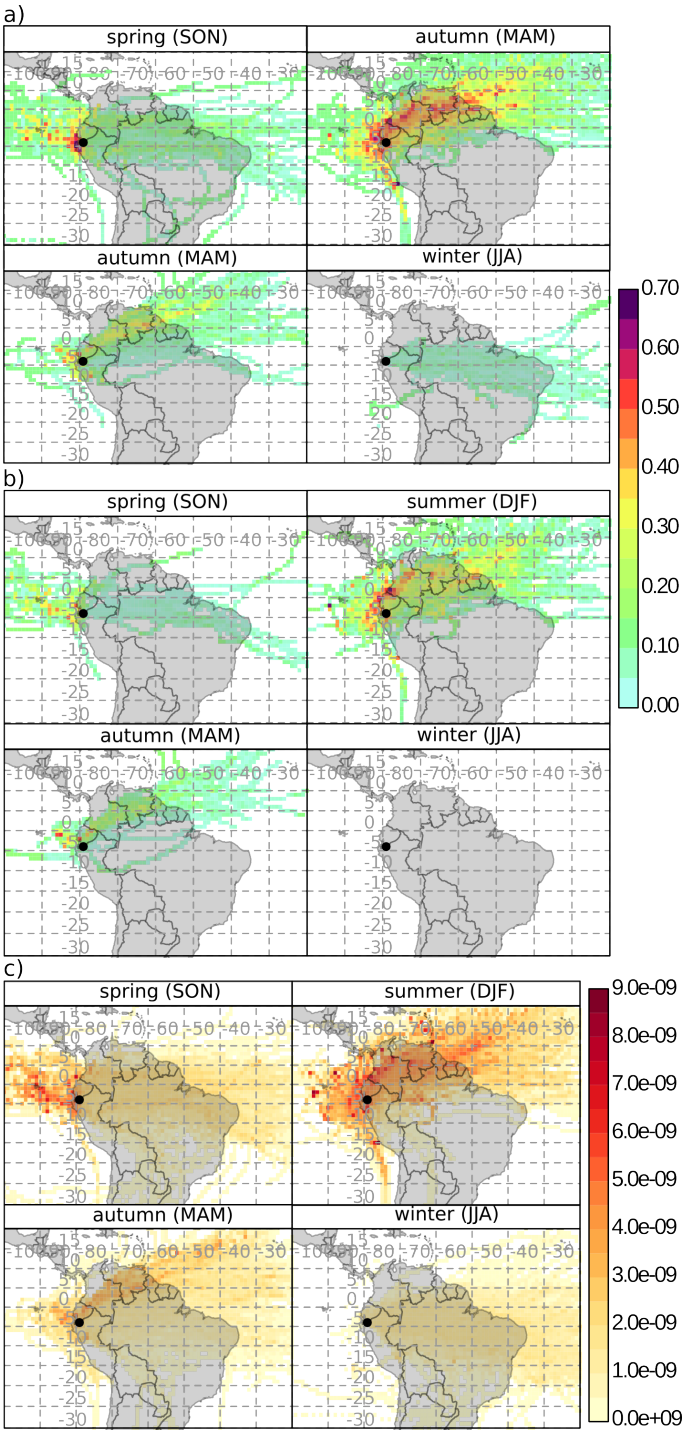

Figure 5.5: Seasonal sea salt source maps according to a) PSCF with concentration threshold at 75th percentile, b) PSCF with concentration threshold at 90th percentile, and c) CWT; the back trajectory starting height is 3180 m at the receptor.

Furthermore, chlorine-containing compounds related to sea salt and biomass burning were likely co-linearly transported during that season, as shown by the high concentration over the northern portion of South America during DJF, and the coincidence of the biomass-burning season in that area (Fig. 5.9). On the other hand, during austral autumn

(MAM) and winter (JJA) the models identified no relevant potential sources of high sea salt concentration.

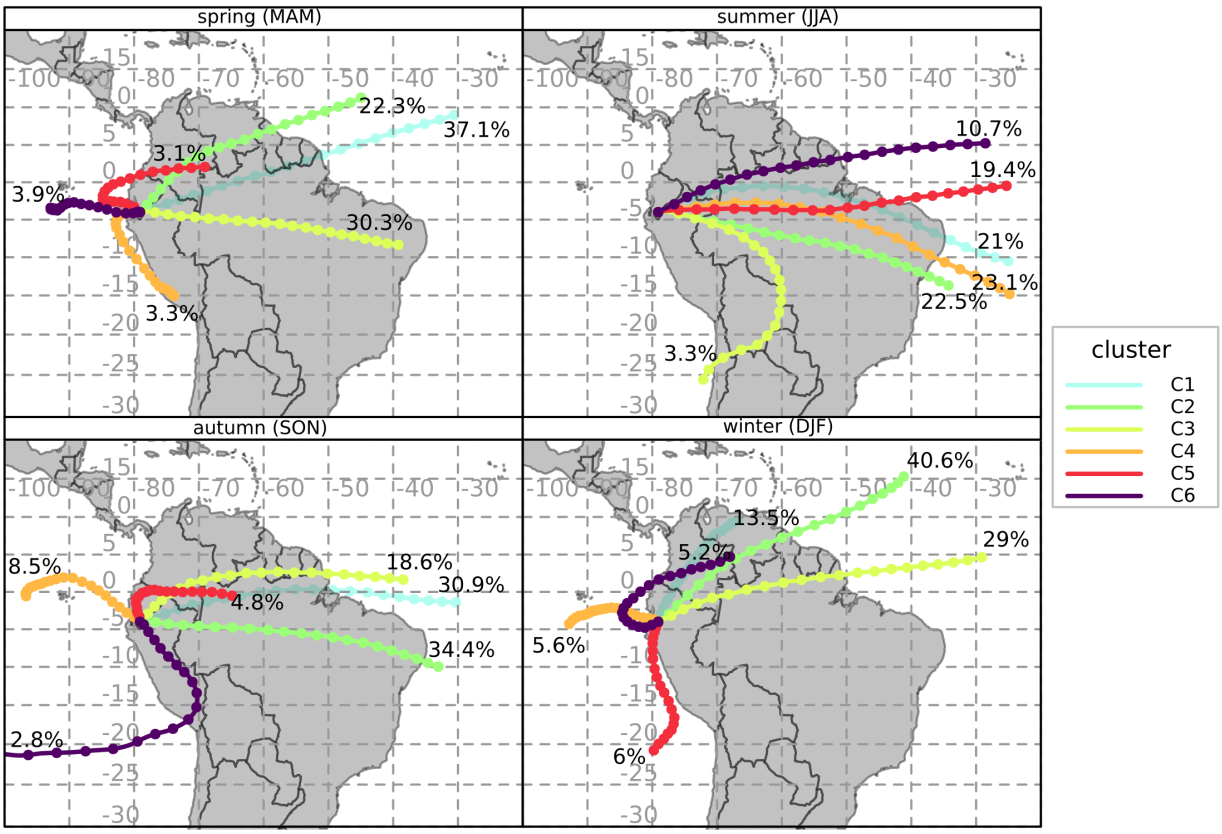

Figure 5.6: Seasonal mean back-trajectory clusters (C1–C6).

After locating the potential geographic sources of sea salt, trajectory cluster analysis was applied to identify the main representative air mass transport patterns, and thus the transport pathways of sea salt (Fig. 5.6). Here, the easterlies were dominant. In the air mass transport, fast flowing east trajectories dominated (from approximately 83 to 97 % of the trajectories, in DJF and JJA, respectively), and slower-moving trajectories from the west appeared rather sporadically (between approximately 2.8 and 17 %). The occurrence of bow-shaped trajectories was common (Fig. 5.6, MAM and DJF) and characterized the coastal wind system associated with the Humboldt current (Bendix et al. 2008a; Emck 2007).

Westerlies mostly evolved during SON and DJF, and to a lesser extent during MAM. Meanwhile, north easterlies were absent during the austral winter (JJA) following the displacement of the ITCZ to the north. The eastern clusters exhibited no seasonal pattern, because they represent the prevailing wind directions throughout the year.

Table 5.3: Mean sea salt concentration and percentage of total concentration for each season at the receptor site associated to the mean trajectory clusters (C1–C6) in the Andes of southern Ecuador. The percentage contribution of the mean clusters to the total concentration is shown in parenthesis

	Mean sea salt concentration (kg kg^{-1}) and relative total concentration (%)					
	C1	C2	C3	C4	C5	C6
Summer (DJF)	5.12E-09	5.18E-09	3.81E-09	5.86E-09	4.57E-09	5.78E-09
	(14.42)	(43.76)	(22.99)	(6.84)	(5.7)	(6.28)
Autumn (MAM)	1.90E-09	3.80E-09	1.35E-09	2.83E-09	3.85E-09	3.82E-09
	(30.34)	(36.42)	(17.6)	(4.04)	(5.18)	(6.43)
Winter (JJA)	1.72E-09	1.83E-09	1.64E-09	1.53E-09	1.81E-09	1.52E-09
	(21.28)	(24.33)	(3.2)	(20.83)	(20.77)	(9.6)
Spring (SON)	2.16E-09	2.33E-09	2.70E-09	6.53E-09	4.18E-09	3.47E-09
	(23.63)	(28.36)	(17.77)	(19.56)	(7.07)	(3.61)

Table 5.3 summarizes the mean sea salt concentration over southern Ecuador related to each cluster object reaching the receptor site for each season. High concentrations of sea salt are associated with westerly and north-easterly trajectories mainly occurring between September and May (Table 5.3), whereas easterly air masses that passed over the Atlantic and continental South America before arriving at the receptor site showed intermediate to lower concentrations. In addition to the cluster-associated mean sea salt concentration, values in parenthesis in Table 5.3 describe the proportion (in percentage) that each cluster contributes to the total concentration during the study period. Cluster C2, representing the north easterlies, was associated with the highest contributions in DJF and MAM. In SON, cluster C2 represented the easterlies and was likewise associated with the highest contributions. SON is the main biomass-burning season in the Brazilian Amazon, which likely contributed to the overall budget. Furthermore, easterlies' transport from September to May was associated with approximately 75–80 % of the total concentration. The remaining 15–20 % were attributed to air flows passing over the Pacific before reaching the receptor site. These highly loaded seasonal Pacific flows took place in the Southern Hemisphere's late spring and summer as easterlies weaken due to the southward shift of the ITCZ. Atlantic air masses contributed to the concentration constantly over the year, also in austral winter (JJA), when the Pacific flows were negligible. However, transport from the Pacific clearly dominated the high peaks at the end and the beginning of each year. The sea salt concentration associated with the easterly clusters was much weaker. However, due to its high frequency, it persistently contributed to the transport from the Atlantic with likely additions from Amazon fires. Similar seasonal patterns were also identified in the measurements as illustrated in Fig. 5.2, the most clearest of which occurred at the highest station, Cerro del Consuelo (Fig. 5.2a). That means that the observed patterns in the measurements can be explained by the large-scale atmospheric circulation patterns.

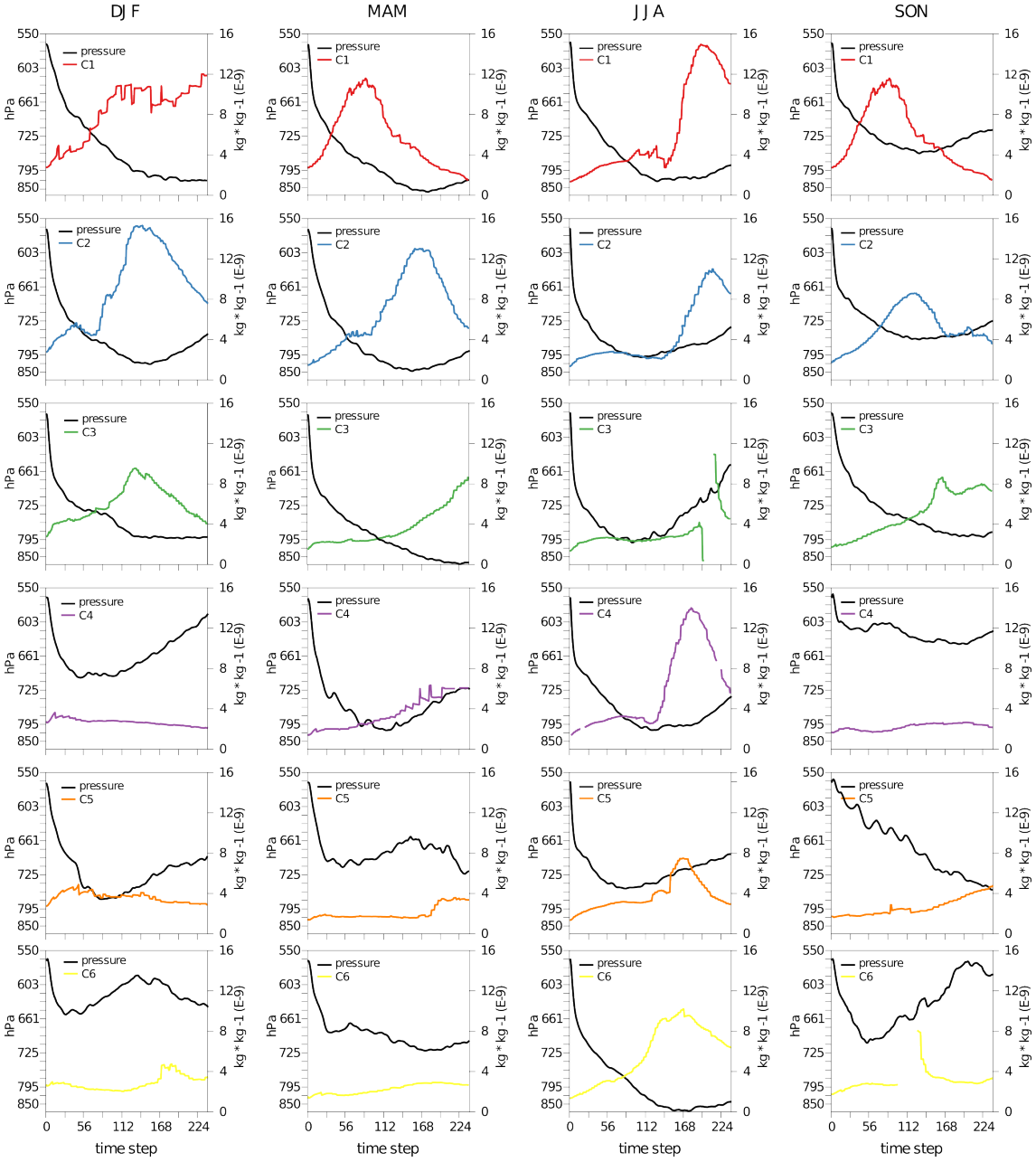

Figure 5.7: Seasonal plots of sea salt concentration and pressure level along mean back-trajectory clusters. The colours of the sea salt concentration lines match those in the trajectory clusters in Fig. 5.6.

Figure 5.7 depicts the sea salt concentration along the cluster mean trajectories and the trajectory height for each season. The north equatorial Atlantic was a great source of sea salt during DJF (Fig. 5.7, column 1), according to the sea salt concentration along the trajectory clusters. Nonetheless, the concentration rapidly decreased as the air masses travelled over the continent. Compared to westerly air masses, easterly air masses were lower in elevation, which increased the probability that they were loaded with aerosols from surface emissions. Those air masses then ascended abruptly as they approached the

Andean range. In comparison, the equatorial Pacific is a less significant source for sea salt. Because of its vicinity to the receptor site and because the air masses spent most of the time over the ocean, the concentration did not sink significantly over time (Fig. 5.7, C4–C6). The concentration peaks in C1 and C2 were due to sea salt intrusions from the Caribbean Sea and canalized by the Andean *cordillera*, as depicted in Fig. 5.8a. The season DJF was also characterized by frequent forest and agricultural fires in northern South America, which likely contributed chlorinated compounds from biomass burning to the budget as well (Fig. 5.9).

A similar situation also occurred in MAM (Fig. 5.7, column 2), where C1–C3 are north-easterly air masses and C4–C6 represent westerly pathways. In C2 the intrusion of sea salt from the Caribbean was also present, but less pronounced than in DJF (Fig. 5.8).

For SON (Fig. 5.7, column 3) most of the budget was transported from the Atlantic and the continent: clusters C1, C2, and C3. Because this period coincided with the Brazilian biomass-burning season (see Fig. 5.9), a considerable quantity of sodium and chloride from the Atlantic (Fig. 5.8a) and from fire emissions were probably transported to the receptor site.

5.5 Discussion

In this study, we examined potential sources of sodium and chloride for the southern escarpment of the Ecuadorian Andes. The investigation analysed chemical ion concentrations in rain and OP samples along an altitudinal gradient, using back-trajectory statistical analysis and source–receptor modelling.

We first explored the distribution of sodium and chloride inputs by rain and OP in relation to altitude. Overall, comparisons between the MSs reveal a difference in the temporal variation of the concentration of sodium and chloride in rain and OP depending on elevation and exposure. The highest MS, Cerro del Consuelo, displays a distinct seasonal pattern, which is otherwise lacking or less pronounced at the remaining MSs. The largest sodium and chloride concentration occurred between September and February, concomitantly with the southward migration of the ITCZ and the more frequent north easterlies (see Fig. 5.2).

Chloride was consistently a larger portion of the concentration than sodium, which agrees with findings by Tardy et al. (2005). Their study investigated the chemical composition of rainwater in the Amazon and found that in places closer to the Atlantic Ocean chloride concentrations were higher than sodium, whereas this ratio inverted for locations

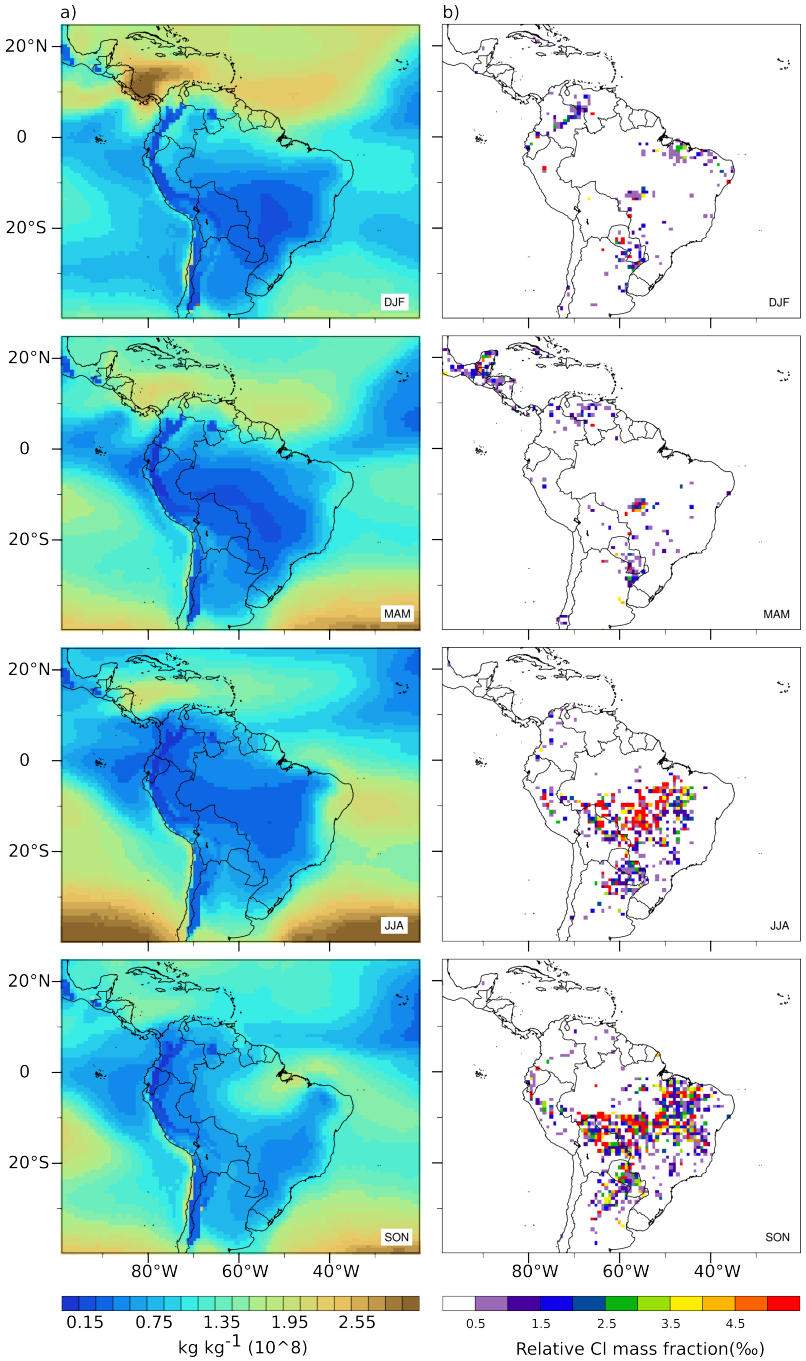

Figure 5.8: a) Seasonal maps of sea salt concentration calculated from the MACC reanalysis model. b) Seasonal maps of biomass-burning Cl mass fraction relative to sea salt. Cl mass ratio to NO_x was estimated based on emission factors from Ferek et al. (1998).

further away from the Atlantic coast. The observed excess in chloride concentration compared to sodium at our study site means that marine sources have a significant impact on the overall sea salt presence. This influence is also demonstrated by the Na^+ / Cl^- molar ratios in samples from the MSs along the altitudinal gradient. Higher altitudes are exposed to synoptic circulation and stations there register Na^+ / Cl^- ratios closer to that in marine air masses. This indicates a gradient of sea salt inputs with relation to terrain height.

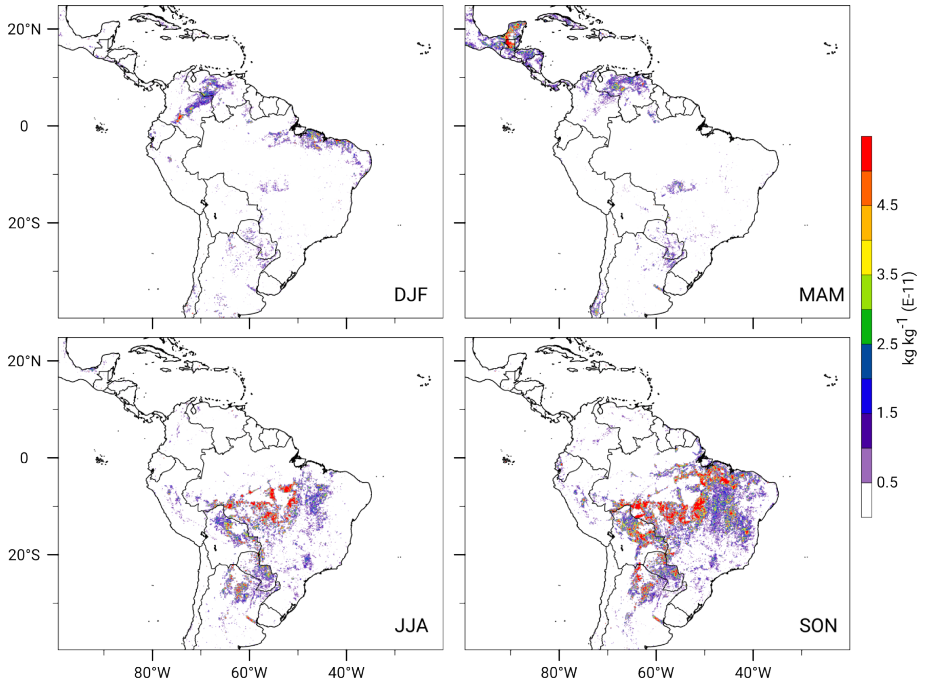

Figure 5.9: Seasonal maps of NO_x fluxes caused by biomass burning. Values were calculated from the MACC reanalysis model.

Common transport histories were identified on the basis of the PFA. As evinced by their prevalence in the first two components, sodium and chloride concentration are very relevant in both rain and OP. The fact that they exclusively load to factor 1 or 2, based on their location in multidimensional space, suggests the likely origin of sodium and chloride is sea salt from either the Pacific or the Atlantic Ocean. Biomass-burning seems to play a minor role in the transport of sodium and chloride, since nitrate and sulfate did not load to the same factor. Although emissions of chloride from fires may be recognizable (Akagi et al. 2011), they are likely irrelevant compared to sea salt (Fabian et al. 2009). Calcium and magnesium (crustal material) loading to factor 2 in OP at TS1 (Table 5.2) reveals the effect local winds have on emissions at lower elevations. The influence of chloride-containing dust blown from the Loja–Zamora road (Fig. 5.1) and plumes from local biomass-burning fires are the most likely causes of the high chloride concentrations at ECSF. Findings by Yokouchi et al. (2002), Spanos (2002), Hildemann et al. (1991), Akagi et al. (2011), and Harrison and Pio (1983) substantiate this assumption. According to these studies, chloride not only stems from sea spray but is also emitted from natural and anthropogenic terrestrial sources, i.e. dust, biomass-burning and biogenic forest emissions.

Concluding from the ion concentration time series (Fig. 5.2) and PFA (Table 5.2), the distribution of chloride and its sources can differ between valleys and mountain tops. In the former, the concentration is influenced by local winds and emissions, while in the latter

the concentration most likely depends on synoptic air-mass transport and emissions from distant sources. This difference in atmospheric circulation between valleys and mountain tops is clearly depicted in Fig. 5.4, in which only the mountain tops are strongly influenced by the synoptic circulation.

The potential sources defined by PSCF and CWT (Fig. 5.5) as well as the cluster-concentration statistics (Table 5.3) concur with the occurrence of the highest sodium and chloride concentration between September and February at the most elevated MSs – El Tiro and Cerro del Consuelo – in the study area (Fig. 5.2a, b and Table 5.3). This corroborates the conclusions reached in previous paragraphs that the transport at higher elevations is more synoptically driven. Thus, medium- to long-range transport (reproduced by back-trajectory modelling) has more of an effect in areas of high elevation than at lower slopes and valleys, which are more affected by local transport.

The results of the PSCF and CWT source–receptor models (Fig. 5.5a, b, c) indicate the areas that contribute to the highest concentration at the receptor site, i.e. the equatorial Pacific in the vicinity of the coast of Ecuador and northern Peru as well as the north equatorial Atlantic and the Caribbean Sea. Nonetheless, according to the spatial distribution of the sea salt concentration illustrated in Fig. 5.8a, the PSCF and CWT models seem to overestimate the contribution of the equatorial Pacific, which exhibits a lower sea salt concentration than the Atlantic Ocean. Analysis of the sea salt concentration along the trajectory clusters reveal a comparable behaviour, wherein the clusters passing over the Pacific contain a lower sea salt concentration. However, the concentration remains quite stable, contrary to the easterly trajectories passing over the continent, where wet scavenging is much more pronounced. Those drier conditions over the equatorial Pacific were clearly seen in DJF, where the concentration among clusters C4, C5, and C6 even increase as the air masses approach the receptor site (Fig. 5.7).

The CWT (Fig. 5.5c) model delivered the best results in that it successfully differentiates the source hot spots over the oceans from those areas of moderate contribution over the continent. In contrast, the PSCF (Fig. 5.5a, b) is less successful in making this distinction. As already reported by Hsu et al. (2003) and Stohl (1996) a drawback of the PSCF method is that the high and extreme values above a defined threshold get similar probabilities, which hamper their distinction. Thus, PSCF results are heavily influenced by the choice of an arbitrary threshold concentration. Pekney et al. (2006) reported that the selection of the threshold value relies on the evaluated concentration time series. The authors found that for low background values and high concentration peaks, the 90th percentile threshold performs better, while the 75th percentile is more appropriate for concentration time series with less variability. In our case, the quite strong seasonal

variations in the sea salt concentration explain why the PSCF performed better with the 90th percentile threshold (Fig. 5.5b) rather than the 75th percentile (Fig. 5.5a).

Table 5.4: Comparison of the mean concentration of Na^+ and Cl^- in precipitation in this study with data from other sites in the Amazon basin. The values represent volume-weighted means expressed in μ eq. L^{-1}

	Na^+	Cl^-	Reference
South Ecuador (RBSF)	7.80	9.60	This study
Central Amazon (Lake Calado)	2.40	4.60	Williams et al. (1997)
Central Amazon (Balbina)	3.80	5.20	Pauliquevis et al. (2012)
Northeast Amazon	16.60	16.90	Forti et al. (2000)
Eastern Amazon (Belem)	18.90	19.50	Mortatti (1995)

To perform a cluster analysis, the trajectories were grouped together and six dominant pathways were identified (C1–C6 in Fig. 5.6). In general, over the entire observation period, the eastern clusters originating on the equatorial and south equatorial Atlantic predominate ($>$ 51 % of the trajectories). However, when seasonally linking the main transport pathways (C1–C6) to the sea salt concentration at the receptor site (see Table 5.3), we notice that those pathways do not have the highest impact on the sea salt concentration in southern Ecuador. Even if easterly and south-easterly transport prevail, larger sea salt loads are transported from the north equatorial Atlantic, the Caribbean Sea, and the equatorial Pacific. The north easterlies originating from the north equatorial Atlantic and Caribbean Sea occurred approximately 29.5 % of the time and accounted for around 56.5 % of the concentration over southern Ecuador. The westerlies from the equatorial Pacific were much less frequent ($\approx$ 9.3 %) and accounted for 26 % of the concentration. That means, despite the barrier effect of the Andes and the low frequency of occurrences of western pathways, Pacific sea salt sources still play a relevant role in transporting sea salt to the receptor site. Together, equatorial Pacific and north equatorial Atlantic sources accounted for around 82.4 % of the total sea salt concentration. Furthermore, large quantities were added solely from the equatorial Pacific and the Caribbean Sea in a short period of time ($\approx$ 16 % of trajectories), contributing up to 46.7 % of the total concentration, which stress the importance of these sources to the atmospheric sea salt budget over southern Ecuador.

Nevertheless, in light of the sea salt concentration along the seasonal trajectory clusters (Fig. 5.7) and sea salt's spatial distribution (Fig. 5.8a), the significance of Pacific sea salt remains questionable. The concentration of sea salt in the equatorial Pacific is less than that in the Atlantic. Therefore, the former's influence may be overestimated, even if the concentration decay over the Pacific is much less pronounced as over continental South America. On the one hand, the greater frequency of the north easterlies, and on the other hand, the higher sea salt concentration in the Atlantic are good reasons that justify a

greater influence of the Caribbean Sea and the north equatorial Atlantic with respect to the atmospheric sea salt budget over southern Ecuador.

Regarding the addition of salt from biomass burning to the chloride budget at the study area, based on the co-occurrence of high NO_x concentration from biomass burning and high sea salt concentration during the main sea salt transport season (SON and DJF, in Figs. 5.8a and 5.9), it is very likely that sea salt is indeed enriched by biomass-burning chloride. However, this assumption is not corroborated by our field samples from southern Ecuador. In the concentration of sodium and chloride from rain and OP samples we did not find any correlation between nitrate and sulfate, the products of biomass burning (Fabian et al. 2009; Makowski Giannoni et al. 2013, 2014), and sodium and chloride (Table 5.2). Furthermore, the mass fraction of biomass-burning sodium (maximum 0.07 %) and chloride (maximum values in the order of 3.5 %, see Fig. 5.8b) are very small and therefore play only a limited role in the sodium and chloride transport to south Ecuador.

5.6 Conclusions

Sodium and chloride ions exhibited different concentrations in rain and OP along the altitudinal gradient of interest to this study. Their concentration levels and temporal variability in the highest and more exposed MSs presented a stronger seasonality linked to global circulation patterns, and thus a greater influence from sea salt, confirmed by Na^+ / Cl^- molar ratios similar to those from marine air masses. Similar seasonal patterns were observed by modelling at a larger scale, using MACC sea salt concentration data and ERA-Interim air mass back trajectories, confirming the influence of the medium- to long-range transport at higher elevations. In contrast, MSs situated at lower altitudes were influenced by the mountain-valley wind systems and local aerosols.

According the sea salt transport analysis by back-trajectory modelling for medium- to long-range sources, the Caribbean Sea, the north equatorial Atlantic, and equatorial Pacific play an important role in the transport of sea salt to southern Ecuador. Here, the Caribbean and north equatorial Atlantic sources have the greatest impact. Equatorial Pacific sources, on the other hand, are less significant: they are seasonally driven with the greatest contributions occurring when the ITCZ migrates further south in austral late spring (SON) and summer (DJF). In total, the north equatorial Atlantic and equatorial Pacific contribute to 56.5 and 26 % of the total concentration in southern Ecuador, respectively, which represents an important addition to the total atmospheric sea salt budget.

A comparison of the sodium and chloride concentrations at our area of investigation with those at other sites further east substantiates the important role played by the identified

sources (Caribbean Sea, north equatorial Atlantic, and equatorial Pacific oceans) on the sea salt transport to our study area (Table 5.4). Even if concentrations in southern Ecuador are lower than in forests close to the Atlantic, they clearly exceed those concentrations measured in the central Brazilian Amazon thousands of kilometres to the east, despite being located further from the Atlantic coast. However, whether the higher sodium and chloride availability observed in southern Ecuador makes this tropical ecosystem less salt deprived than other similar ecosystems in the western Amazon is still an open question deserving of investigation.

5.7 Data availability

The MACC sea salt and biomass-burning NO_x fluxes are available at `http://apps.ecmwf.int/datasets/data/macc-reanalysis/levtype=ml/` and `http://apps.ecmwf.int/datasets/data/cams-gfas/`, respectively. The ERA Interim reanalysis data can be accessed at `http://apps.ecmwf.int/datasets/data/interim-full-daily/levtype=sfc/`. The precipitation chemistry data and climate data from in-situ meteorological stations are accessible at the Platform for Biodiversity and Ecosystem Monitoring and Research in South Ecuador: `http://www.tropicalmountainforest.org/data_pre.do?cmd=showall`.

Acknowledgements

We thank the German Academic Exchange Service (DAAD) for funding the PhD thesis of S. Makowski Giannoni (ref. no. A/08/98222) and the German Research Foundation (DFG) for funding this work in the scope of the Research Unit RU816 (funding no. BE 1780/15-1). We also thank Thorsten Peters for providing meteorological data. We are grateful to Giulia F. Curatola Fernández and Tim Appelhans for their valuable help. We also thank the foundation Nature & Culture International (NCI) Loja and San Diego for logistic support. Last but not least we are very thankful to Jeffrey Reid from the U.S. Naval Research Laboratory for his valuable comments on the manuscript.

Edited by: R. Krejci
Reviewed by: J. Reid and two anonymous referees

Appendix A5

Table A5.1: The 6-year average ion concentration (2004–2009) in rain and OP, precipitation volume, and electrical conductivity at MSs along an altitudinal gradient in southern Ecuador.

Site	Collector	Elev. (m)	P (mm)	pH	eC (μ S cm^{-1})	NH_4^-	Ca^+	Cl^-	PO_4^-	Mg^+ (mg L^{-1})	NO_3^-	K^+	Na^+	SO_4^-
C. del Consuelo	OP	3180	105.59	5.4	12	0.55	0.17	0.42	0.085	0.059	0.82	0.15	0.22	1
C. del Consuelo	Rain	3180	472.65	5.3	3.5	0.18	0.1	0.29	0.16	0.05	0.11	0.098	0.14	0.26
ECSF	OP	1960	7.26	5	13	0.17	0.42	0.86	0.098	0.073	0.14	0.23	0.22	0.44
ECSF	Rain	1960	142.48	5.3	4.3	0.15	0.11	0.43	0.13	0.048	0.077	0.16	0.18	0.24
El Tiro	OP	2825	75.41	6	20	0.8	0.19	0.45	0.12	0.07	1.4	0.3	0.31	1.6
El Tiro	Rain	2825	142.37	5.4	5.4	0.22	0.14	0.36	0.15	0.047	0.12	0.15	0.24	0.39
TS1	OP	2660	34.15	5.3	5.2	0.25	0.12	0.5	0.16	0.054	0.16	0.12	0.25	0.32
TS1	Rain	2660	279	5.4	4	0.18	0.077	0.36	0.13	0.047	0.084	0.13	0.18	0.26

Bibliography

Akagi, S. K., Yokelson, R. J., Wiedinmyer, C., Alvarado, M. J., Reid, J. S., Karl, T., Crounse, J. D., and Wennberg, P. O.: Emission factors for open and domestic biomass burning for use in atmospheric models, Atmos. Chem. Phys., 11, 4039–4072, doi: 10.5194/acp-11-4039-2011, URL http://www.atmos-chem-phys.net/11/4039/2011/, 2011.

Beck, E., Makeschin, F., Haubrich, F., Richter, M., Bendix, J., and Valarezo, C.: The Ecosystem (Reserva Biológica San Francisco), in: Gradients in a tropical mountain ecosystem of Ecuador, edited by Beck, E., Bendix, J., Kottke, I., Makeschin, F., and Mosandl, R., chap. 1, pp. 1–14, Springer, URL http://www.springer.com/life+sciences/ecology/book/978-3-540-73525-0, 2008.

Bendix, J., Rollenbeck, R., and Reudenbach, C.: Diurnal patterns of rainfall in a tropical Andean valley of southern Ecuador as seen by a vertically pointing K-band Doppler radar, Int. J. Climatol., 26, 829–846, doi:10.1002/joc.1267, URL http://onlinelibrary.wiley.com/doi/10.1002/joc.1267/fullhttp://doi.wiley.com/10.1002/joc.1267, 2006.

Bendix, J., Rollenbeck, R., Göttlicher, D., Nauß, T., Fabian, P., Goettlicher, D., Nauss, T., and Fabian, P.: Seasonality and diurnal pattern of very low clouds in a deeply incised valley of the eastern tropical Andes (South Ecuador) as observed by a cost-effective webcam system, Meteorol. Appl., 15, 281–291, doi:10.1002/met, URL http://onlinelibrary.wiley.com/doi/10.1002/met.72/abstract, 2008a.

Bendix, J., Rollenbeck, R., Richter, M., Fabian, P., and Emck, P.: Climate, in: Gradients in a tropical mountain ecosystem of Ecuador, edited by Beck, E., Bendix, J., Kottke, I., Makeschin, F., and Mosandl, R., chap. 1, pp. 63–74, Springer Berlin / Heidelberg, ecological edn., URL http://dx.doi.org/10.1007/978-3-540-73526-7{\protect\T1\textbraceleft}{_}{\protect\T1\textbraceright}8, 2008b.

Bendix, J., Beck, E., Bräuning, A., Makeschin, F., Mosandl, R., Scheu, S., and Wilcke, W., eds.: Ecosystem services, biodiversity and environmental change in a tropical mountain ecosystem of South Ecuador, vol. 221 of *Ecological Studies*, Springer Berlin / Heidelberg, doi:10.1007/978-3-642-38137-9, URL http://link.springer.com/10.1007/978-3-642-38137-9, 2013.

Benedetti, A., Morcrette, J., Boucher, O., Dethof, A., Engelen, R. J., Fisher, M., Flentje, H., Huneeus, N., Jones, L., Kaiser, J. W., Kinne, S., Mangold, A., Razinger, M., Simmons,

A. J., and Suttie, M.: Aerosol analysis and forecast in the European Centre for Medium-Range Weather Forecasts Integrated Forecast System: 2. Data assimilation, J. Geophys. Res., 114, D13 205, doi:10.1029/2008JD011115, URL http://doi.wiley.com/10.1029/2008JD011115, 2009.

Bobbink, R., Hicks, K., Galloway, J., Spranger, T., Alkemade, R., Ashmore, M., Bustamante, M., Cinderby, S., Davidson, E., Dentener, F., Emmett, B., Erisman, J. W., Fenn, M., Gilliam, F., Nordin, A., Pardo, L., and De Vries, W.: Global assessment of nitrogen deposition effects on terrestrial plant diversity: a synthesis, Ecol. Appl., 20, 30–59, doi:10.1890/08-1140.1, URL http://www.esajournals.org/doi/abs/10.1890/08-1140.1, 2010.

Carslaw, D. C. and Ropkins, K.: Openair - An R package for air quality data analysis, Environ. Model. Softw., 27-28, 52–61, doi:10.1016/j.envsoft.2011.09.008, URL http://linkinghub.elsevier.com/retrieve/pii/S1364815211002064, 2012.

Clarke, N., Zlindra, D., Ulrich, E., Mosello, R., Derome, J., Derome, K., König, N., Lövblad, G., Draaijers, G., Hansen, K., Thimonier, A., and Waldner, P.: Sampling and analysis of deposition: part XIV, in: Manual on methods and criteria for harmonized sampling, assessment, monitoring and analysis of the effects of air pollution on forests, chap. 14, UNECE, ICP Forests, Hamburg, URL http://icp-forests.net/page/icp-forests-manual, 2010.

Dee, D. P., Uppala, S. M., Simmons, A. J., Berrisford, P., Poli, P., Kobayashi, S., Andrae, U., Balmaseda, M. A., Balsamo, G., Bauer, P., Bechtold, P., Beljaars, A. C. M., van de Berg, L., Bidlot, J., Bormann, N., Delsol, C., Dragani, R., Fuentes, M., Geer, A. J., Haimberger, L., Healy, S. B., Hersbach, H., Hólm, E. V., Isaksen, L., Kållberg, P., Köhler, M., Matricardi, M., McNally, A. P., Monge-Sanz, B. M., Morcrette, J.-J., Park, B.-K., Peubey, C., de Rosnay, P., Tavolato, C., Thépaut, J.-N., and Vitart, F.: The ERA-Interim reanalysis: configuration and performance of the data assimilation system, Q. J. R. Meteorol. Soc., 137, 553–597, doi:10.1002/qj.828, URL http://doi.wiley.com/10.1002/qj.828, 2011.

Dentener, F., Drevet, J., Lamarque, J. F., Bey, I., Eickhout, B., Fiore, A. M., Hauglustaine, D., Horowitz, L. W., Krol, M., Kulshrestha, U. C., Lawrence, M., Galy-Lacaux, C., Rast, S., Shindell, D., Stevenson, D., Van Noije, T., Atherton, C., Bell, N., Bergman, D., Butler, T., Cofala, J., Collins, B., Doherty, R., Ellingsen, K., Galloway, J., Gauss, M., Montanaro, V., Müller, J. F., Pitari, G., Rodriguez, J., Sanderson, M., Solmon, F., Strahan, S., Schultz, M., Sudo, K., Szopa, S., and Wild, O.: Nitrogen and sulfur deposition on regional and global scales: a

multimodel evaluation, Global Biogeochem. Cycles, 20, GB4003, doi:10.1029/2005GB002672, URL http://dx.doi.org/10.1029/2005GB002672http://www.agu.org/pubs/crossref/2006/2005GB002672.shtml, 2006.

Draxler, R. and Hess, G.: An overview of the HYSPLIT_4 modeling system of trajectories, dispersion, and deposition, Aust. Meteorol. Mag., 47, 295–308, 1998.

Dudley, R., Kaspari, M., and Yanoviak, S. P.: Lust for salt in the western Amazon, Biotropica, 44, 6–9, doi:10.1111/j.1744-7429.2011.00818.x, URL http://doi.wiley.com/10.1111/j.1744-7429.2011.00818.x, 2012.

Emck, P.: A climatology of South Ecuador, Phd thesis, Fachbereich Geographie der Friedrich-Alexander-Universität Erlangen-Nürnberg, Germany, URL http://www.opus.ub.uni-erlangen.de/opus/volltexte/2007/656/, 2007.

Fabian, P., Rollenbeck, R., Spichtinger, N., Brothers, L., Dominguez, G., and Thiemens, M.: Sahara dust, ocean spray, volcanoes, biomass burning: pathways of nutrients into Andean rainforests, Adv. Geosci., 22, 85–94, doi:10.5194/adgeo-22-85-2009, URL http://www.adv-geosci.net/22/85/2009/, 2009.

Ferek, R. J., Reid, J. S., Hobbs, P. V., Blake, D. R., and Liousse, C.: Emission factors of hydrocarbons, halocarbons, trace gases and particles from biomass burning in Brazil, J. Geophys. Res. Atmos., 103, 32 107–32 118, doi:10.1029/98JD00692, URL http://doi.wiley.com/10.1029/98JD00692, 1998.

Fleming, Z. L., Monks, P. S., and Manning, A. J.: Review: untangling the influence of air-mass history in interpreting observed atmospheric composition, Atmos. Res., 104-105, 1–39, doi:10.1016/j.atmosres.2011.09.009, URL http://linkinghub.elsevier.com/retrieve/pii/S0169809511002948, 2012.

Forti, M. C., Melfi, A. J., Astolfo, R., and Fostier, A.-H.: Rainfall chemistry composition in two ecosystems in the northeastern Brazilian Amazon (Amapá State), J. Geophys. Res., 105, 28 895, doi:10.1029/2000JD900235, URL http://doi.wiley.com/10.1029/2000JD900235, 2000.

Galloway, J. N., Townsend, A. R., Erisman, J. W., Bekunda, M., Cai, Z., Freney, J. R., Martinelli, L. A., Seitzinger, S. P., and Sutton, M. A.: Transformation of the nitrogen cycle: recent trends, questions, and potential solutions., Science, 320, 889–92, doi:10.1126/science.1136674, URL http://www.ncbi.nlm.nih.gov/pubmed/18487183, 2008.

Griffith, K. T., Ponette-González, A. G., Curran, L. M., and Weathers, K. C.: Assessing the influence of topography and canopy structure on Douglas fir throughfall with LiDAR

and empirical data in the Santa Cruz mountains, USA., Environ. Monit. Assess., 187, 4486, doi:10.1007/s10661-015-4486-6, URL http://www.ncbi.nlm.nih.gov/pubmed/25893759, 2015.

Guelle, W., Schulz, M., Balkanski, Y., and Dentener, F.: Influence of the source formulation on modeling the atmospheric global distribution of sea salt aerosol, J. Geophys. Res., 106, 27 509, doi:10.1029/2001JD900249, URL http://doi.wiley.com/10.1029/2001JD900249, 2001.

Harrison, R. M. and Pio, C. A.: Major ion composition and chemical associations of inorganic atmospheric aerosols., Environ. Sci. Technol., 17, 169–74, doi:10.1021/es00109a009, URL http://dx.doi.org/10.1021/es00109a009, 1983.

Hildemann, L. M., Markowski, G. R., and Cass, G. R.: Chemical composition of emissions from urban sources of fine organic aerosol, Environ. Sci. Technol., 25, 744–759, doi:10.1021/es00016a021, URL http://dx.doi.org/10.1021/es00016a021, 1991.

Homeier, J., Hertel, D., Camenzind, T., Cumbicus, N. L., Maraun, M., Martinson, G. O., Poma, L. N., Rillig, M. C., Sandmann, D., Scheu, S., Veldkamp, E., Wilcke, W., Wullaert, H., and Leuschner, C.: Tropical andean forests are highly susceptible to nutrient inputs–rapid effects of experimental N and P addition to an ecuadorian montane forest., PLoS One, 7, e47 128, doi:10.1371/journal.pone.0047128, URL http://www.pubmedcentral.nih.gov/articlerender.fcgi?artid=3468540{&}tool=pmcentrez{&}rendertype=abstract, 2012.

Hsu, Y.-K., Holsen, T. M., and Hopke, P. K.: Comparison of hybrid receptor models to locate PCB sources in Chicago, Atmos. Environ., 37, 545–562, doi:10.1016/S1352-2310(02)00886-5, URL http://linkinghub.elsevier.com/retrieve/pii/S1352231002008865, 2003.

Inness, A., Baier, F., Benedetti, A., Bouarar, I., Chabrillat, S., Clark, H., Clerbaux, C., Coheur, P., Engelen, R. J., Errera, Q., Flemming, J., George, M., Granier, C., Hadji-Lazaro, J., Huijnen, V., Hurtmans, D., Jones, L., Kaiser, J. W., Kapsomenakis, J., Lefever, K., Leitão, J., Razinger, M., Richter, A., Schultz, M. G., Simmons, A. J., Suttie, M., Stein, O., Thépaut, J.-N., Thouret, V., Vrekoussis, M., and Zerefos, C.: The MACC reanalysis: an 8 yr data set of atmospheric composition, Atmos. Chem. Phys., 13, 4073–4109, doi:10.5194/acp-13-4073-2013, URL http://www.atmos-chem-phys.net/13/4073/2013/, 2013.

Jaeglé, L., Quinn, P. K., Bates, T. S., Alexander, B., and Lin, J.-T.: Global distribution of sea salt aerosols: new constraints from in situ and remote

sensing observations, Atmos. Chem. Phys., 11, 3137–3157, doi:10.5194/acp-11-3137-2011, URL http://www.atmos-chem-phys.net/11/3137/2011/acp-11-3137-2011.html, 2011.

Kaiser, J. W., Heil, A., Andreae, M. O., Benedetti, A., Chubarova, N., Jones, L., Morcrette, J.-J., Razinger, M., Schultz, M. G., Suttie, M., and van der Werf, G. R.: Biomass burning emissions estimated with a global fire assimilation system based on observed fire radiative power, Biogeosciences, 9, 527–554, doi:10.5194/bg-9-527-2012, URL http://www.biogeosciences.net/9/527/2012/, 2012.

Kaspari, M., Yanoviak, S. P., and Dudley, R.: On the biogeography of salt limitation: a study of ant communities., Proc. Natl. Acad. Sci. U.S.A., 105, 17 848–51, doi:10.1073/pnas.0804528105, URL http://www.pubmedcentral.nih.gov/articlerender.fcgi?artid=2584704{&}tool=pmcentrez{&}rendertype=abstract, 2008.

Kaspari, M., Yanoviak, S. P., Dudley, R., Yuan, M., and Clay, N. A.: Sodium shortage as a constraint on the carbon cycle in an inland tropical rainforest., Proc. Natl. Acad. Sci. U.S.A., 106, 19 405–9, doi:10.1073/pnas.0906448106, URL http://www.pnas.org/content/106/46/19405.abstract, 2009.

Keene, W. C., Pszenny, A. A. P., Galloway, J. N., and Hawley, M. E.: Sea-salt corrections and interpretation of constituent ratios in marine precipitation, J. Geophys. Res., 91, 6647, doi:10.1029/JD091iD06p06647, URL http://doi.wiley.com/10.1029/JD091iD06p06647, 1986.

Kirchner, M., Fegg, W., Römmelt, H., Leuchner, M., Ries, L., Zimmermann, R., Michalke, B., Wallasch, M., Maguhn, J., Faus-Kessler, T., and Jakobi, G.: Nitrogen deposition along differently exposed slopes in the Bavarian Alps, Sci. Total Environ., 470-471, 895–906, doi:10.1016/j.scitotenv.2013.10.036, URL http://www.sciencedirect.com/science/article/pii/S0048969713011807, 2014.

Koehler, B., Corre, M. D., Veldkamp, E., Wullaert, H., and Wright, S. J.: Immediate and long-term nitrogen oxide emissions from tropical forest soils exposed to elevated nitrogen input, Glob. Chang. Biol., 15, 2049–2066, doi:10.1111/j.1365-2486.2008.01826.x, URL http://doi.wiley.com/10.1111/j.1365-2486.2008.01826.x, 2009.

Lee, A. T. K., Kumar, S., Brightsmith, D. J., and Marsden, S. J.: Parrot claylick distribution in South America: do patterns of "where" help answer the question "why"?, Ecography, doi:10.1111/j.1600-0587.2009.05878.x, URL http://doi.wiley.com/10.1111/j.1600-0587.2009.05878.x, 2009.

Lizcano, D. J. and Cavelier, J.: Características químicas de salados y hábitos alimenticios de la Danta de montaña (Tapirus pinchaque Roulin, 1829) en los Andes Centrales de Colombia, Mastozoología Neotrop., 11, 193–201, URL http://www.scielo.org.ar/scielo.php?script=sci{_}arttext{&}pid=S0327-93832004000200004{&}lng=es{&}nrm=iso{&}tlng=es, 2004.

Lovett, G. and Kinsman, J.: Atmospheric pollutant deposition to high-elevation ecosystems, Atmos. Environ., 24, 2767–2786, URL http://www.sciencedirect.com/science/article/pii/096016869090164I, 1990.

Mahowald, N. M., Artaxo, P., Baker, A. R., Jickells, T. D., Okin, G. S., Randerson, J. T., and Townsend, A. R.: Impacts of biomass burning emissions and land use change on Amazonian atmospheric phosphorus cycling and deposition, Global Biogeochem. Cycles, 19, n/a–n/a, doi:10.1029/2005GB002541, URL http://doi.wiley.com/10.1029/2005GB002541, 2005.

Makowski Giannoni, S., Rollenbeck, R., Fabian, P., and Bendix, J.: Complex topography influences atmospheric nitrate deposition in a neotropical mountain rainforest, Atmos. Environ., 79, 385–394, doi:10.1016/j.atmosenv.2013.06.023, URL http://www.sciencedirect.com/science/article/pii/S1352231013004780http://linkinghub.elsevier.com/retrieve/pii/S1352231013004780, 2013.

Makowski Giannoni, S., Rollenbeck, R., Trachte, K., and Bendix, J.: Natural or anthropogenic? On the origin of atmospheric sulfate deposition in the Andes of southeastern Ecuador, Atmos. Chem. Phys., 14, 11 297–11 312, doi:10.5194/acp-14-11297-2014, URL http://www.atmos-chem-phys.net/14/11297/2014/, 2014.

Malm, W. C., Johnson, C. E., and Bresch, J. F.: Application of principal component analysis for purposes of identifying source-receptor relationships, in: Recept. methods source apportionment, edited by Pace, T. G., Air pollution control association, Pittsburgh, PA, 1986.

Matson, A. L., Corre, M. D., and Veldkamp, E.: Nitrogen cycling in canopy soils of tropical montane forests responds rapidly to indirect N and P fertilization., Glob. Chang. Biol., 20, 3802–13, doi:10.1111/gcb.12668, URL http://www.ncbi.nlm.nih.gov/pubmed/24965673, 2014.

Matson, P., Lohse, K. A., and Hall, S. J.: The globalization of nitrogen deposition: Consequences for terrestrial ecosystems, Ambio, 31, 113–119, URL http://www.jstor.org/stable/4315223, 2002.

Millero, F.: Treatise on Geochemistry, Elsevier, doi:10.1016/B978-0-08-095975-7.00601-X, URL http://www.sciencedirect.com/science/article/pii/B978008095975700601X, 2014.

Morcrette, J., Boucher, O., Jones, L., Salmond, D., Bechtold, P., Beljaars, A., Benedetti, A., Bonet, A., Kaiser, J. W., Razinger, M., Schulz, M., Serrar, S., Simmons, A. J., Sofiev, M., Suttie, M., Tompkins, A. M., and Untch, A.: Aerosol analysis and forecast in the European Centre for Medium-Range Weather Forecasts Integrated Forecast System: forward modeling, J. Geophys. Res., 114, D06 206, doi:10.1029/2008JD011235, URL http://doi.wiley.com/10.1029/2008JD011235, 2009.

Mortatti, J.: Erosão na Amazonia: processos, modelos e balanço, Phd thesis, São Paulo, Brazil, 1995.

Pauliquevis, T., Lara, L. L., Antunes, M. L., and Artaxo, P.: Aerosol and precipitation chemistry measurements in a remote site in Central Amazonia: the role of biogenic contribution, Atmos. Chem. Phys., 12, 4987–5015, doi:10.5194/acp-12-4987-2012, URL http://www.atmos-chem-phys.net/12/4987/2012/acp-12-4987-2012.html, 2012.

Pekney, N. J., Davidson, C. I., Zhou, L., and Hopke, P. K.: Application of PSCF and CPF to PMF-modeled sources of PM 2.5 in Pittsburgh, Aerosol Sci. Technol., 40, 952–961, doi:10.1080/02786820500543324, URL http://www.tandfonline.com/doi/abs/10.1080/02786820500543324, 2006.

Peñuelas, J., Poulter, B., Sardans, J., Ciais, P., van der Velde, M., Bopp, L., Boucher, O., Godderis, Y., Hinsinger, P., Llusia, J., Nardin, E., Vicca, S., Obersteiner, M., and Janssens, I. A.: Human-induced nitrogen-phosphorus imbalances alter natural and managed ecosystems across the globe., Nat. Commun., 4, 2934, doi:10.1038/ncomms3934, URL http://www.nature.com/ncomms/2013/131217/ncomms3934/full/ncomms3934.html, 2013.

Pett-Ridge, J. C.: Contributions of dust to phosphorus cycling in tropical forests of the Luquillo Mountains, Puerto Rico, Biogeochemistry, 94, 63–80, doi:10.1007/s10533-009-9308-x, URL http://link.springer.com/10.1007/s10533-009-9308-x, 2009.

Phoenix, G. K., Hicks, K. W., Cinderby, S., Kuylenstierna, J. C. I., Stock, W. D., Dentener, F. J., Giller, K. E., Austin, A. T., Lefroy, R. D. B., Gimeno, B. S., Ashmore, M. R., and Ineson, P.: Atmospheric nitrogen deposition in world biodiversity hotspots: the need for a greater global perspective in assessing N deposition impacts, Glob. Chang. Biol., 12, 470–476, doi:10.1111/j.1365-2486.2006.01104.x, URL http://dx.doi.org/10.1111/j.1365-2486.2006.01104.x, 2006.

Powell, L. L., Powell, T. U., Powell, G. V. N., and Brightsmith, D. J.: Parrots take it with a grain of salt: available sodium content may drive collpa (Clay Lick) selection in south-eastern Peru, Biotropica, 41, 279–282, doi:10.1111/j.1744-7429.2009.00514.x, URL http://doi.wiley.com/10.1111/j.1744-7429.2009.00514.x, 2009.

Pozzer, A., de Meij, A., Pringle, K. J., Tost, H., Doering, U. M., van Aardenne, J., and Lelieveld, J.: Distributions and regional budgets of aerosols and their precursors simulated with the EMAC chemistry-climate model, Atmos. Chem. Phys., 12, 961–987, doi:10.5194/acp-12-961-2012, URL http://www.atmos-chem-phys.net/12/961/2012/, 2012.

Reid, J. S., Prins, E. M., Westphal, D. L., Schmidt, C. C., Richardson, K. A., Christopher, S. A., Eck, T. F., Reid, E. A., Curtis, C. A., and Hoffman, J. P.: Real-time monitoring of South American smoke particle emissions and transport using a coupled remote sensing/box-model approach, Geophys. Res. Lett., 31, n/a–n/a, doi:10.1029/2003GL018845, URL http://doi.wiley.com/10.1029/2003GL018845, 2004.

Richter, M., Beck, E., Rollenbeck, R., and Bendix, J.: The study area, in: Ecosystem services, biodiversity and environmental change in a tropical mountain ecosystem of South Ecuador, edited by Bendix, J., Beck, E., Brauning, A., Makeschin, F., Mosandl, R., Scheu, S., and Wilcke, W., chap. 1, Springer Berlin / Heidelberg, Berlin, Germany, doi:10.1007/978-3-642-38137-9_1, URL http://link.springer.com/chapter/10.1007/978-3-642-38137-9{_}1, 2013.

Riuttanen, L., Hulkkonen, M., Dal Maso, M., Junninen, H., and Kulmala, M.: Trajectory analysis of atmospheric transport of fine particles, SO_2, NO_x and O_3 to the SMEAR II station in Finland in 1996-2008, Atmos. Chem. Phys., 13, 2153–2164, doi:10.5194/acp-13-2153-2013, URL http://www.atmos-chem-phys.net/13/2153/2013/, 2013.

Robinson, N. H., Newton, H. M., Allan, J. D., Irwin, M., Hamilton, J. F., Flynn, M., Bower, K. N., Williams, P. I., Mills, G., Reeves, C. E., McFiggans, G., and Coe, H.: Source attribution of Bornean air masses by back trajectory analysis during the OP3 project, Atmos. Chem. Phys., 11, 9605–9630, doi:10.5194/acp-11-9605-2011, URL http://www.atmos-chem-phys.net/11/9605/2011/acp-11-9605-2011.html, 2011.

Rollenbeck, R., Bendix, J., Fabian, P., Boy, J., Wilcke, W., Dalitz, H., Oesker, M., and Emck, P.: Comparison of different techniques for the measurement of precipitation in tropical montane rain forest regions, J. Atmos. Ocean. Technol., 24, 156–

168, doi:10.1175/JTECH1970.1, URL http://journals.ametsoc.org/doi/abs/10.1175/JTECH1970.1, 2007.

Rollenbeck, R., Bendix, J., and Fabian, P.: Spatial and temporal dynamics of atmospheric water inputs in tropical mountain forests of South Ecuador, Hydrol. Process., 25, 344–352, doi:10.1002/hyp.7799, URL http://doi.wiley.com/10.1002/hyp.7799, 2011.

Schemenauer, R. S. and Cereceda, P.: A proposed standard fog collector for use in high-elevation regions, J. Appl. Meteorol., 33, 1313–1322, URL http://adsabs.harvard.edu/abs/1994JApMe..33.1313S, 1994.

Schulz, M., de Leeuw, G., and Balkanski, Y.: Sea-salt aerosol source functions and emissions, in: Emiss. Atmos. Trace Compd., pp. 333–359, Springer Netherlands, doi:10.1007/978-1-4020-2167-1_9, URL http://link.springer.com/chapter/10.1007/978-1-4020-2167-1{_}9, 2004.

Seibert, P., Kromb-Kolb, H., Baltensperger, U., Jost, D., and Schwikowski, M.: Trajectory analysis of high-alpine air pollution data, in: NATO challenges Mod. Soc., edited by Gryning, S.-E. and Millán, M. M., pp. 595–596, Springer US, doi:10.1007/978-1-4615-1817-4_65, URL http://link.springer.com/chapter/10.1007/978-1-4615-1817-4{_}65, 1994.

Spanos, T.: Environmetric modeling of emission sources for dry and wet precipitation from an urban area, Talanta, 58, 367–375, doi:10.1016/S0039-9140(02)00285-0, URL http://www.sciencedirect.com/science/article/pii/S0039914002002850, 2002.

Stohl, A.: Trajectory statistics–A new method to establish source-receptor relationships of air pollutants and its application to the transport of particulate sulfate in Europe, Atmos. Environ., 30, 579–587, doi:10.1016/1352-2310(95)00314-2, URL http://linkinghub.elsevier.com/retrieve/pii/1352231095003142, 1996.

Talbot, R. W., Andreae, M. O., Berresheim, H., Artaxo, P., Garstang, M., Harriss, R. C., Beecher, K. M., and Li, S. M.: Aerosol chemistry during the wet season in central Amazonia: the influence of long-range transport, J. Geophys. Res., 95, 16 955–16 969, URL http://dx.doi.org/10.1029/JD095iD10p16955, 1990.

Tanner, E. V. J., Vitousek, P. M., and Cuevas, E.: Experimental investigation of nutrient limitation of forest growth on wet tropical mountains, Ecology, 79, 10–22, doi:10.1890/0012-9658(1998)079[0010:EIONLO]2.0.CO;2, URL http://www.esajournals.org/doi/abs/10.1890/0012-9658(1998)079[0010:EIONLO]2.0.CO;2, 1998.

Tardy, Y., Bustillo, V., Roquin, C., Mortatti, J., and Victoria, R.: The Amazon. Biogeochemistry applied to river basin management, Appl. Geochemistry, 20, 1746–1829, doi:10.1016/j.apgeochem.2005.06.001, URL http://linkinghub.elsevier.com/retrieve/pii/S0883292705001113, 2005.

Tipping, E., Benham, S., Boyle, J. F., Crow, P., Davies, J., Fischer, U., Guyatt, H., Helliwell, R., Jackson-Blake, L., Lawlor, A. J., Monteith, D. T., Rowe, E. C., and Toberman, H.: Atmospheric deposition of phosphorus to land and freshwater., Environ. Sci. Process. Impacts, 16, 1608–17, doi:10.1039/c3em00641g, URL http://www.ncbi.nlm.nih.gov/pubmed/24526176, 2014.

Vet, R., Artz, R. S., Carou, S., Shaw, M., Ro, C. U., Aas, W., Baker, A., Bowersox, V. C., Dentener, F., Galy-Lacaux, C., Hou, A., Pienaar, J. J., Gillett, R., Forti, M. C., Gromov, S., Hara, H., Khodzher, T., Mahowald, N. M., Nickovic, S., Rao, P. S. P., and Reid, N. W.: A global assessment of precipitation chemistry and deposition of sulfur, nitrogen, sea salt, base cations, organic acids, acidity and pH, and phosphorus, Atmos. Environ., 93, 3–100, doi:10.1016/j.atmosenv.2013.10.060, URL http://www.sciencedirect.com/science/article/pii/S1352231013008133, 2014.

Vitousek, P. M.: Litterfall, nutrient cycling, and nutrient limitation in tropical forests, 65, 285–298, URL http://www.esajournals.org/doi/abs/10.2307/1939481, 1984.

Voigt, C. C., Capps, K. A., Dechmann, D. K. N., Michener, R. H., and Kunz, T. H.: Nutrition or detoxification: why bats visit mineral licks of the Amazonian rainforest, PLoS One, 3, e2011, doi:10.1371/journal.pone.0002011, URL http://journals.plos.org/plosone/article?id=10.1371/journal.pone.0002011, 2008.

Wang, F., Li, J., Wang, X., Zhang, W., Zou, B., Neher, D. A., and Li, Z.: Nitrogen and phosphorus addition impact soil N_2O emission in a secondary tropical forest of South China., Sci. Rep., 4, 5615, doi:10.1038/srep05615, URL http://www.nature.com/srep/2014/140708/srep05615/full/srep05615.html, 2014.

Wilcke, W., Leimer, S., Peters, T., Emck, P., Rollenbeck, R., Trachte, K., Valarezo, C., and Bendix, J.: The nitrogen cycle of tropical montane forest in Ecuador turns inorganic under environmental change, Global Biogeochem. Cycles, 27, 1194–1204, doi:10.1002/2012GB004471, URL http://doi.wiley.com/10.1002/2012GB004471, 2013.

Williams, M. R., Fisher, T. R., and Melack, J. M.: Chemical composition and deposition of rain in the central Amazon, Brazil, Atmos. Environ., 31, 207–217, doi:10.1016/1352-2310(96)00166-5, URL http://www.sciencedirect.

com/science/article/pii/1352231096001665http://www.sciencedirect.com/science/article/B6VH3-3SVHG1X-8/2/d033b026107388fe3f991cd9b492e31c, 1997.

Wolf, K., Veldkamp, E., Homeier, J., and Martinson, G. O.: Nitrogen availability links forest productivity, soil nitrous oxide and nitric oxide fluxes of a tropical montane forest in southern Ecuador, Global Biogeochem. Cycles, 25, GB4009, doi:10.1029/2010GB003876, URL http://www.agu.org/pubs/crossref/2011/2010GB003876.shtml, 2011.

Wullaert, H.: Response of nutrient cycles of an old-growth montane forest in Ecuador to experimental low-level nutrient amendments, Phd thesis, Fachbereich Chemie, Pharmazie und Geowissenschaften der Johannes Gutenberg-Universität Mainz, Germany, URL http://ubm.opus.hbz-nrw.de/volltexte/2010/2312/, 2010.

Yokouchi, Y., Ikeda, M., Inuzuka, Y., and Yukawa, T.: Strong emission of methyl chloride from tropical plants., Nature, 416, 163–5, doi:10.1038/416163a, URL http://dx.doi.org/10.1038/416163a, 2002.

Yu, H., Chin, M., Yuan, T., Bian, H., Remer, L. A., Prospero, J. M., Omar, A., Winker, D., Yang, Y., Zhang, Y., Zhang, Z., and Zhao, C.: The fertilizing role of african dust in the Amazon rainforest: a first multiyear assessment based on CALIPSO lidar Observations, Geophys. Res. Lett., 42, 1984–1991, doi:10.1002/2015GL063040, URL http://doi.wiley.com/10.1002/2015GL063040, 2015.

Zeng, Y. and Hopke, P.: A study of the sources of acid precipitation in Ontario, Canada, Atmos. Environ., 23, 1499–1509, doi:10.1016/0004-6981(89)90409-5, URL http://www.sciencedirect.com/science/article/pii/0004698189904095, 1989.

Chapter 6

Conclusions and outlook

6.1 Conclusions

This work represents a first effort to resolve the complex interaction between the atmospheric deposition of ecosystem-relevant nutrients/pollutants in a complex terrain area, atmospheric transport, and contribution of emission sources. The general objective was to investigate the inputs of nitrate, sulfate, and salts (NaCl) by OP and rain in a complex terrain area of the South-eastern Ecuadorian Andes as a function of present-day atmospheric circulation and source-emission patterns. To accomplish this, the first aim of the current thesis was to analyze the deposition patterns along an altitudinal gradient, for which precipitation chemistry data from four MSs at different topographical locations were used. Our second aim was to shed light on the sources and atmospheric circulation patterns driving the observed deposition. This was done by using two source-receptor models, depending on whether emission data was available or not for the analyzed constituent, and other back-trajectory techniques.

A similar methodological framework was used to evaluate the defined hypotheses for each of the following elements: nitrate, sulfate, and sea salt (sodium and chloride). For each of these atmospheric constituents, which were the topics of the scientific publications in chapters 3-5, the hypotheses in section 1.2 were tested. The conclusions that arise from the evaluation of these hypotheses are developed in the following paragraphs.

The atmospheric deposition of nitrate, a limiting nutrient for vegetation growth, was the topic of the first article (chapter 3) in which **H1** was tested.

We found that topographic position, aspect, and elevation are important parameters influencing the nitrate deposition. The nitrate deposition was higher at crest MSs, where the contribution of OP to the total water input is more important. Crest MSs revealed

a very clear synoptical pattern, while lower valley MSs were characterized by local mountain-valley winds. However, specifically at crests, there were also some differences in the transport-deposition relationship depending on the type of precipitation (OP or rain). Accordingly, in the OP samples the relation of nitrate deposition and the synoptical transport was clearly evident, because the cloud droplets are deposited directly onto the collector without traversing the atmosphere below the clouds. In contrast, local pollutants were washed out by rain droplets due to below-cloud scavenging, blurring the correlation to the synoptical transport from remote sources. We conclude that, given the strong influence of the different wind systems, the precipitation type, and the topography in the deposition, **H1a** is accepted.

With regard to the sources, on the one hand, biomass-burning from the Amazon lowlands was found as the most important source of atmospheric nitrate, affecting mostly the higher elevated areas, which confirms **H1b**. The location of the biomass-burning emission sources closer to the receptor site and in the path of the predominant air masses, as well as the big spatial dimension of the area burned and the intensity of the emissions explain the strong influence of these sources in the observed deposition. On the other hand, the lack of influence of urban/transportation emissions from cities at the east coast of the continent is also explained by the distant location of these sources as well as its dispersed distribution which generally did not coincide well with the predominant air mass pathways to the receptor site in South Ecuador.

Sulfate deposition can contribute to the acidification of soils and in high concentration even cause damage to plant leaves (Delmelle et al. 2002; Kuylenstierna et al. 2001). This type of deposition and its related transport pathways and potential emission sources was addressed in the second article (chapter 4).

Considering that the concentration of sulfate presented a similar distribution with altitude as that of nitrate, and that preliminary work in the first article showed that higher areas are more vulnerable to higher deposition, here only the two uppermost MSs were evaluated.

The altitude of the measurement sites was an important parameter that conditioned the type of deposition. Thus, biomass-burning contributed to OP sulfate deposition at El Tiro and Cerro del Consuelo MSs, whereas the contribution of volcanoes differed between both sites. At Cerro del Consuelo higher intensities of OP deposition were recorded while at El Tiro rain the deposition was more pronounced. A strong signal of the synoptical transport was observed in both elevated MSs. Nonetheless, the higher and the better exposed the MS, the stronger the influence of the synoptical transport from all wind directions because the surrounding topography does not play a relevant role. These results

lead to the acceptance of **H2a**.

Concerning the sources of sulfate, the results of the source allocation study indicated that, although the vicinity of volcanic emission and some weak urban/industrial anthropogenic sources, biomass-burning emissions dominate the deposition at the San Francisco valley, because of its location in the pathway of the preponderant air masses and the great dimension of the source areas. Eruptive and passive emissions from volcanoes contribute only in a limited time window and play a marginal role in the deposition. With this, **H2b** is rejected because biomass-burning emission sources are dominating the observed sulfate deposition at the study area in southeastern Ecuador.

Salt availability has been shown to influence the behavior of several essential species regarding ecosystem health (Dudley et al. 2012; Kaspari et al. 2008, 2009). In South-America salt availability was observed to decline as a function of the distance from the Atlantic coast (Talbot et al. 1990; Tardy et al. 2005). Given the special position of the study site at a topographic depression in the Andes, the subject of a third scientific publication was to evaluate the influence of Pacific and Atlantic sea salt aerosols on the deposition of salt at this special location in the tropical Andes (chapter 5).

Since no adequate emission inventories for source-receptor modelling as in the first and second publications were available, in this article source-receptor modelling approaches that did not require emission data were used, namely the PSCF and the CWT function. On top of that, the reason for the inclusion of the complete set of MSs along the altitudinal gradient was the notably different distribution of the sodium and chloride data in comparison to nitrate and sulfate. Additionally, they differ in their origins, which lead to a completely different deposition pattern.

The concentration time series at the uppermost MSs exhibited a higher seasonality which was also observed in the sea salt medium-to-large-scale transport. In the lower MSs this seasonality was absent in the concentration time series. Additionally, the Na^+ / Cl^- molar ratios at the elevated MSs are closer to the ratio of fresh sea salt than low elevation MSs. Hence, this indicates that the more elevated MSs are, less affected by the surrounding topography and therefore more influenced by the synoptical transport. In contrast, the MSs at lower elevations are affected by the local circulation. The high chloride concentration in OP at the low altitude ECSF MS reveals the differentiated effect of local winds and emissions with respect to the type of precipitation. Here, only fog collectors captured local pollution transport by the mountain-valley breeze system. The chemical composition of the samples also changed according to the precipitation type, with a sea salt factor dominating the variability in rain and biomass-burning components being dominant in OP.

Hence, hypothesis **H3a** is accepted.

Concerning the sources of sea salt, the interplay between the location of the Pacific sources close to the receptor site, under the influence of the westerly winds, and the low altitude of the Andean mountain range at the latitude of the study area was decisive for the final balance of the source contributions. In the end, the transport from the Equatorial Pacific considerably contributed to the sea-salt deposition at the study area, even if the westerly flows were highly seasonal and featured a quite low frequency of occurrence, leading to the confirmation of **H3b**. When compared to other sites in the Amazon, the sea-salt deposition at the TMF of south-eastern Ecuador seems to follow the patterns of near-ocean regions more closely than the patterns of continental sites. This conclusion follows from the higher sodium and chloride concentration in the study area than that observed in sites of the central Amazon and from the higher Cl^- concentration with respect to that of Na^+ which match the observations in near-ocean sites. The importance of the contribution of Pacific sea-salt aerosol inputs can in part alleviate from the salt deprivation reported for similar ecosystems. This is of course out of the scope of this research, but could be an interesting and important topic for future research in the area.

The described sources and transport pathways of the different atmospheric constituents in the study area are illustrated in a synthesis map in Fig. 6.1.

6.2 Outlook

The transport of nutrients and pollutants through the atmosphere remains a very complex phenomenon which involves multiple parameters (emissions, state of the atmosphere, particles and gases chemistry and physics) and their interactions, making its study a very challenging task. On the basis of the conclusions of this work, a valuable advance in the attribution of deposition sources would be the implementation of a dispersion model like FLEXPART (Stohl et al. 2005), as well as the incorporation of data from a regional climatic model, such as the WRF model. These advances would mean a significant progress, because regional turbulence, convection, and dry and wet scavenging along transport would be taken into account (Brioude et al. 2012, 2013; Hernández-Ceballos et al. 2014). This higher complexity would likely allow for more precise differentiation between local and distant sources, and probably among local sources as well.

The expansion of the rain and OP deposition measurement network on leeward and windward slopes and at different elevations would also represent an interesting improvement. This would allow to bring the quantification of the deposition to the landscape scale as done by the LandMod deposition model by Weathers et al. (2006),

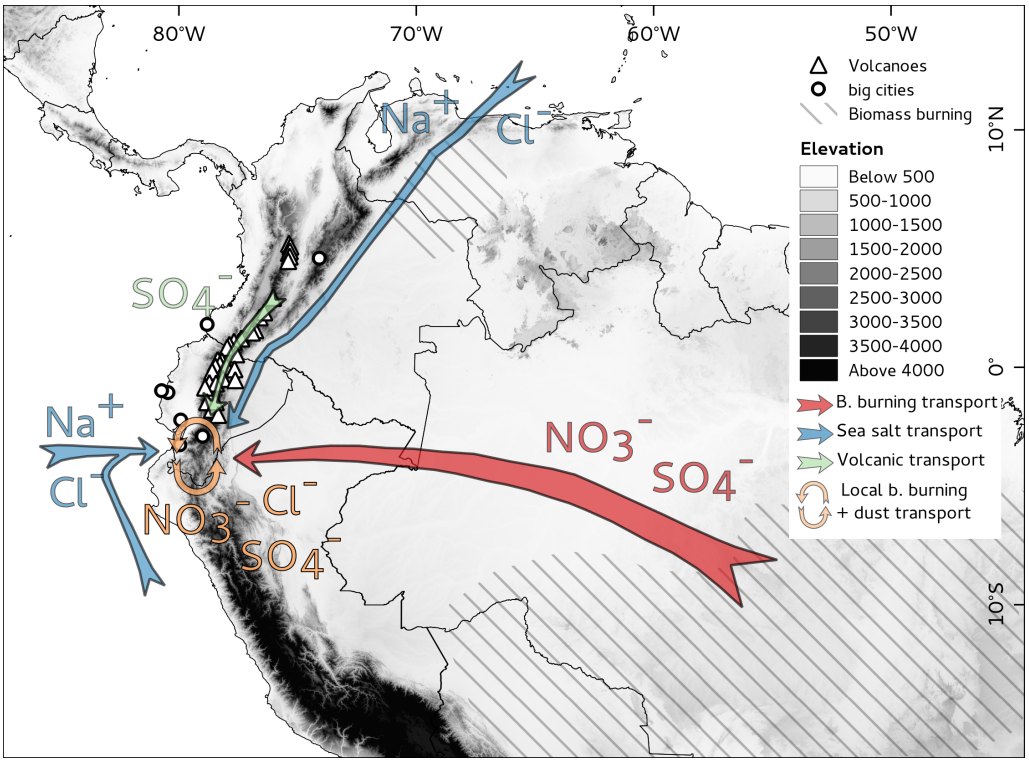

Figure 6.1: Synthesis map of nitrate, sulfate, sodium, and chloride's sources and atmospheric pathways. Because of the mountainous terrain the reader should keep in mind that distant sources affect mostly elevated and well exposed areas, while local sources will affect less elevated areas exposed to the local winds.

which would be of high relevance for emission policy decision makers.

Bibliography

Brioude, J., Angevine, W. M., McKeen, S. A., and Hsie, E.-Y.: Numerical uncertainty at mesoscale in a Lagrangian model in complex terrain, Geosci. Model Dev., 5, 1127–1136, doi:10.5194/gmd-5-1127-2012, URL http://www.geosci-model-dev.net/5/1127/2012/, 2012.

Brioude, J., Arnold, D., Stohl, A., Cassiani, M., Morton, D., Seibert, P., Angevine, W., Evan, S., Dingwell, A., Fast, J. D., Easter, R. C., Pisso, I., Burkhart, J., and Wotawa, G.: The Lagrangian particle dispersion model FLEXPART-WRF version 3.1, Geosci. Model Dev., 6, 1889–1904, doi:10.5194/gmd-6-1889-2013, URL http://www.geosci-model-dev.net/6/1889/2013/, 2013.

Delmelle, P., Stix, J., Baxter, P. J., and Garcia-Alvarez, J.: Atmospheric dispersion, environmental effects and potential health hazard associated with the low-altitude gas plume of Masaya volcano, Nicaragua, Bull. Volcanol., 64, 423–434, doi:10.1007/s00445-002-0221-6, URL http://link.springer.com/10.1007/s00445-002-0221-6http://link.springer.com/article/10.1007/s00445-002-0221-6, 2002.

Dudley, R., Kaspari, M., and Yanoviak, S. P.: Lust for salt in the western Amazon, Biotropica, 44, 6–9, doi:10.1111/j.1744-7429.2011.00818.x, URL http://doi.wiley.com/10.1111/j.1744-7429.2011.00818.x, 2012.

Hernández-Ceballos, M. A., Skjøth, C. A., García-Mozo, H., Bolívar, J. P., and Galán, C.: Improvement in the accuracy of back trajectories using WRF to identify pollen sources in southern Iberian Peninsula., Int. J. Biometeorol., 58, 2031–43, doi:10.1007/s00484-014-0804-x, URL http://link.springer.com/10.1007/s00484-014-0804-x, 2014.

Kaspari, M., Yanoviak, S. P., and Dudley, R.: On the biogeography of salt limitation: a study of ant communities., Proc. Natl. Acad. Sci. U.S.A., 105, 17 848–51, doi:10.1073/pnas.0804528105, URL http://www.pubmedcentral.nih.gov/articlerender.fcgi?artid=2584704{&}tool=pmcentrez{&}rendertype=abstract, 2008.

Kaspari, M., Yanoviak, S. P., Dudley, R., Yuan, M., and Clay, N. A.: Sodium shortage as a constraint on the carbon cycle in an inland tropical rainforest., Proc. Natl. Acad. Sci. U.S.A., 106, 19 405–9, doi:10.1073/pnas.0906448106, URL http://www.pnas.org/content/106/46/19405.abstract, 2009.

Kuylenstierna, J. C. I., Rodhe, H., Cinderby, S., and Hicks, K.: Acidification in developing countries: ecosystem sensitivity and the critical load ap-

proach on a global scale, Ambio, 30, 20–28, doi:10.1579/0044-7447-30.1.20, URL http://www.bioone.org/doi/pdf/10.1579/0044-7447-30.1.20http://dx.doi.org/10.1579/0044-7447-30.1.20, 2001.

Stohl, A., Forster, C., Frank, A., Seibert, P., and Wotawa, G.: Technical note: the Lagrangian particle dispersion model FLEXPART version 6.2, Atmos. Chem. Phys., 5, 2461–2474, doi:10.5194/acp-5-2461-2005, URL http://www.atmos-chem-phys.net/5/2461/2005/, 2005.

Talbot, R. W., Andreae, M. O., Berresheim, H., Artaxo, P., Garstang, M., Harriss, R. C., Beecher, K. M., and Li, S. M.: Aerosol chemistry during the wet season in central Amazonia: the influence of long-range transport, J. Geophys. Res., 95, 16 955–16 969, URL http://dx.doi.org/10.1029/JD095iD10p16955, 1990.

Tardy, Y., Bustillo, V., Roquin, C., Mortatti, J., and Victoria, R.: The Amazon. Biogeochemistry applied to river basin management, Appl. Geochemistry, 20, 1746–1829, doi:10.1016/j.apgeochem.2005.06.001, URL http://linkinghub.elsevier.com/retrieve/pii/S0883292705001113, 2005.

Weathers, K. C., Simkin, S. M., Lovett, G. M., and Lindberg, S. E.: Empirical modeling of atmospheric deposition in mountainous landscapes, Ecol. Appl., 16, 1590–1607, doi:10.1890/1051-0761(2006)016[1590:EMOADI]2.0.CO;2, 2006.

Erklärung

Ich erkläre an Eidesstatt, dass ich meine Dissertation

Sources, pathways, and deposition of nutrients and pollutants in an Ecuadorian tropical mountain forest

selbstständig und ohne unerlaubte Hilfe angefertigt und mich dabei keinerlei anderen als der von mir ausdrücklich bezeichneten Quellen und Hilfen bedient habe.

Die Dissertation wurde in der jetzigen oder einer ähnlichen Form noch an keiner anderen Hochschule eingereicht und hat noch keinen sonstigen Prüfungszwecken gedient.

Marburg, 17.08.2016

Sandro Makowski Giannoni